CAN SILICON CARBIDE NANOTUBES BE EFFECTIVE STORAGE MEDIUM FOR HYDROGEN STORAGE?

by

SOUPTIK MUKHERJEE

Presented to the Faculty of the Graduate School of

The University of Texas at Arlington in Partial Fulfillment

of the Requirements

for the Degree of

MASTER OF SCIENCE IN PHYSICS

THE UNIVERSITY OF TEXAS AT ARLINGTON

November 2008

ACKNOWLEDGEMENTS

I would like to express my deep gratitude to my thesis advisor, Prof. Dr. A. K. Ray who made this whole work possible. All throughout my research and writing of this thesis his suggestions has been simulating and encouraging. My experience of working as a student of Prof. A. K. Ray has been a cherished experience, which will benefit my entire life. I also would like to extend my thanks to my committee members, Dr. Zhang and Dr. Fry. Their advice and opinions have enriched my work and have helped me to get valuable insight. Finally I would like to thank the entire physics department for providing me with an excellent work environment.

Also, my research group members; Raymond, Somil, Kazi, Pratik, Fakrul and Shafaq have given help and valuable hints from time to time and it was my pleasure working with them. The group meetings have helped to increase my expanse of knowledge and have been quite enjoyable. The UTA Physics department has always treated me like a member of a family. The departmental activities have been a great platform to build up social networks, gain vital insights into latest developments in science and technology and help improve my overall personality.

Finally, I would like to acknowledge the continuous support and encouragement of my family members which have helped me complete this work. I would also like to gratefully acknowledge the partial support from the Welch Foundation, Houston, Texas (Grant No. Y-1525).

November 25, 2008

ABSTRACT

CAN SILICON CARBIDE NANOTUBES BE EFFECTIVE STORAGE MEDIUM FOR HYDROGEN STORAGE?

SOUPTIK MUKHERJEE

The University of Texas at Arlington, 2008

Supervising Professor: A. K. Ray

A systematic study of molecular hydrogen adsorption on three different atomic configurations of armchair SICNTs has been performed. In the first stage of our study, first principles calculations using both density functional theory (DFT) and hybrid density functional theory (HDFT) as well as the finite cluster approximation have been performed to study the adsorption of molecular hydrogen on three types of armchair (9, 9) silicon carbide nanotubes. The distances of molecular hydrogen from the outer wall of the nanotubes have been optimized manually using the B3LYP and PW91 functionals and results have been compared in detail with published literature results. In the second part of our study, hydrogen molecule has been adsorbed from both inside as well as from the outer wall of nanotubes ranging from (3, 3) to (6, 6) and for all three types. A detailed comparison of the binding energies, equilibrium positions and Mulliken charges has been performed for all three types of nanotubes and for all possible sites in those nanotubes. In the third phase, co-adsorption of two hydrogen molecules has been carried out. In some cases, during co-adsorption, the binding energy obtained has increased in certain structures like type 2 (4, 4) compared to single hydrogen molecular adsorption. Possibilities of hydrogen storage have been explored in detail.

TABLE OF CONTENTS

LIST OF ILLUSTRATIONS

LIST OF TABLES

CHAPTER 1

INTRODUCTION

Hydrogen has long been recognized as a clean source of energy and is often referred to as the fuel of the future. When used in a fuel cell, hydrogen produces only water as a byproduct. Electric vehicles using hydrogen fuel cells hold great promise. Recently, it has been announced by the Daimler Chrysler Corporation that it would be the first automaker worldwide to offer fuel cell vehicles on the market during the next several years [1]. However, to put hydrogen electric vehicles into large-scale practical utilization, several challenges need to be met. One of the major challenges is the lack of a safe and efficient onboard storage technology, which can dramatically influence the vehicle's cost, range, performance, and fuel economy. It can also shape the scale, investment requirements, energy use, and potential emissions of a hydrogen-refueling infrastructure. Hence the development of onboard storage technology will directly determine the schedule of hydrogen-powered vehicles coming into the market [2].

One method employed for storage is the formation of metal hydrides due to reaction of solids like metals and alloys with hydrogen. Using cryogenic conditions for adsorption on various solids, including carbon, has also been suggested as an alternative storage method [3-5]. Another method tried out by Schwarz et al. is the adsorption of hydrogen on molecularly engineered carbon at -150 ℃ [4, 5]. They reported that a storage capacity of 0.5 g of H2/kg of carbon at 20 Atm pressure can be achieved using this material. Dillon et al. [6] used another storage material, 1 mg of unpurified soot that consisted of a mixture of carbonaceous materials, for hydrogen storage. It contained 0.1-0.2 wt % of single-walled carbon nanotubes as

well as a large fraction of cobalt catalyst particles (20 wt %). Using this material, a storage capacity of 5% of hydrogen at 0 ℃ was achieved.

Interaction of hydrogen with various isotopes of carbon with graphitic surface has been studied extensively for hydrogen storage [7, 8]. Alkali-intercalated graphite [9, 10] has also been suggested as a possible storage material. Up to 0.137 L (STP) of H_2/gm of carbon can be absorbed as reported. It has also been found that at liquid nitrogen temperature, repeated cycles of absorption and release of hydrogen causes no damage to the material.

However, critical problems associated with conventional storage mediums like metals and intermetallics is the limitation on the storage capacity and the reversibility of stored hydrogen under normal conditions [11-14]. The United States Department of Energy (DOE) has set a goal of developing a hydrogen storage system having a capacity of 6 wt % by 2010 and 9 wt % by 2015, [15]. It is to be noted that these targets are for the hydrogen storage system, not the hydrogen storage material. Thus while a material may store 6 wt% H_2, a working system using that material may only achieve 3 wt% when the weight of tanks, temperature and pressure control equipment, etc., is considered. A light weight nanostructure with a large surface-to-bulk ratio is ideal for hydrogen storage. As a result the hydrogen storage capacity of single walled nanostructures has become extremely important. Since the synthesis of carbon nanotubes by Iijima, [16] the synthesis and application of one dimension, nanometer scaled structures have increased considerably. Dillon *et al*. [17] have reported that carbon nanotubes (CNTs) can be used for hydrogen storage and have measured the H_2 adsorption capacity of SWCNT which ranges from 5 -10 wt %. Recent theoretical studies indicate that the binding energies of molecular hydrogen on boron-nitride nanotubes (BNNTs) exceed that of CNTs considerably [18]. Hence the possibility of hydrogen storage in similar polar nanotubes, made up of two different atoms, such as SiC becomes an interesting study.

Silicon carbide (SiC) in bulk form is one of the hardest materials and is very suitable for operations in extreme environments. Group IV elements, with the exception of carbon, have

significant energy difference between sp^2 and sp^3 bonds [19]. This large energy difference is also seen in case of SiC bonds. Different groups have successfully synthesized SiCNTs [20-26]. For brevity; only few of the methods have been discussed here. Synthesis of SiCNTs resulting from the reaction of silicon (via disproportionation of SiO) and multiwalled carbon nanotubes (as templates) have been successfully reported by Sun *et al*. [20]. Synthesis of SiCNTs using high-temperature reactions between silicon powders and multi-walled carbon nanotubes have been reported by Borowiak-Palen *et al*. [22]. Very recently, using periodic boundary conditions and the DMol suite of software, Meng *et al.* have studied hydrogen adsorption in silicon carbide nanotubes coated with Ti metal atoms [27]. They concluded that SiCNT materials could be used as an excellent hydrogen storage media. There are certain advantages SiC nanotubes enjoy over carbon nanotubes. They have high reactivity of exterior surface, stability at high temperature and can form harsh environment nanotube and nanofibre reinforced ceramics [28]. Similar work has been carried out using boron and nitrogen doped SiCNTs [29]. In order to study hydrogen storage in SiCNTs experimentally Rong-an He *et al*. [30] synthesized SiCNTs from multi walled carbon nanotubes (MWCNTs) via chemical vapour reaction (CVR) and purification. Measurements carried out on SiCNTs by them have revealed that the hydrogen storage capacity of SiCNTs is superior to those of MWCNTs.

Most stable SiC nanotubes have been found to possess one to one ratio of Si and C atoms in their atomic arrangement as any other ratio would collapse the tube into nanowire or clusters with solid interiors [31]. Two atomic arrangements of SiC nanotubes (type 1 and type 2) had already been studied by M. Menon *et al*. [32]. Recently, it has been found out that there can be three types of armchair nanotube types, based on spatial configuration [33] and that the armchair structures show more stability as more compared to zigzag configurations.

In case of type 1, SiC atomic arrangement can be discussed as rows of alternating Si and C atoms perpendicular to the nanotube axis. Each Si atoms has three C neighbors and vice versa with only Si-C bonds. In type 2 atomic configuration each layer has either Si or C atoms

perpendicular to the nanotube axis. C atom has two Si neighbors and one C neighbor and vice versa. Type 2 nanotubes contain C-C and Si-Si bonds in addition to Si-C bonds. Calculations have revealed that type 1 SiC nanotubes with alternating Si and C atoms are energetically preferred over the SiC nanotubes that contain C-C and Si-Si bonds. [33]. The type 3 SiC nanotube [33] has the same number of Si and C atoms, with similar one to one ratio, but differs in the relative atomic arrangement of Si and C atoms. In type 3 arrangements each Si has two C and one Si neighbors, similar to type 2, but Si and C atoms are arranged alternatively in each layer (the layer perpendicular to the tube axis) similar to type 1. All three nanotube structures are close in energy but type 1 is more stable as compared to type 2 and type 3. Mpourmpakis *et al*. [34] has mentioned that the storage capacity in SiC nanotubes exceed that of CNTs by 20%. They also stated that the binding can increase further under low temperature and high pressure conditions. Thus, according to them SiCNTs are more suitable material for hydrogen storage as compared to pure CNTs. However, only one nanotube type and only a specific adsorption site in that type has been considered in their study. These considerations along with the previous work on SiC nanotubes done in our group [33] has guided us to study a detailed adsorption site-specific study of the interaction of hydrogen molecules with the three armchair SiC nanotubes (all three atomic configuration types). The hydrogen molecule has been studied for adsorption both from inside the nanotube and from the outer wall of the nanotube. This also helps us to explore the possibility of utilizing SiC nanotubes as an effective medium for hydrogen storage.

This thesis has been organized into five chapters. In the first chapter we have given an introduction to SiC nanotubes. In the second chapter the density functional theory and computational details have been discussed. In the third chapter the hydrogen molecular adsorption from the outer wall for three types of (9, 9) armchair SiC nanotubes [35] have been discussed and the results form these studies have been compared to previous studies. Studies on the hydrogen molecular interaction, with the hydrogen molecule adsorbed from inside the

nanotube have been done and have been compared with the outer wall adsorption. We have chosen nanotubes ranging from (3, 3) to (6, 6) for this purpose. Previous studies done on armchair SiC nanotubes ranging from (3, 3) to (11, 11) have indicated that beyond (6, 6), the binding energy of the nanotubes saturates [33]. Hence to simplify some of the computational constraints involving more atoms and for reasons above we have limited our study to (6, 6) armchair nanotubes. By choosing a smaller nanotube we expect to study the inner wall interaction of the hydrogen molecules in more details. The results of our study have been discussed in the later part of the chapter. Apart from single molecular adsorption we have also done co-adsorption of two hydrogen molecules in order to explore the possibility of getting better binding energy. For each of the sites where a single molecule has been adsorbed there are several unique co-adsorption sites available. Co-adsorption of the hydrogen molecules have been carried out for (3, 3) to (6, 6) armchair nanotube structures. As in single hydrogen molecular adsorption, in case of co-adsorption too, both inner wall as well as outer wall adsorption has been studied. The results of our study have been laid out in chapter 4. The last chapter deals with the conclusions and contains suggestions for future work.

CHAPTER 2

THEORY

2.1 Density Functional Theory

Hartree-Fock (HF) theory and density functional theory (DFT) are the two standard methods in computational condensed matter physics. Both of these theories are simplistic versions of the full problem of many electrons moving in the potential field. Amongst both the theories density functional theory, which results from work of Hohenberg, Kohn and Sham [36-43] has been the most popular method. Time-independent Schrödinger equation can be used in many cases to study problems related to electronic structures. In case of an isolated system with N electrons in the Born-Oppenheimer nonrelativistic approximation, this is given by

$$H\Psi = E\Psi \tag{2.1}$$

Where H is the Hamiltonian in atomic units,

$$H = \sum_{i=1}^{N} (-\frac{1}{2}\nabla_i^2) + \sum_{i=1}^{N} v(r_i) + \sum_{i<j}^{N} \frac{1}{r_{ij}} \tag{2.2}$$

in which

$$v(r) = -\sum_{\alpha} \frac{Z_\alpha}{|r_i - R_\alpha|} \tag{2.3}$$

is taken to be the "external" potential due to nuclei of charges Z_α acting on the i^{th} electron. The electronic energy is given by E and $\Psi = \Psi(x_i, x_2, ..., x_n)$ is the many-electron wave function, where x_i denote the particle coordinates and spins. For the last few decades physics have strived to solve the many particle problems. There are essentially two ways in which physicists approach this problem. One is by considering the many-electron wave

function $\Psi(x_i, x_2, ..., x_n)$ [44]. The many-electron wave function is constructed from the product of single particle functions.

$$\Psi(x_i, x_2, ..., x_n) = \Psi_1(x_1)\Psi_2(x_2)...\Psi_n(x_n) \quad (2.4)$$

Each of the functions $\Psi_1(x_1)$ satisfies a one-electron Schrödinger equation with a potential term arising from the average field of the other electrons,

$$\left[-\frac{h^2}{2m}\nabla^2 + V_{ext} + \Phi_i\right]\Psi_i(x) = \varepsilon_i\Psi_i(x) \quad (2.5)$$

where the Coulomb potential Φ_i is given by Poisson's equation

$$\nabla^2\Phi_i = 4\pi e^2 \sum_{j=1, i\neq j}^{N} |\Psi_j|^2 \quad (2.6)$$

and where V_{ext} is the potential due to the nuclei. Now, the simple product wave function can be replaced by a single determinantal function, which leads to the so-called Hartree-Fock approximation [45-46] which results from the Pauli Exclusion Principle. The total energy calculation improves after the inclusion of Fermi statistics thereby introducing an additional, nonlocal exchange term. However the single particle picture, with the wave function described in terms of orbital with particular spins and occupation numbers remains unchanged. Since the lowest-lying configuration is generally only one of many comparable energies, it has been observed that a single configuration (Slater determinant) wave function inevitably lead to a poor energy. A better approximation would result from taking a linear combination [47]. This approach is known as "configuration interaction" (CI). It also includes the correlation effects beyond Hartree-Fock approximation by improving the many-particle wave functions. CI in principle provides an exact solution of the many-electron problems. The number of configurations with increasing electron number has increased explosively in real practice limiting its application to only small systems having relatively few electrons. Also, due to the complexity

of the resulting solutions it has become increasingly difficult to interpret the results. Another alternative approach which is based on the density of electrons in the system n(r) is the Thomas-Fermi model [48-49].

$$n(r) = N \int dr_2 ... \int dr_n \Psi^*(r_1, r_2, ..., r_n)\Psi(r_1, r_2, ..., r_n). \quad (2.7)$$

The Thomas-Fermi model is based on the assumption that the motions of the electrons are uncorrelated. It also assumes that the local approximation based on the results for uniform electron gas, $[n(r)]^{5/3}$ can describe the corresponding kinetic energy. The fact that by incorporating a term derived from the exchange energy density in a homogenous system was described by Dirac [50] very shortly there after. In a system of variable density the exchange potential could be approximated by a term. This term has a local dependence ~ $[n(r)]^{1/3}$ based on electron density. In fact, the concept of the "exchange" or "Fermi" hole helps to explain this dependence on the density. In other words this concept is based on the fact that the region near an electron is avoided by electrons of the same spin, and not on the exchange potential in a homogenous system. A prototype for modern density functional theory was given by the Thomas-Fermi model and is based upon two Hohenberg-Kohn theorems [37].

It is to be noted that the number of electrons is represented by N Hamiltonian in (2.2), and the external potential is represented by $v(r)$ in the Hamiltonian (2.2) Because of that all properties for the ground state are determined are determined by $v(r)$ and N . The use of electron density $n(r)$ as the basic variable has been permitted to be used in place of N and $v(r)$, by the first two Hohenberg-Kohn theorems. The Hohenberg-Kohn theorem states the following: *The external potential* $v(r)$ *is determined, within a trivial additive constant, by the electron density* $n(r)$.

The proof of the Hohenberg-Kohn theorem is quite straightforward. For some N-electron system, the number of electrons is determined by Consider the electron density for the

non-degenerate ground state of some N-electron system. It determines the number of electrons by

$\int n(r)dr = N$, where $n(r)$ is the electron density for the non degenerate ground state (2.8)

We know that $v(r)$ is determined from $n(r)$. Hence the ground-state wave function Ψ is determined from $n(r)$. Similarly, other electronic properties can also be determined from $n(r)$. Let us consider two external potentials v and v_1. Taking into fact that they differ by more than a constant, and each give the same $n(r)$ for its ground state. It is possible to construct two Hamiltonians H and H_1 whose normalized wave functions Ψ and Ψ_1 are different, although their ground-state densities are the same.

$$H\Psi = E\Psi \tag{2.9}$$

$$H_1\Psi_1 = E_1\Psi_1 \tag{2.10}$$

H and H_1 have the ground-state energies E and E_1 respectively. Hence for Ψ_1 its expectation value H would be greater than E,

$$E < \langle \Psi_1 | H | \Psi_1 \rangle = \langle \Psi_1 | H + H_1 - H_1 | \Psi_1 \rangle$$

$$= \langle \Psi_1 | H_1 | \Psi_1 \rangle + \langle \Psi_1 | H - H_1 | \Psi_1 \rangle \tag{2.11}$$

$$= E_1 + \int n(r)[v(r) - v_1(r)]dr$$

In a similar way, in Ψ, the expectation value of H_1 in would be greater than E_1,

$$E_1 < \langle \Psi | H_1 | \Psi \rangle = \langle \Psi | H_1 + H - H | \Psi \rangle$$

$$= \langle \Psi | H | \Psi \rangle + \langle \Psi | H - H_1 | \Psi \rangle \tag{2.12}$$

$$= E + \int n(r)[v(r) - v_1(r)]dr$$

By adding (2.11) and (2.12), we get

$$E + E_1 < E_1 + E \tag{2.13}$$

But two different external potentials cannot give the same ground-state densities. Otherwise there would be a contradiction.

Thus, all properties of the ground state are determined $n(r)$ determines both N and v and hence. Therefore, the ground state total energy can be written as a functional of the electron density,

$$E[n] = T[n] + V_{ne}[n] + V_{ee}[n] = \int n(r)v(r)dr + F_{HK}[n] \tag{2.14}$$

where $T[n]$ is the kinetic energy, $V_{ne}[n]$ is the nuclei-electron interaction energy and $V_{ee}[n]$ is the electron-electron Coulomb interaction energy and $F_{HK}[n]$ is a universal functional of $n(r)$ in a sense that $F_{HK}[n]$ is defined independently of the external potential $v(r)$,

$$F_{HK}[n] = T[n] + V_{ee}[n] \tag{2.15}$$

The second Hohenberg-Kohn theorem states: *For a trial density* $n_1(r)$*, such that* $n_1(r) \geq 0$ *and* $\int n_1(r)dr = N$,

$$E_0 \leq E[n_1] \tag{2.16}$$

Where $E[n_1]$ *is the energy functional of (2.14).*

This theorem gives the energy variational principle. It means that the ground-state electron density as the density that minimizes $E[n]$. Since the first theorem assures that $n_1(r)$ which determines its own v_1, Hamiltonian H_1, and wave function Ψ_1, can be taken as a trial function for the Hamiltonian H of interest with external potential v. Thus,

$$\langle \Psi_1 \mid H \mid \Psi_1 \rangle = \int n_1(r)v(r)dr + F_{HK}[n_1] = E[n_1] \geq E[n] \tag{2.17}$$

The variational principle (2.16) requires that the ground-state density satisfy the following stationary principle,

$$\delta\left\{E[n]-\mu\left[\int n(r)dr-N\right]\right\}=0 \tag{2.18}$$

which gives the Euler-Lagrange equation

$$\mu=\frac{\delta \mathrm{E}[n]}{\delta n(r)}=v(r)+\frac{\delta F_{HK}[n]}{\delta n(r)} \tag{2.19}$$

where the quantity μ is the chemical potential.

Knowing the exact $F_{HK}[n]$ (2.18) gives an exact equation for the ground-state density. Once an explicit form of $F_{HK}[n]$ either approximate or accurate is found, this method can be applied to any system. Equation (2.19) is the basic working equation of density-functional theory. However, accurate computational implementations of the density-functional theory are far from easy to achieve, due to the difficulty in obtaining the explicit form of the functional $F_{HK}[n]$. Although the Hohenberg-Kohn theorems are not insightful of actual methods of calculation, as it is usually $v(r)$ rather than $n(r)$ that is known, they provide confidence that it is sensible to seek solutions based on the density rather than the wave functions for many-body problems.

Early attempts to approximate the universal functional $F_{HK}[n]$ used the Thomas-Fermi approximation for the kinetic component $T[n]$. However only very crude answers can be obtained with this local functional for the kinetic energy, no matter how sophisticated the approximation for the $V_{ee}[n]$ component is. Kohn and Sham thereafter proposed a highly nonlocal functional giving the major part of the kinetic energy and the scheme making the density functional theory practical. They invoked a non-interacting reference system, with the Hamiltonian,

$$H_s=\sum_i^N(-\frac{1}{2}\nabla_i^{\,2})+\sum_i^N v_{eff}(r_i) \tag{2.20}$$

For which the ground-state electron density is exactly $n(r)$. Thus, for this system, there will be an exact ground-state wave function.

$$\Psi_s = \frac{1}{\sqrt{N!}} \det\left[\Psi_1 \Psi_2 ... \Psi_n\right] \tag{2.21}$$

where the Ψ_i are the N lowest eigenstates of the one-electron Hamiltonian h_s:

$$h_s \Psi_i = \left[-\tfrac{1}{2}\nabla^2 + v_{eff}(r)\right]\Psi_i = \varepsilon_i \Psi_i \tag{2.22}$$

and

$$n(r) = \sum_i^N \sum_s \left|\Psi_i(r,s)\right|^2 \tag{2.23}$$

The kinetic energy is then given by $T_s[n]$,

$$T_s[n] = \sum_{i=1}^{N} \left\langle \Psi_i \left| -\frac{1}{2}\nabla^2 \right| \Psi_i \right\rangle \tag{2.24}$$

The kinetic energy of the independent electrons in their ground state (i.e. electrons without mutual Coulomb repulsion), under the action of an external potential such that their ground state density is $n(r)$ is given by the equation above. Now the universal functional can now be restructured as

$$\begin{aligned} F_{HK}[n] &= T[n] + V_{ee}[n] \\ &= T_s[n] + J[n] + \left(T[n] - T_s[n] + V_{ee}[n] - J[n]\right) \\ &= T_s[n] + J[n] + E_{xc}[n] \end{aligned} \tag{2.25}$$

Where $J[n]$ is the classical Coulomb interaction energy.

$$J[n] = \frac{1}{2}\int \frac{n(r)n(r')}{\left|r - r'\right|} dr dr' \tag{2.26}$$

While the defined quantity

$$E_{xc}[n] \equiv T[n] - T_s[n] + V_{ee}[n] - J[n] \tag{2.27}$$

is called the exchange-correlation energy. It is to be noted that $T_s[n]$ here is not the true kinetic energy of the interacting system whose ground state density is $n(r)$, but is in fact much closer to the kinetic energy $T[n]$, in the final optimized description, than it is to the Thomas-Fermi kinetic energy. There are two parts of contributions to the exchange correlation energy $E_{xc}[n]$: one is from the non-classical effects of the electron-electron interactions and the other is from the kinetic energy. The Euler equation now becomes

$$\mu = v_{eff}(r) + \frac{\delta T_s[n]}{\delta n(r)} \tag{2.28}$$

where the Kohn-Sham effective potential is defined by

$$v_{eff}(r) = v(r) + \frac{\delta J[n]}{\delta n(r)} + \frac{\delta E_{xc}[n]}{\delta n(r)} \tag{2.29}$$

$$= v(r) + \int \frac{n(r')}{|r - r'|} dr' + v_{xc}(r)$$

Which the exchange-correlation potential

$$v_{xc}(r) = \frac{\delta E_{xc}[n]}{\delta n(r)} \tag{2.30}$$

As seen in Figure 2.1, the Kohn-Sham computational scheme for DFT is shown as a flowchart. The effective potential v_{eff} as we see from equation (2.29) is also a functional of the electron density, such that equations (2.22) to (2.30) have to be solved self-consistently. To start with a guessed density $n_0(r)$ is assumed which is usually constructed from the atomic wave functions. Then the effective potential v_{eff} is calculated through equation (2.29) and is used in equation (2.22) to solve the single-electron Schrödinger equation. Using equation (2.23), a new electron

density $n(r)$ can be formed (2.23). The total energy from equations (2.14, 2.24 to 2.27), can be computed once the convergent requirement is achieved.

The single Euler equation (2.22) includes a more general local effective potential incorporating the exchange and correlation interactions between electrons but has the same form as the Hartree equation. Therefore, to solve the Hartree equations the computational efforts would be the same as required to solve the Kohn-Sham equations and significantly less than to solve the Hartree-Fock equations. In principle, the exact ground state properties are given by Kohn-Sham equations provided the exact exchange correlation potential is given. However, methods to provide the explicit exchange and correlation functionals is not given by Kohn-Sham scheme and therefore, approximations need to be considered.

2.2 Exchange and Correlation Functionals

The exchange correlation functionals can be approximated in three distinct ways, according to DFT. They are the local density approximation (LDA), the generalized gradient approximation (GGA) and the hybrid approximation.

2.2.1. Local Density Approximation

Kohn and Sham proposed the local density approximation. They showed that it is possible to apply it to the limiting case of a slowly varying density [58].

$$E_{xc}^{LDA}[n] = \int n(r)\varepsilon_{xc}(n)dr \tag{2.31}$$

Where for a uniform electron gas of density $n(r)$, $\varepsilon_{xc}(n)$ is the exchange and correlation energy per particle. The local approximation to the Kohn-Sham exchange-correlation potential is given by the functional derivative of $E_{xc}^{LDA}[n]$.

$$v_{xc}^{LDA}(r) = \frac{\delta E_{xc}^{LDA}}{\delta n(r)} = \varepsilon_{xc}(n(r)) = n(r)\frac{\delta \varepsilon_{xc}(n)}{\delta n} \tag{2.32}$$

The Kohn-Sham equation becomes

$$\left[-\frac{1}{2}\nabla^2 + v(r) + \int \frac{n(r')}{|r-r'|}dr' + v_{xc}^{LDA}(r)\right]\Psi_1 = \varepsilon_i \Psi_i \tag{2.33}$$

$$\varepsilon_{xc}(n) = \varepsilon_x(n) + \varepsilon_c(n) \tag{2.34}$$

Where for a homogeneous electron gas $\varepsilon_x(n)$ is the exchange energy per particle.

$$\varepsilon_{xc}(n) = -\frac{3}{4}\left(\frac{3}{\pi}\right)^{1/3} n(r)^{1/3} = -\frac{0.4582}{r_s} \tag{2.35}$$

and for a homogenous electron gas, $\varepsilon_c(n)$ is the correlation energy per particle

$$\varepsilon_c(n) = \frac{1}{2}\left(\frac{g_0}{r_s} + \frac{g_1}{r_s^{3/2}} + \frac{g_2}{r_s^{2}} + ...\right) \qquad \text{for } r_s >> 1 \tag{2.36}$$

Here r_s is the Wigner-Seitz radius,

$$\frac{4}{3}\pi r_s^3 = \frac{1}{n} \tag{2.37}$$

By replacing the scalar external potential $v(r)$ by a spin dependent potential $v_{\alpha\beta}(r)$ and also replacing the charge density $n(r)$ by the density matrix $n_{\alpha\beta}(r)$ [51-53], the Kohn-Sham-LDA is further extended to the spin dependent case. The electron densities can be treated separately, with spin projection up $n_\alpha(r)$ and down $n_\beta(r)$. Similarly, one can deal with $n(r) = n_\alpha(r) + n_\beta(r)$, along with the polarization $\zeta(r) = \left[n_\alpha(r) - n_\beta(r)\right]/n(r)$. ζ takes values between -1 (fully polarized downwards) and +1 (fully polarized upwards). In a similar way it is possible to deal with $n(r)$ as well. The spin-up and spin-down Kohn-Sham wave functions generate the spin-up and spin-down densities. LDA for atomic and molecular systems with unpaired spins was improved by local spin density (LSD) approximation.

The knowledge of the uniform electron gas to predict properties of the in homogenous electron gases that occurs in atoms, molecules and solids can be used by LDA and its spin

generalization LSD. The success and importance of LDA and LSD computational schemes in can hardly be exaggerated as far as the solid state computations are concerned. Particularly, for most systems of interest, LSD usually has moderate accuracy. Errors of order 5-10% have been reported. It makes the same kind of mistake in every system it's applied to and hence in a way its reliable. The fact that the exchange-correlation hole $n_{xc}^{LDA}(r_1, r_2)$ is spherically symmetric and that it obeys the sum rule which corresponds to the fact that, if an electron has been found at r_1 , then there is one less electron left to find elsewhere (i.e , by integral over all r_2), can be majorly attributed to the success of LDA and LSD.

$$\int n_{xc}^{LDA}(r_1, r_2) dr_2 = -1 \tag{2.38}$$

Where the exchange-correlation hole $n_{xc}^{LDA}(r_1, r_2)$ is defined by

$$V_{ee} = \iint \frac{1}{r_{12}} n_2(r_1, r_2) dr_1 dr_2 = J[n] + \frac{1}{2} \iint \frac{1}{r_{12}} n(r_1) n_{xc}^{LDA}(r_1, r_2) dr_1 dr_2 \tag{2.39}$$

with $J[n]$ being the classical Coulomb interaction. This is true because for every r_1, $n_{xc}^{LDA}(r_1, r_2)$ is the exact exchange-correlation hole of a homogenous electron gas having a density $n(r_1)$. Hence, the total charge of $n_{xc}^{LDA}(r_1, r_2)$ is correctly described by LDA and LSD .

2.2.2. Generalized Gradient Approximation

The LDA formula for E_{xc} is formally justified for systems with slow varying densities, and hence it seems to be a logical extension seek gradient corrections to E_{xc}^{LDA} by the gradient expansion approximation (GGA), thereby expanding the functional in a Taylor series in gradients of the density [54],

$$E_{xc}^{GEA}[n_\alpha, n_\beta] = E_{xc}^{LSD}[n_\alpha, n_\beta] + \sum_{\alpha\beta} \int C_{\alpha\beta}(n_\alpha(r), n_\beta(r)) \frac{\nabla n_\alpha(r)}{n_\alpha^{2/3}} . \frac{\nabla n_\beta(r)}{n_\beta^{2/3}} d^3 r \tag{2.40}$$

However, for systems such as atom and molecule, GGA does not give better energy than LDA. The reasons are following: (1) GGA exchange-correlation hole at only short separations can improve the LDA hole. However, at large separations it is poorly damped and oscillatory. (2) The sum rule of the exchange-correlation hole is violated by GGA .That made it possible for Perdew to introduce the so-called generalized gradient approximation [55-60] which makes it possible for the exchange correlation energy which can now be written as a functional of both the density and its gradient:

$$E_{xc}^{GGA}[n_\alpha, n_\beta] = \int d^3 r f(n_\alpha(r), n_\beta(r), \nabla n_\alpha(r), \nabla n_\beta(r)) \quad (2.41)$$

The first modern GGA was that of Langreth and Mehl [87]. They were the first to propose the idea of truncating the gradient expansion for the exchange-correlation hole. Perdew *et al*. [59, 60] proposed several versions of GGA functional which removed some of the problems encountered by GGA. He introduced the real-space cutoff procedure on the hole thereby restoring the sum rule or the normalization and negativity conditions on the GGA hole and generating a short-ranged hole whose angular and system average was much closer to the true hole. No free parameters were incorporated by the Perdew-Wang 1991 (PW91) GGA functional [60]. It is also possible to entirely determine it from uniform electron gas properties .The Perdew-Burke-Ernzerhof [59] functional is a simplified and refined version of the PW91 functional. Becke [56]. The exchange functional known as B88 was derived which incorporated the known behavior of the exchange hole at large distances outside a finite system. The correlation energy as an explicit functional of the density was obtained by Lee, Yang and Parr [57] and it's gradient and Laplacian are now generally known as the "LYP" functional.

The well-known GGA functionals in some calculations, approach the accuracy of traditional quantum chemical (e.g. Configuration Interaction) methods, at much less computational cost. It also systematically improves the LDA. However, the quasilocal nature of GGA, fails to describe the dispersion or long-ranged van der Waals interaction arising from long-ranged correlated electronic density fluctuations in the weak bonding systems such as

noble gas dimmers. Neither LDA nor GGA can accurately describe. GGA, like LDA has the difficulty to describe the hole centered for from the electron causing the hole.

2.2.3. Hybrid Density Functional Method

Based on local or semi local nature of LDA and GGA, Becke proposed the so-called Hybrid Density Functional method incorporating the exact treatment of exchange by Hartree-Fock theory with DFT approximations for dynamical correlation. This idea was inspired by re-examination of the adiabatic connection,

$$H_\lambda = T + \lambda V_{ee} + \sum_i v_\lambda(r_i) \tag{2.42}$$

Where λ is an inter-electronic coupling-strength parameter that "switches on" the $1/r_{12}$ coulomb repulsion between electrons. $\lambda = 0$ corresponds to the non-interacting Kohn-Sham reference system, while $\lambda = 1$ corresponds to the fully interacting real system, with $n(r)$ being fixed as the exact ground state density of H_λ. The $E_{xc}[n]$ can be written as

$$E_{xc}[n] = \int_0^1 d\lambda U_{xc}^{\lambda}[n] \tag{2.43}$$

where,

$$U_{xc}^{\lambda}[n] = \left\langle \Psi_n^{\lambda} \mid V_{ee} \mid \Psi_n^{\lambda} \right\rangle - J[n] \tag{2.44}$$

The obvious first approximation for the λ dependence of the integrated in equation (2.43) is a linear interpolation, resulting in the Becke's half-and-half functional:

$$E_{xc}^{h\&h}[n] = \frac{1}{2}\left(U_{xc}^{0} + U_{xc}^{1}\right) \tag{2.45}$$

Where U_{xc}^{o} is the exact exchange energy of the KS determinant. U_{xc}^{1} represents the potential energy contribution to the exchange-correlation energy of the fully interacting system. This half and half functional has the potential of having a finite slope as $\lambda \to 0$. It becomes exact if

$E_{xc,\lambda=1}^{DFT}$ is exact and when the system has high density. However, a good quality of the total energy is not provided by it and the uniform gas limit is not obtained. Based on the above facts, Becke proposed the semi-empirical generalization of 3-parameter hybrid exchange-correlation functional

$$E_{xc}^{B3} = E_{xc}^{LSDA} + a_o(E_x^{exact} - E_x^{LSDA}) + a_x \Delta E_x^{GGA} + a_c \Delta E_c^{GGA} \quad (2.46)$$

Where, a_o, a_x and a_c are semiempirical coefficients an appropriate fit to experimental data helps to determine them. E_x^{exact} represents the exchange energy of the Slater determinant of the Kohn-Sham orbitals. ΔE_c^{GGA} represents the gradient correction for the correlation and ΔE_x^{GGA} represents the gradient correction for the exchange and.

Both methods based on Hartree-Fock (HF) theory and density functional theory (DFT) have their advantages and disadvantages.[36-39,61] For example, DFT within the local spin density approximation (LSDA) calculations underestimate the band gaps of semiconductors. The discontinuity of exchange-correlation Kohn-Sham potential results in this discrepancy between theoretical and experimental band gaps. [62, 63] On the other hand, hybrid density functional theory incorporating HF exchange with DFT exchange-correlation has proved to be an efficient method for many systems. It has been recently verified that hybrid functionals can reproduce the band gaps of semiconductors and insulators quite well. [64, 65] In particular, screened hybrid functionals can accurately reproduce band gaps in carbon based materials. [66-69]

2.3 Computational Method

In this work, we have opted to use hybrid density functional theory and compare the results using pure density functional theory for initial outer wall hydrogen molecular adsorption in (9, 9) armchair nanotube. That is because the primary objective of the (9, 9) outer wall adsorption study had been to compare out results with those made by Mpourmpakis *et. al.* [34]

Later calculations involving hydrogen molecular adsorption and co-adsorption for armchair structures ranging from (3, 3) to (6, 6) have been performed using hybrid density functional theory for a detailed step by step investigation of SiC nanotubes. In particular, we have used the B3LYP [56, 57] hybrid functional and the PW91, [70] pure density functional as implemented in the Gaussian 03 suite of programs [71] The dangling bonds have been terminated by hydrogen atoms to simulate the effect of infinite nanotubes.

2.3.1 Dimer Calculations

Using the B3LYP method, the ionization potential and electron affinity of the Si atom are 8.14eV and 0.80eV, to be compared with the experimental values of 8.15eV and 1.39eV, respectively. For C atom, our theoretically computed values are 11.44eV and 0.37eV, and the experimental values are 11.26eV and 1.2eV, respectively. In case of SiC dimer, our values for the theoretical ionization potential and electron affinity are 8.86eV and 1.79eV, to be compared with the experimental values of 9.29eV and 3.8eV, respectively. The calculated bond length of the SiC dimer is 1.72 Å and the corresponding experimental value is 1.89 Å. For PW91, the ionization potential and electron affinity for Si atom are 8.25eV and 0.98eV, respectively. For C atom, our theoretically computed, corresponding values are 11.48eV and 0.21eV. In the case of the SiC dimer, our values for the theoretical ionization potential and electron affinity are 8.92eV and 1.92eV. The calculated bond length of the SiC dimer is 1.74 Å. Also for Si, C, H, SiC, SiH and CH dimers the B.E/atom values for B3LYP are 1.55eV, 3.08eV, 2.43eV, 2.15eV, 1.64eV and 1.83eV, respectively. The corresponding values using PW91 are 1.75eV, 3.45eV, 2.34eV, 2.41eV, 1.60eV and 1.53eV. The corresponding experimental values are 1.69eV, 3.15eV, 2.26eV, 2.34eV, 1.55eV and 1.75eV. Thus, the methods and the basis set used are deemed to be quite satisfactory.

2.3.2 Basis sets and functionals used for various calculations

The basis set chosen was 3-21G* where the exponents of the polarization functions were optimized to yield the energy minima at the experimental dimer bond lengths. The d

exponent for the C atom was found to be 0.91 and the p exponent for the H atom was 1.04 [Figure. 2.2-2.3]. The same basis set has been used consistently for all calculations. However the functional used in case of adsorption of the hydrogen molecule from outside the nanotube at various uniquely available sites in case of the (9, 9) armchair structures, is B3LYP and PW91. Manual optimization of the vertical distance of the hydrogen molecule has been carried out by optimizing the binding energy with the hydrogen molecule placed at different vertical distances from the adsorption sites. The results that are obtained using both B3LYP and PW91 functional are compared to determine how the sites stack up with respect to binding of the hydrogen molecule.

After optimization of the bare SiCNT armchair (9, 9) structure using 3-21G* basis set, for both B3LYP and PW91 methods, it is found that for SiCNT type 1 structures, more electronegative C atoms move outward and more electropositive Si atoms move inward resulting in two concentric cylinders [Figure. 2.4]. The tube diameter for type 1 optimized structure using B3LYP functional is 15.492 Å and the radial buckling in this case is 0.030 Å. Using the PW91 functional, the tube diameter for the type 1 optimized structure is 15.542 Å and the corresponding radial buckling is 0.035 Å. This results in stretching of the sp^3 hybridized Si-C bonds and thus, weakening the bonds in the process. For type 2 SiCNT, upon optimization of the bare SiCNT structures, using 3-21G* basis set, for both B3LYP and PW91 methods, the average radial distance of Si atoms were higher than that for C atoms [Figure. 2.4], because in those structures in addition to Si-C bonds there are Si-Si and C-C covalent type bonds as well. The tube diameter for type 2 structure is 15.942 Å using B3LYP functional and 15.993 Å using the PW91 functional. The corresponding radial buckling are 0.102 Å and 0.106 Å for B3LYP and PW91, respectively. In case of type 3 structures the tube diameter using the B3LYP method is 15.648 Å and 15.678 Å using the PW91 method. The corresponding radial buckling is 0.0025 Å, using the B3LYP method and 0.0027 Å, using the PW91 method. Thus, we find using both the B3LYP and PW91 methods, the type 3 structures become slightly C coated. However, the radial

buckling can be considered insignificant for type 3 structures optimized using both B3LYP and PW91 functional.

Now when the hydrogen molecule is absorbed from inside and outside the nanotube for all armchair structures ranging from (3, 3) to (6, 6) and for all three types, the bare nanotube structures are first optimized using B3LYP functional. The structures are optimized once again with the hydrogen molecule absorbed both from inside as well as outside the nanotube at various uniquely available sites and using the same functional.

In case of co-adsorption of hydrogen molecules at various uniquely available site arrangement for all armchair structures ranging from (3, 3) to (6, 6) and for all three types, with a hydrogen molecule already adsorbed at a particular site, the functional used is again B3LYP. All computations reported here have been performed using the supercomputing facilities at the University of Texas at Arlington.

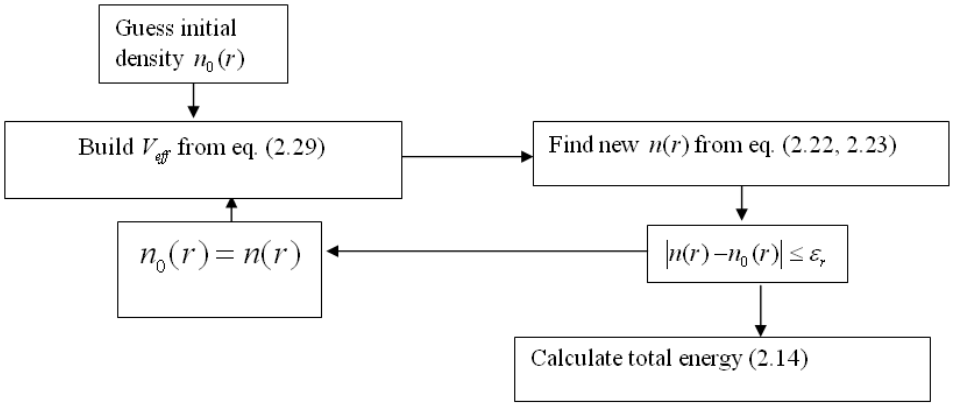

Figure 2.1 Flowchart for DFT calculations.

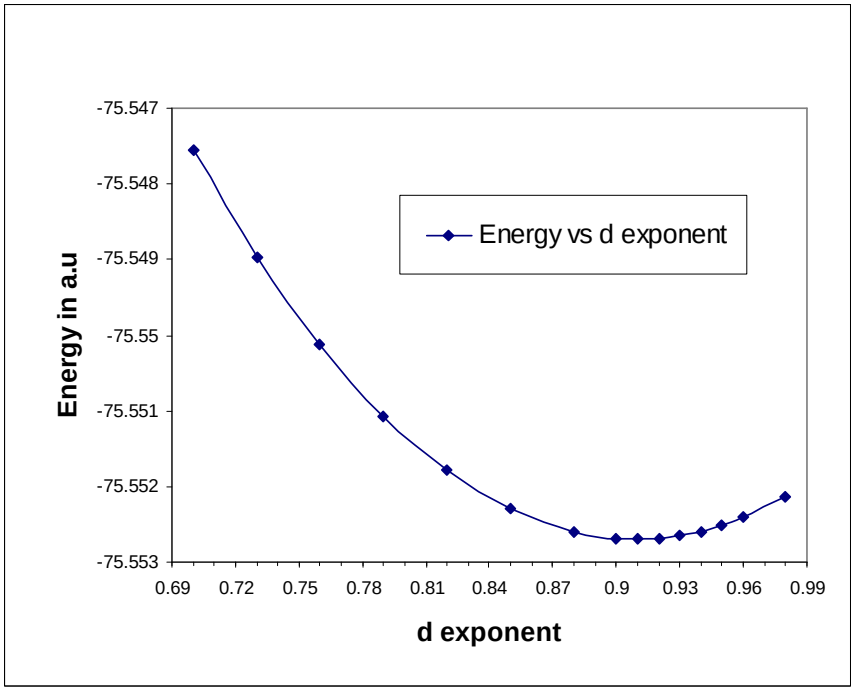

Figure 2.2: Ground state energy in a.u vs. d exponent for carbon dimer using 3-21G* basis set.

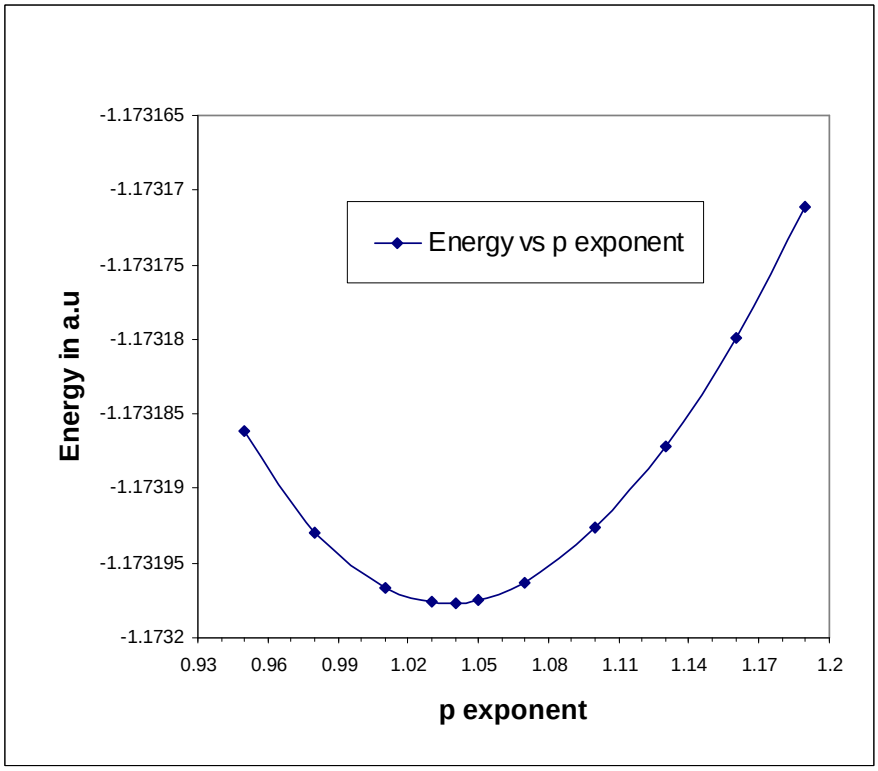

Figure 2.3: Ground state energy in a.u vs. p exponent for hydrogen dimer using 3-21G* basis set.

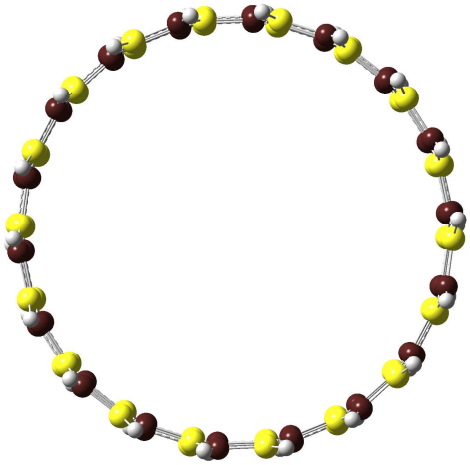

Type 1 SiCNT (9, 9)
Tube diameter = 15.492 Å
Radial buckling = 0.030 Å

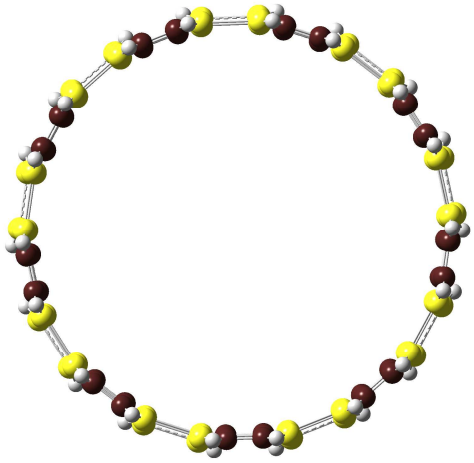

Type 2 SiCNT (9, 9)
Tube diameter = 15.942 Å
Radial buckling = 0.102 Å

Type 3 SiCNT (9, 9)
Tube diameter = 15.648 Å
Radial buckling = 0.0025 Å

Figure 2.4: Tube diameter and buckling. The carbon atoms are shown in brown and the silicon atoms are shown in yellow. All the above structures have been optimized using B3LYP method. In case of Type 1, the carbon atoms move outwards but for type 2, the silicon atoms move outwards. In case of type 3, the buckling is insignificant.

CHAPTER 3

MOLECULAR HYDROGEN ADSORPTION IN SIC NANOTUBES

3.1 Construction of different types of nanotubes

SiC nanotubes have been constructed using finite cluster-CNT based approach where a graphene-like sheet of Si and C are rolled to form a nanotube. The two sites of the two dimensional graphene-like sheet which are crystographically equivalent are connected and the rolling can be described in terms of a chiral vector C_h. This chiral vector is an integer multiple of the two basis vectors a_1 and a_2, which is $C_h = na_1 + ma_2$. It maps an atom from the left hand border onto an atom on the right border line. The chiral vector is thus determined from the integer pair (n, m) which also describes the geometry of any nanotube. In the case of an armchair nanotube n=m and the chiral angle is 30°. As has been mentioned before, armchair nanotubes having type 1 arrangement, there is no adjacent silicon and carbon atoms and are placed alternatively in each layer perpendicular to the tube axis. However the basic difference between type 2 and type 3 is the difference in relative spatial position of silicon and carbon atoms. In type 2 each silicon atom is surrounded by two carbon and a silicon atom and vice versa. Also each layer perpendicular to the nanotube axis has only silicon or carbon atoms. Thus along the nanotube axis there are alternate layers of silicon and carbon atoms. In type 3 as in case of type 2 each silicon atom is surrounded by two carbon and a silicon atom, and vice versa. However for each of the layers perpendicular to the nanotube axis, type 3 is very similar to type 1. The layers have no adjacent silicon or carbon atoms and are placed alternately. The relative positions of silicon and carbon atoms are shown in [Figure. 3.1].

3.2 Adsorption of hydrogen molecule in (9, 9) armchair nanotubes

Exohedral interactions of a hydrogen molecule with a (9, 9) armchair SiC nanotube has been considered. Of course, the molecule can also approach the nanotube wall from inside in a

direction such that the hydrogen molecular axis can make any angle between 0° and 90°. To start with, we have specifically studied the vertical approach of hydrogen molecule to the outer part of the tube wall. The binding energy (BE) is obtained by comparing the total energy of the spin-optimized composite system SiCNT+H2 with the total energies of the optimized separated systems, namely SiCNT and H2 with the 3-21G* basis set:

BE = E (SiCNT) + E (H2) – E (SiCNT+H2) (1)

For type 1, which has only one type of bond, we have five different sites available [Figure. 3.1]. In the first case, the hydrogen molecule approaches the nanotube vertically on top of the carbon atom. We call this site type 1 carbon top (T1CT). In the second case the hydrogen molecule approaches the silicon atom vertically. This site is called type 1 silicon top (T1SIT). The third site, called type 1 hollow site (T1HS), lies at the centre of the hexagon. The fourth site is the centre of the silicon and carbon bond. There are two such bond orientations available. One is the normal bond and the other the zigzag bond. The corresponding sites are type 1 carbon silicon normal bridge (T1CSINB) and the Type 1 carbon silicon zigzag bridge (T1CSIZB). The graphs in [Figure. 3.2] show the BE of the hydrogen molecule as a function of the distance of the nearest hydrogen atom, of the approaching hydrogen molecule, from the tube wall, using both B3LYP and PW91 for all sites. [Table 3.1] shows the BE versus the distance of the nearest hydrogen atom, of the approaching hydrogen molecule, and the optimized values of both quantities using both the B3LYP and the PW91 functionals. For type 1 structure using B3LYP method, the order of the binding energies is as follows:

BE (T1CSINB) > BE (T1CSIZB) > BE (T1HS) > BE (T1CT) > BE (T1SIT). (2)

The minimum value of the binding energy obtained in this case is 0.044 kcal/mol and the maximum value obtained is 0.277 kcal/mol. There is significantly less dispersion in the values of the optimized distances, either 3.5 Å or 3.3 Å. The SiH bond has the lowest binding energy amongst the three bonds SiH, CH and SiC, the corresponding values being 1.64eV, 1.83eV and 1.93eV, respectively. We believe that this contributes to the low BE for T1SIT site. Also our

analysis shows that the HOMO contribution of C-Si normal bridge bond site is higher than that of other sites. This explains why the T1CSINB site is the most preferred site [Figure. 3.5].

For the type 1 structure using PW91 functional, the BE is significantly higher, as expected, for all sites, from 0.701 kcal/mol to 1.134 kcal/mol and the hydrogen molecular distances are either 2.9 Å or 3.1 Å. Thus, the choice of the functional has lower effect on the adsorption geometry than on the adsorption energy. The ordering of the binding energies is as follows:

BE (T1CT) > BE (T1CSINB) > BE (T1CSIZB)> BE (T1HS) > BE (T1SIT) (3)

Thus, from our study we can say that there are more preferred bonding sites compared to T1HS which is different from the conclusions reported by Mpourmpakis *et al*. [34]. We also note that for B3LYP functional, as the BE increases the distance of the hydrogen molecule from the nanotube decreases. For T1CSINB which has the highest BE, this distance is 3.3 Å and 3.5 Å in case of T1SIT which has the lowest BE. However, this conclusion does not hold true for the PW91 functional.

For type 2, there are seven different bonding sites available and three different types of bonds, namely C-C, Si-Si and Si-C. First two sites in type 2, carbon top (T2CT) and silicon top (T2SIT) are similar to T1CT and T1SIT. Taking the hydrogen adsorption site at the middle of the three different types of bonds, the next three different sites are carbon silicon bridge (T2CSIB), silicon silicon bridge (T2SISIB) and the carbon carbon bridge (T2CCB). Two different hollow sites are type 2 first hollow site (T2H1S) and type 2 second hollow site (T2H2S). The adsorption energy obtained for different sites using the B3LYP method is of the following order [Table 3.2]:

BE (T2CCB) > BE (T2CT) > BE (T2H2S) > BE (T2SISIB) > BE (T2CSIB) > BE (T2SIT) >
BE (T2H1S) (4)

Thus, T2H1S has the lowest BE (0.079 kcal/mol) with the BE for the T2H2S (0.263 kcal/mol) being higher compared to that of T2H1S. In case of T2H1S the atoms of the hexagon are compactly arranged as compared to T2H2S causing possible electron-electron repulsion to occur [Figure. 3.1]. In case of T2H2S the atoms are spaced apart further. Hence the electron-

electron repulsion may be less in this case. The BE of T2SIT is 0.143 kcal/mol. The low BE of silicon top site may be attributed to the low binding energy of Si-H bond. The BE of T2CCB is highest. The difference in enthalpies between sp^2 and sp^3 lattices in case of carbon is small. This allows carbon to shift between sp^2 and sp^3 hybridized states easily. When a hydrogen molecule approaches the centre of the bond the carbon atoms have a tendency to form a sp^3 hybridized bond with hydrogen molecule while other bonds, like Si-Si which are already sp^3 hybridized may fail to do so. This possibly contributes to the T2CCB and the T2CT sites as the more preferred hydrogen adsorption sites, with adsorption energies of 0.303 kcal/mol and 0.284 kcal/mol, respectively, as compared to the other sites. This is also evident from the HOMO plots where the HOMO contribution of C atoms is bound to be significantly more than that of Si atoms [Figure. 3.5]. The distance of the hydrogen molecule from the nanotube for the most preferred site T2CCB is found to be 3.1 Å. The binding energies obtained for different sites using PW91 method is of the following order:

BE (T2H2S) > BE (T2CT) > BE (T2CSIB) > BE (T2SISIB) > BE (T2CCB) > BE (T2SIT) > BE (T2H1S) (5)

T2H1S has the lowest BE (1.206 kcal/mol), with the BE of T2H2S being the highest, 1.423 kcal/mol. The BE of T2SIT is 1.241 kcal/mol. The low BE of silicon top sites may again be attributed to the low binding energy of Si-H bond. The BE of T2SISIB and T2CCB is almost the same, being 1.283 kcal/mol and 1.276 kcal/mol, with the BE of T2CSIB being 1.340 kcal/mol.

For type 3, we have three different types of bonds as in the case of type 2 [Figure. 3.1]. They are C-C, C-Si, and Si-Si. In addition to that, two different types of C-Si bonds, one normal to the tube axis and one in the zigzag direction, exist. Also there is only one hollow site possible since the hexagons in the structure are all similar. Consequently, the seven different sites are type 3 carbon top (T3CT), silicon top (T3SIT), carbon silicon zigzag bridge (T3CSIZB), carbon silicon normal bridge (T3CSINB), carbon carbon bridge (T3CCB), silicon silicon bridge

(T3SISIB) and the hollow site (T3HS). The binding energies using B3LYP method is of the following order [Table 3.3].

BE (T3CCB) > BE (T3CT) > BE (T3CSIZB) > BE (T3CSINB) > BE (T3SISIB) > BE (T3HS) > BE (T3SIT) (6)

The most preferred site is T3CCB. The possible explanation behind the BE of T3CCB being more than that of other adsorption sites is the sp^3 hybridization factor as explained in type 2 before. The same kind of explanation holds for the carbon-top site. Significantly the BE of carbon-carbon bridge site for both type 2 as well as type 3 using the B3LYP method is same, which is equal to 0.303 kcal/mol.

Similarly the binding energies using PW91 method is of the following order:

BE (T3CCB) > BE (T3CT) > BE (T3CSIZB) > BE (T3SISISB) > BE (T3SIT) > BE (T3HS) > BE (T3CSINB) (7)

Here also the T3CCB site is the most preferred site followed by T3CT. Amongst all sites, where binding of hydrogen molecule has been studied using B3LYP method, the T2CCB or T3CCB site has been found to be the best. We specifically comment on the T2CCB site. The Mulliken charge analysis for the bare type 2 SiCNT nanotube using B3LYP method gives the average Mulliken charge for carbon as -0.531 e, average Mulliken charge for hydrogen as 0.037 e and the average Mulliken charge for silicon as 0.494 e. The overall charge distribution has been shown in [Figure. 3.6]. When the hydrogen molecule is placed vertically on top of the T2CCB site at 3.1 Å, which is the optimized distance, the corresponding average Mulliken charges for carbon is -0.529 e, 0.034 e for hydrogen atoms and 0.495 e for silicon atoms. The approaching hydrogen molecule, has zero charge on each of the hydrogen atoms initially, but gets polarized as it approaches this site. At the optimized distance, the hydrogen atom, in the approaching hydrogen molecule, which is closest to the nanotube wall has a Mulliken charge of 0.014 e, while the other hydrogen atom, in the approaching hydrogen molecule, which is farthest from the nanotube wall has a Mulliken charge of -0.016 e. This has been shown in

[Figure. 3.8]. Similarly for all possible sites, where binding of hydrogen molecule has been studied using PW91 method, the T2H2S site has been found to be the best. The Mulliken charge analysis for the bare type 2 SiCNT nanotube, using PW91 method, gives the average Mulliken charge for carbon as -0.530 e, average Mulliken charge for hydrogen as 0.060 e and the average Mulliken charge for silicon as 0.470 e. The overall charge distribution has been shown in [Figure. 3.6]. When the hydrogen molecule is placed vertically on top of the T2H2S site at 2.7 Å, which is the optimized distance, the corresponding average Mulliken charge for carbon atoms is -0.527 e, 0.056 e for hydrogen atoms and 0.471 e for Si atoms. The approaching hydrogen molecule, has zero charge on each of the hydrogen atoms initially, but gets polarized as it approaches the site. At the optimized distance, the hydrogen atom which is closest to the nanotube wall has a Mulliken charge of 0.015 e, while the hydrogen atom in the approaching hydrogen molecule which is farthest from the nanotube wall has a Mulliken charge of -0.010 e. This has been shown in [Figure. 3.8]. The BE obtained for different sites in SiCNT is not significantly high. However certain superior properties of SiCNT like high reactivity of exterior surface and stability at high temperature allows SiCNT nanotubes to possess certain advantage over other nanotubes. This makes possible the use of SiCNT nanotubes as a storage medium under harsh environmental conditions [72].

3.3 Outer and Inner wall adsorption of hydrogen molecule in armchair nanotubes

To study the hydrogen molecular interaction, with the hydrogen molecule adsorbed from inside the nanotube and compare with the outside adsorption, we have chosen nanotubes ranging from (3, 3) to (6, 6) for all the three armchair types and all possible sites in each of these nanotube structures. Studies done before on armchair SiC nanotubes ranging from (3, 3) to (11, 11) have indicated that there beyond (6, 6) the binding energy of the nanotubes saturates. [33] Hence, we have chosen nanotubes ranging from (3, 3) to (6, 6) armchair configuration, thereby chosen a shorter diameter to study the adsorption of the hydrogen molecule from inside the nanotube in more details. In this study, a hydrogen molecule is placed

at different sites in three different types of nanotubes. The hydrogen molecule is made to approach the tubes at various sites both from inside as well as from outer wall of the nanotube. Our aim is to explore the binding energies of hydrogen molecule for the various sites. As a precursor to the current work, we have studied hydrogen molecule adsorption on the outside, on a SiC (9, 9) nanotube [73]. In this paper, as mentioned before, we have carried out a more detailed study on all available sites from (3, 3) to (6, 6) structures, for hydrogen molecule adsorption, both from inside and outside the nanotube. The various sites in different types of nanotubes and the relative arrangement of silicon and carbon atoms, for all three types have been shown [Figure. 3.1]. In the case of type 1 nanotube, having only Si-C bonds, silicon and carbon atoms are placed alternatively without any adjacent Si or C atoms. In type 2 and type 3 nanotube structure having Si-C, Si-Si, and C-C bonds, the nearest neighbors of each Si atom consist of two C atoms and another Si atom and vice versa. The difference between type 2 and type 3 structures lies in the relative spatial positions of the Si and C atoms. If we consider one layer perpendicular to the tube axis, in type 3, Si and C atoms are alternately arranged, while in type 2 each layer contains either Si or C atoms. Type 1 has five different adsorption sites and types 2 and 3 nanotubes have seven different adsorption sites each.

For each of the structures, there are three major adsorption sites: top, bridge, and hollow. T1CT for type one, T2CT for type 2 and T3CT for type 3 are C top adsorption sites directly perpendicular to the tube wall along the C atoms. Similarly, T1SIT, T2SIT and T3SIT are Si top adsorption sites directly perpendicular to the tube wall along the Si atoms, for three different types, type 1, type 2 and type 3 respectively. Also there are two major bridge sites named as normal and zigzag bridge. The relative orientation of these bridge sites with respect to the tube axis is clearly visible in [Figure. 3.1]. These two bridge sites are named according to their adjacent atoms. Hollow sites are located at the middle of the hexagons. In types 1 and 3 there is only one type of hexagon present and hence there is only one hollow site. In type 2, two different hexagons are present and this gives rise to two different hollow sites, T2H1S and

T2H2S. T2H1S is associated with the hexagon containing four C and two Si atoms, whereas T2H2S is positioned along the center perpendicular to hexagon containing two C and four Si atoms.

The binding energy (B.E) for the adsorbed hydrogen molecule, approaching the tube wall from either inside or outside the tube is obtained from the expression below.

Binding energy= E (SiCNT) + E (H2) - E (H2+SiCNT) (1)

Where, E (SiCNT) and E (H2) are the ground state energies of the bare nanotube and the hydrogen molecule respectively. E (H2 + SiCNT) represent the ground state energy of the hydrogen molecule, adsorbed in SiCNT. [Table 3.5] shows the binding energies of the hydrogen molecule adsorbed inside the nanotubes for type 1, the distance of the adsorbed hydrogen molecule from the nanotube wall, distance of the molecule from nearest C and Si atoms, the bond length of the adsorbed hydrogen molecule and the Mulliken charge of the hydrogen atom, belonging to the adsorbed molecule. Similar information with regards to the adsorption of the hydrogen molecule on the outer wall of type 1 nanotubes has been shown in [Table 3.6]. From the data, it is quite noticeable, that there is a slight difference between the distances of hydrogen molecule from the tube wall and the corresponding distances of the molecule from the nearest carbon atom for carbon top sites. Similarly there is a difference when compared with the distance of the molecule from the nearest silicon atom in case of silicon top site. This is due to the difference in electro negativities of the C and Si atoms. In case of Type 1 nanotubes, the best adsorption binding energy is obtained for (5, 5) structures, for hydrogen molecular adsorption, both for inside adsorption as well as for adsorption on the outer wall of the nanotube. The most favorable site for both inside and outer wall adsorption in case of type 1 (5, 5) tubes, is found to be TICT site, having an adsorption binding energy of 0.52 kcal/mol and 1.11 kcal/mol for inside and outer wall adsorption respectively. From the Mulliken charge analysis, it is found, that the charge transfer between hydrogen atoms, belonging to the adsorbed hydrogen molecule, is slightly higher, in case of the hydrogen molecule approaching

the tube from the outer wall, as compared to the molecule approaching the tube wall from inside [Figure. 3.9 - 3.10]. It is 0.011e, in case of adsorption from outside as compared to 0.008e, in case of adsorption from inside. In both cases, the charge transfer from the nanotube mostly occurs from the carbon atom of the T1CT site, which is also the C atom closest to the approaching hydrogen molecule. In case of outside adsorption, the Mulliken charge of the closest carbon atom is 0.944e and 0.941e, in case of inside adsorption. In both cases, the carbon atom is loosing charge and the hydrogen atom of the approaching hydrogen molecule is gaining charge. The Mulliken charge of the hydrogen atom, belonging to the adsorbed hydrogen molecule closest to the tube wall, has been analyzed for various sites and structures. In all cases the approaching hydrogen atom is gaining charge. However, no trend between amount of charge transfer and adsorption energy of the site has been found here, suggesting that the local structure as a whole determines the amount of charge transfer as well as the binding strength of the adsorbent. Type 1 (3, 3) and (4, 4) structures have been found not to display any binding for any of the sites when the hydrogen molecule approaches the various sites from inside. For type 1 (5, 5) structures, only T1CT and T1CSINB site show binding, when the hydrogen molecule approaches the nanotube wall from inside. For other sites in type 1 (5, 5) structures, in case of hydrogen molecular adsorption from inside, the hydrogen molecule does not bind at all and in case of type 1 (6, 6) only the T1HS site is found to display binding. The interaction is however weak and a binding energy of only 0.02 kcal/mol is observed. In case of the hydrogen molecule approaching the type 1 nanotube structures from the outer wall, all structures from (3, 3) to (6, 6) binds the incoming hydrogen molecule. However only 2 sites in (3, 3),5 sites in (4, 4),3 sites in (5, 5) and 4 sites in (6, 6) show binding with the hydrogen molecule during outer wall adsorption. The total electron charge density plot for type 1 (5, 5) TICT site and type 1 (5, 5) T1CSINB site, when the hydrogen molecule has been adsorbed from inside has been shown [Figure. 3.11]. We note that in case of type 1 (5, 5), TICT site, there is significant overlap between the charge of the hydrogen molecule and the SiCNT, as compared to type 1 (5, 5)

T1CSINB site, during inside adsorption. Similarly in case of hydrogen molecule adsorbed from the outer wall of the nanotube, the charge overlap of the hydrogen molecule with SICNT is significant in case of type 1 (5, 5) T1CT as compared to type 1 (5, 5) T1CSIZB site. The electron charge density plot has a strong relationship to binding energy values in all cases. The binding energy value when the hydrogen molecule is adsorbed from outside the nanotube has been found to be significantly more as compared to when adsorption takes place from inside the nanotube. The reason being, due to buckling, the bonds in these structures stretch outwardly and may facilitate strong binding. From the values of binding energy in case of type 1 structures, we find that the adsorption of the hydrogen molecule is mostly physosorption in nature. This is substantiated from the PDOS plot, plotted using GaussSum [74] of type 1 (5, 5) T1CT site, where the hydrogen molecular adsorption is taking place from outside the nanotube. The plot shows that binding energy just below E_F has no major contribution from hydrogen s orbitals [Figure. 3.12]. All these point out to a pure physosorption taking place. However, it is worth noting that for both inside and outside adsorption, the T1CT site is most preferable and is always more preferable than the T1SIT site. Using the DMol3 suite of software, for Ti adsorption on type 1 (5, 5) SiCNT, Meng *et al*. [75] found the most favorable site to be the C top site. The reason behind it is that, the binding energy/atom of the C-H bond, according to our dimmer calculations is 1.83eV while the binding energy/atom of the Si-H bond is 1.64eV. The HOMO plots for type 1 (5, 5) bare SiCNT and the type 1 (5, 5) TICT site for both inside and outside adsorption of the hydrogen molecule have been shown [Figure. 3.13]. In all cases it has been found that the delocalization of the HOMO initially present in the bare nanotube remains unchanged after the adsorption. This is due to the bonding being physosorption in nature. For all the four structures studied in type 1, for outer wall interactions of the hydrogen molecule, the average binding energy, which is the binding energy of different sites averaged out for any particular structure, increases from (3, 3) to (5, 5) and decreases thereafter [Figure. 3.14].

Though type 1 bare nanotubes were found to be most stable [33], we note from [Table. 3.5-3.10] that type 2 tubes have the strongest interactions with hydrogen molecules followed by type 3 and then type 1, both for adsorption from inside and outside the nanotube. The type 2 (4, 4) structure in particular shows a very strong interaction with the hydrogen molecule, both when the molecule is placed inside and outside the nanotube. When the hydrogen molecule is placed inside the nanotube at T2CCB site, a high adsorption binding energy of 29.50 kcal/mol is obtained. This is the only site where chemisorption takes place, in the case of hydrogen adsorption from inside the nanotube. Adsorption in all other sites is physosorption in nature. From the Mulliken charge analysis it can be seen that type 2 (4, 4) T2CCB structure is highly charge symmetric [Figure. 3.15]. Usually for all other sites in various structures, one of the atoms in the adsorbed hydrogen molecule gains charge, while the other one looses charge. Here both the hydrogen atoms gain an equal charge of 0.004e. In the optimized structure, the hydrogen molecule is found to be at the centre of nanotube, with both the atoms at equal distance from the opposite walls of the nanotube. The geometrical symmetry of the final optimized structure as well as the charge symmetry may be responsible for the high adsorption binding energy, in this case. For outside adsorption of the hydrogen molecule for type 2 (4,4) T2CT site, the Mulliken charge analysis shows strong charge transfer from neighboring carbon and silicon atoms where the adsorption takes place. While comparing with the bare nanotube, this becomes quite evident [Figure. 3.16]. Also, from the electron charge density plots, we find that there is considerable charge overlap between the hydrogen molecule and the bare SiCNT, when the hydrogen molecule is adsorbed from inside at T2CCB site [Figure. 3.17]. In this case, the charge overlap is quite prominent visually and can be seen to take up the whole space inside the nanotube. Similar plot for the T2CSIB site, showing interaction of the hydrogen molecule with bare nanotube shows considerably free space inside the nanotube. This site has a binding energy of 0.36 kcal/mol compared to 29.50 kcal/mol for the T2CCB site. The HOMO plots for type 2 (4, 4) bare SiCNT, the type 2 (4, 4) T2CCB site with hydrogen molecule

adsorbed inside and T2CT site with hydrogen molecule adsorbed from outside the nanotube have been shown [Figure. 3.18]. In case of type 2 (4, 4) T2CCB site, the HOMO moves from one of the ends of the nanotube, the end where the molecule is placed and gets localized at the centre. The other end remains unaffected. In case of type 2 (4, 4) T2CT site, the HOMO delocalization initially present in the bare nanotube remains unchanged after the adsorption. From the electron charge density plot for the type 2 (4,4) T2CT site, with the hydrogen molecule adsorbed from outside the nanotube, considerable charge overlap is observed as compared to its type 2 (4,4) T2CSIB site, where the molecular adsorption is from the outer wall [Figure. 3.17]. Clearly, most of the sites in type 2 (4, 4) show strong chemisorption, during outer wall interaction with the hydrogen molecule. In this case, the T2CT site is the most preferred site having a binding energy of 37.52 kcal/mol. The PDOS plot for this site also shows strong contribution from the s orbital of the adsorbed hydrogen molecule and the p orbital of the C atom on which it is adsorbed [Figure. 3.19]. This justifies the high binding energy for this site. The average binding energy for outside interaction shows a steep increase from type 2 (3, 3) to type 2 (4, 4) and a steep fall thereafter [Figure. 3.20]. Type 2 (3, 3) has an average binding energy of 0.26 kcal/mol while type 2 (4, 4) has an average binding energy of 27.09 kcal/mol. In case of type 2 (5, 5), two sites T2CCB and T2H1S show very strong interaction with the hydrogen molecule adsorbed from outside the nanotube. T2CCB has a binding energy of 15.20 kcal/mol and T2H1S has a binding energy of 13.95 kcal/mol. For type 2 (5, 5) structure, the hydrogen storage capacity has been calculated to be 7.45%. Hence by reducing the diameter of the nanotube, and modifying the atomic configuration, it is possible to obtain the desired storage weight percentage.

In case of type 3 structures, for adsorption of the hydrogen molecule from inside the nanotube, it has been found, that the (3, 3) structure shows strong binding. We have compared the geometry of the type 3 (3,3) optimized structure, with the hydrogen molecule placed inside the tube, at the most preferred sites in that structure, to the bare SiCNT [Figure. 3.21]. It has been

found that the introduction of the hydrogen molecule changes the geometry of the bare SiCNT structure and makes it tapered towards the end, closer to the adsorbed molecule. The change in geometry can also be observed from the Mulliken charge analysis plot [Figure. 3.22]. From the Mulliken charge analysis plot, it has been found that there is a considerable change in the charges of the carbon and silicon atoms closest to the hydrogen molecule. The bare SiCNT has -0.551e as the partial charge on the carbon atom closest to the hydrogen molecule and the neighboring silicon atom has a partial charge of 0.535e. The carbon atom is loosing charge and the silicon atom is gaining charge. After the introduction of the hydrogen molecule, the corresponding carbon atom gain charge and has a partial charge of -0.493e and the corresponding silicon atom loose charge and has a partial charge of 0.432e. Same is observed for other sites in type 3 (3, 3), inside molecular adsorption, as well. For other type 3 structures like (4, 4) and (5, 5), most of the sites do not display any binding with the hydrogen molecule, when the hydrogen molecule is adsorbed from inside. Also a site where interaction does occur, the binding is extremely weak. However type 3 (6, 6) shows binding with the hydrogen molecule, inside the nanotube for all available sites. The interaction is however weak and the structure as a whole determines the binding energy. In case of type 3, when the hydrogen molecule is adsorbed from outside, the (6, 6) structure has the maximum number of sites where adsorption takes place. For type 3 structures, when the hydrogen molecule is adsorbed from outside the nanotube, the average binding energy increases with diameter from (4, 4) to (6,6). For (4, 4) structures the average binding energy is 0.32 kcal/mol and for (6, 6) structures the binding energy is 0.72 kcal/mol. From the Mulliken charge analysis of type 3 (6, 6), T3CSINB site, which is the most preferred adsorption site for outside adsorption, it has been found that no considerable change occurs in the values of the partial charges of the atoms neighboring the site [Figure. 3.23]. This is also evident from the electron charge density plots, where the charge overlap for both type 3 (6, 6), T3CSINB and T3SIT sites is minimal, with the hydrogen molecule adsorbed from outside. The electron charge density plot, in case of the hydrogen molecule

adsorbed from inside the nanotube, for both type 3 (3,3) T3CSIZB and T3CSINB sites, has been found to display considerable charge overlap [Figure. 3.24]. The HOMO plots for the above sites show no major change from bare SiCNT due to the hydrogen molecular adsorption [Figure. 3.25]. The PDOS plot for type 3 (6,6) T3CSINB site, with the hydrogen molecule adsorbed from outside shows that at E_F the contribution from p orbital of carbon and p orbital of silicon is significant [Figure. 3.26]. However the contribution from the s orbital of hydrogen is minimal, thereby indicating a physosorption.

Table 3.1 BE in kcal/mol for different sites in type 1 (9, 9) armchair nanotube, outside adsorption and the corresponding optimized vertical distance in Å of the hydrogen molecule from the nanotube wall.

Site Name	BE (B3LYP)	BE (PW91)	D (B3LYP)	D (PW91)
T1CT	0.059	1.134	3.5	3.1
T1SIT	0.044	0.701	3.5	3.1
T1HS	0.068	0.800	3.3	2.9
T1CSINB	0.277	0.970	3.3	2.9
T1CSIZB	0.115	0.962	3.3	2.9

Table 3.2 BE in kcal/mol for different sites in type 2 (9, 9) armchair nanotube, outside adsorption and the corresponding optimized vertical distance in Á of the hydrogen molecule from the nanotube wall.

Site Name	BE (B3LYP)	BE (PW91)	D (B3LYP)	D (PW91)
T2CT	0.284	1.354	3.1	2.9
T2SIT	0.143	1.241	3.3	3.1
T2CSIB	0.196	1.340	3.3	2.9
T2SISIB	0.207	1.283	3.5	3.1
T2CCB	0.303	1.276	3.1	3.1
T2H1S	0.079	1.206	3.3	3.1
T2H2S	0.263	1.423	3.1	2.7

Table 3.3 BE in kcal/mol for different sites in type 3 (9, 9) armchair nanotube, outside adsorption and the corresponding optimized vertical distance in Á of the hydrogen molecule from the nanotube wall.

Site Name	BE (B3LYP)	BE (PW91)	D (B3LYP)	D (PW91)
T3CT	0.257	1.193	3.1	2.9
T3SIT	0.052	1.109	3.5	3.1
T3CSIZB	0.159	1.190	3.3	2.9
T3CSINB	0.124	1.102	3.3	3.1
T3CCB	0.303	1.265	3.1	2.9
T3SISIB	0.117	1.164	3.3	3.1
T3HS	0.084	1.103	3.5	3.1

Table 3.4 Different nanotube structures from (3, 3) to (6, 6) and their corresponding diameter and buckling.

Type name and armchair structure	Diameter in Å	Buckling in Å
Type 1 (3,3)	5.204	0.115
Type 1 (4,4)	6.925	0.076
Type 1 (5,5)	8.631	0.050
Type 1 (6,6)	10.350	0.044
Type 2 (3,3)	5.186	0.224
Type 2 (4,4)	7.098	0.208
Type 2 (5,5)	8.869	0.161
Type 2 (6,6)	10.640	0.135
Type 3 (3,3)	5.259	0.173
Type 3 (4,4)	7.023	0.002
Type 3 (5,5)	8.742	0.005
Type 3 (6,6)	10.460	0.012

Table 3.5 Adsorption binding energies of hydrogen molecule, distances of hydrogen molecule from tube walls, nearest C-hydrogen molecule distances, nearest Si-hydrogen molecule distances, bond lengths of adsorbed hydrogen molecules and Mulliken charges of hydrogen atom nearest to the wall, belonging to the adsorbed molecule, adsorbed on type 1 armchair SiCNT from inside.

Nanostructure name / Site name	Binding energy in kcal/mol	Distance of hydrogen molecule from nanotube wall in Å	Distance from nearest C atom in Å	Distance from nearest Si atom in Å	Bond length of adsorbed hydrogen molecule in Å	Mulliken charge of the hydrogen atom nearest to the wall
TYPE 1 (5,5)/ T1CT	0.52	3.599	3.608	3.621	0.748	0.008
TYPE 1 (5,5)/ T1CSINB	0.13	3.321	3.350	3.298	0.748	0.009
TYPE 1 (6,6)/ T1HS	0.02	3.347	3.498	3.455	0.748	0.010

Table 3.6 Adsorption binding energies of hydrogen molecule, distances of hydrogen molecule from tube walls, nearest C-hydrogen molecule distances, nearest Si-hydrogen molecule distances, bond lengths of adsorbed hydrogen molecules and Mulliken charges of hydrogen atom nearest to the wall, belonging to the adsorbed molecule, adsorbed on type 1 armchair SiCNT from outside.

Nanostructure name / Site name	Binding energy in kcal/mol	Distance of hydrogen molecule from nanotube wall in Å	Distance from nearest C atom in Å	Distance from nearest Si atom in Å	Bond length of adsorbed hydrogen molecule in Å	Mulliken charge of the hydrogen atom nearest to the wall
TYPE 1 (3,3)/ T1CSINB	0.50	2.751	2.961	3.160	0.749	0.018
TYPE 1 (3,3)/ T1CSIZB	0.42	2.935	3.101	3.396	0.748	0.012
TYPE 1 (4,4)/ T1CT	1.02	3.071	3.061	3.677	0.748	0.017
TYPE 1 (4,4)/ T1CSIZB	0.63	3.074	3.141	3.867	0.748	0.015
TYPE 1 (4,4)/ T1CSINB	0.55	2.955	3.073	3.406	0.748	0.017
TYPE 1 (4,4)/ T1SIT	0.36	3.271	3.806	3.351	0.747	0.005
TYPE 1 (4,4)/ T1HS	0.09	3.038	3.634	3.684	0.748	0.013
TYPE 1 (5,5)/ T1CT	1.11	3.453	3.448	4.040	0.747	0.011
TYPE 1 (5,5)/ T1SIT	0.59	3.535	4.057	3.605	0.747	0.004
TYPE 1 (5,5)/ T1CSIZB	0.16	3.149	3.257	3.382	0.748	0.011

Table 3.6 – *Continued*

Nanostructure name / Site name	Binding energy in kcal/mol	Distance of hydrogen molecule from nanotube wall in Å	Distance from nearest C atom in Å	Distance from nearest Si atom in Å	Bond length of adsorbed hydrogen molecule in Å	Mulliken charge of the hydrogen atom nearest to the wall
TYPE 1 (6,6)/ T1CSINB	0.46	2.881	3.105	3.172	0.748	0.009
TYPE 1 (6,6)/ T1HS	0.33	3.023	3.469	3.677	0.747	0.012
TYPE 1 (6,6)/ T1CSIZB	0.14	3.036	3.068	3.524	0.748	0.014
TYPE 1 (6,6)/ T1CT	0.09	2.982	3.000	3.610	0.748	0.015

Table 3.7 Adsorption binding energies of hydrogen molecule, distances of hydrogen molecule from tube walls, nearest C-hydrogen molecule distances, nearest Si-hydrogen molecule distances, bond lengths of adsorbed hydrogen molecules and Mulliken charges of hydrogen atom nearest to the wall, belonging to the adsorbed molecule, adsorbed on type 2 armchair SiCNT from inside.

Nanostructure name / Site name	Binding energy in kcal/mol	Distance of hydrogen molecule from nanotube wall in Å	Distance from nearest C atom in Å	Distance from nearest Si atom in Å	Bond length of adsorbed hydrogen molecule in Å	Mulliken charge of the hydrogen atom nearest to the wall
TYPE 2 (4,4)/ T2CCB	29.50	3.174	2.937	3.341	0.749	0.004
TYPE 2 (4,4)/ T2SIT	1.30	2.920	3.213	3.003	0.750	0.000
TYPE 2 (4,4)/ T2CT	1.22	3.098	3.004	3.543	0.749	0.003
TYPE 2 (4,4)/ T2H2S	1.16	3.043	3.305	3.174	0.749	0.003
TYPE 2 (4,4)/ T2SISIB	1.09	2.895	3.279	3.016	0.748	0.001
TYPE 2 (4,4)/ T2H1S	1.02	3.051	3.048	3.511	0.748	0.003
TYPE 2 (4,4)/ T2CSIB	0.36	3.039	3.044	3.219	0.747	0.003
TYPE 2 (5,5)/ T2CSIB	0.17	3.581	3.591	3.712	0.748	0.006
TYPE 2 (5,5)/ T2SIT	0.11	3.676	3.731	3.883	0.748	0.005
TYPE 2 (5,5)/ T2SISIB	0.11	3.73	3.938	3.835	0.747	0.005

Table 3.7 – *Continued*

Nanostructure name / Site name	Binding energy in kcal/mol	Distance of hydrogen molecule from nanotube wall in Å	Distance from nearest C atom in Å	Distance from nearest Si atom in Å	Bond length of adsorbed hydrogen molecule in Å	Mulliken charge of the hydrogen atom nearest to the wall
TYPE 2 (5,5)/ T2H2S	0.11	3.560	3.877	3.649	0.748	0.006
TYPE 2 (6,6)/ T2CT	1.31	4.798	4.702	5.062	0.747	0.000
TYPE 2 (6,6)/ T2CCB	0.18	3.157	3.087	3.678	0.748	0.009
TYPE 2 (6,6)/ T2H2S	0.10	3.264	3.551	3.421	0.747	0.008
TYPE 2 (6,6)/ T2H1S	0.07	3.488	3.579	3.877	0.747	0.007
TYPE 2 (6,6)/ T2CSIB	0.16	3.063	3.077	3.202	0.748	0.008

Table 3.8 Adsorption binding energies of hydrogen molecule, distances of hydrogen molecule from tube walls, nearest C-hydrogen molecule distances, nearest Si-hydrogen molecule distances, bond lengths of adsorbed hydrogen molecules and Mulliken charges of hydrogen atom nearest to the wall, belonging to the adsorbed molecule, adsorbed on type 2 armchair SiCNT from outside.

Nanostructure name / Site name	Binding energy in kcal/mol	Distance of hydrogen molecule from nanotube wall in Å	Distance from nearest C atom in Å	Distance from nearest Si atom in Å	Bond length of adsorbed hydrogen molecule in Å	Mulliken charge of the hydrogen atom nearest to the wall
TYPE 2 (3,3)/ T2SIT	0.53	3.835	4.304	3.304	0.749	0.028
TYPE 2 (3,3)/ T2CCB	0.38	2.795	3.705	3.140	0.747	0.012
TYPE 2 (3,3)/ T2SISIB	0.36	3.729	4.733	3.478	0.747	0.019
TYPE 2 (3,3)/ T2H2S	0.29	2.701	3.516	3.352	0.747	0.010
TYPE 2 (3,3)/ T2H1S	0.15	3.750	4.675	3.860	0.747	0.011
TYPE 2 (3,3)/ T2CSIB	0.08	3.521	3.705	3.444	0.748	0.015
TYPE 2 (4,4)/ T2CT	37.52	2.827	3.863	3.125	0.748	0.006
TYPE 2 (4,4)/ T2SIT	33.98	3.133	3.947	3.428	0.747	0.003
TYPE 2 (4,4)/ T2CCB	29.76	3.329	3.601	4.043	0.747	0.008
TYPE 2 (4,4)/ T2SISIB	29.59	7.175	7.482	6.555	0.747	0.001

Table 3.8 – *Continued*

Nanostructure name / Site name	Binding energy in kcal/mol	Distance of hydrogen molecule from nanotube wall in Å	Distance from nearest C atom in Å	Distance from nearest Si atom in Å	Bond length of adsorbed hydrogen molecule in Å	Mulliken charge of the hydrogen atom nearest to the wall
TYPE 2 (4,4)/ T2H2S	28.56	3.302	3.947	3.428	0.747	0.008
TYPE 2 (4,4)/ T2H1S	29.14	3.342	4.351	3.670	0.748	0.009
TYPE 2 (4,4)/ T2CSIB	1.05	3.341	3.799	3.625	0.747	0.008
TYPE 2 (5,5)/ T2CCB	15.20	2.940	3.795	3.249	0.747	0.012
TYPE 2 (5,5)/ T2H1S	13.95	3.345	3.239	3.828	0.747	0.012
TYPE 2 (5,5)/ T2CT	0.26	2.940	3.193	3.641	0.748	0.013
TYPE 2 (5,5)/ T2SIT	0.14	3.239	3.892	3.208	0.749	0.006
TYPE 2 (5,5)/ T2CSIB	0.09	2.657	3.589	3.450	0.747	0.009
TYPE 2 (5,5)/ T2SISIB	0.01	3.291	4.581	3.575	0.747	0.003
TYPE 2 (6,6)/ T2CCB	0.28	2.824	3.086	3.831	0.747	0.017
TYPE 2 (6,6)/ T2SIT	0.09	2.991	3.659	3.000	0.748	0.004
TYPE 2 (6,6)/ T2H2S	0.07	2.709	3.366	3.421	0.747	0.016

Table 3.9 Adsorption binding energies of hydrogen molecule, distances of hydrogen molecule from tube walls, nearest C-hydrogen molecule distances, nearest Si-hydrogen molecule distances, bond lengths of adsorbed hydrogen molecules and Mulliken charges of hydrogen atom nearest to the wall, belonging to the adsorbed molecule, adsorbed on type 3 armchair SiCNT from inside.

Nanostructure name / Site name	Binding energy in kcal/mol	Distance of hydrogen molecule from nanotube wall in Å	Distance from nearest C atom in Å	Distance from nearest Si atom in Å	Bond length of adsorbed hydrogen molecule in Å	Mulliken charge of the hydrogen atom nearest to the wall
TYPE 3 (3,3)/ T3CSIZB	8.36	2.410	2.420	2.952	0.741	0.010
TYPE 3 (3,3)/ T3HS	8.34	2.338	2.838	3.467	0.741	0.002
TYPE 3 (3,3)/ T3SIT	8.33	2.416	2.737	3.314	0.742	0.006
TYPE 3 (3,3)/ T3CT	8.27	2.416	2.829	3.233	0.741	0.010
TYPE 3 (3,3)/ T3CSINB	5.52	2.283	2.419	2.506	0.744	0.024
TYPE 3 (4,4)/ T3SISIB	0.17	2.956	3.159	3.074	0.749	0.004
TYPE 3 (5,5)/ T3CCB	0.03	3.130	3.177	3.411	0.746	0.010
TYPE 3 (6,6)/ T3SIT	0.61	3.946	3.936	3.977	0.747	0.002
TYPE 3 (6,6)/ T3CCB	0.60	4.436	4.460	4.574	0.747	0.001
TYPE 3 (6,6)/ T3HS	0.54	4.724	4.738	4.759	0.747	0.001

Table 3.9 – *Continued*

Nanostructure name / Site name	Binding energy in kcal/mol	Distance of hydrogen molecule from nanotube wall in Å	Distance from nearest C atom in Å	Distance from nearest Si atom in Å	Bond length of adsorbed hydrogen molecule in Å	Mulliken charge of the hydrogen atom nearest to the wall
TYPE 3 (6,6)/ T3CSIZB	0.49	4.446	4.491	4.499	0.747	0.001
TYPE 3 (6,6)/ T3SISIB	0.47	4.446	4.569	4.523	0.747	0.001
TYPE 3 (6,6)/ T3CT	0.23	4.431	4.408	4.469	0.747	0.001
TYPE 3 (6,6)/ T3CSINB	0.18	4.504	4.488	4.498	0.747	0.001

Table 3.10 Adsorption binding energies of hydrogen molecule, distances of hydrogen molecule from tube walls, nearest C-hydrogen molecule distances, nearest Si-hydrogen molecule distances, bond lengths of adsorbed hydrogen molecules and Mulliken charges of hydrogen atom nearest to the wall, belonging to the adsorbed molecule, adsorbed on type 3 armchair SiCNT from outside.

Nanostructure name / Site name	Binding energy in kcal/mol	Distance of hydrogen molecule from nanotube wall in Å	Distance from nearest C atom in Å	Distance from nearest Si atom in Å	Bond length of adsorbed hydrogen molecule in Å	Mulliken charge of the hydrogen atom nearest to the wall
TYPE 3 (4,4)/ T3CT	0.39	2.858	3.004	3.755	0.748	0.019
TYPE 3 (4,4)/ T3SISIB	0.39	3.296	3.672	3.313	0.748	0.011
TYPE 3 (4,4)/ T3CSINB	0.37	2.911	3.128	3.542	0.748	0.019
TYPE 3 (4,4)/ T3CSIZB	0.32	2.518	3.175	3.287	0.747	0.012
TYPE 3 (4,4)/ T3SIT	0.28	3.285	3.910	3.329	0.748	0.006
TYPE 3 (4,4)/ T3CCB	0.16	2.886	3.004	3.755	0.748	0.021
TYPE 3 (5,5)/ T3CSINB	0.21	3.062	3.322	3.332	0.748	0.009
TYPE 3 (5,5)/ T3CCB	0.12	3.154	3.267	3.968	0.748	0.017
TYPE 3 (5,5)/ T3CT	0.07	3.162	3.199	3.771	0.747	0.015
TYPE 3 (5,5)/ T3CSIZB	0.02	3.285	3.292	3.313	0.748	0.011

Table 3.10 – *Continued*

Nanostructure name / Site name	Binding energy in kcal/mol	Distance of hydrogen molecule from nanotube wall in Å	Distance from nearest C atom in Å	Distance from nearest Si atom in Å	Bond length of adsorbed hydrogen molecule in Å	Mulliken charge of the hydrogen atom nearest to the wall
TYPE 3 (6,6)/ T3CSINB	0.91	3.082	3.324	3.331	0.748	0.009
TYPE 3 (6,6)/ T3HS	0.81	2.864	3.417	3.567	0.748	0.010
TYPE 3 (6,6)/ T3CCB	0.76	3.12	3.243	3.952	0.748	0.017
TYPE 3 (6,6)/ T3CT	0.75	3.078	3.116	3.709	0.748	0.016
TYPE 3 (6,6)/ T3CSIZB	0.75	3.760	3.569	3.089	0.748	0.017
TYPE 3 (6,6)/ T3SISIB	0.58	3.403	4.253	3.620	0.748	0.007
TYPE 3 (6,6)/ T3SIT	0.49	3.188	3.223	3.773	0.748	0.008

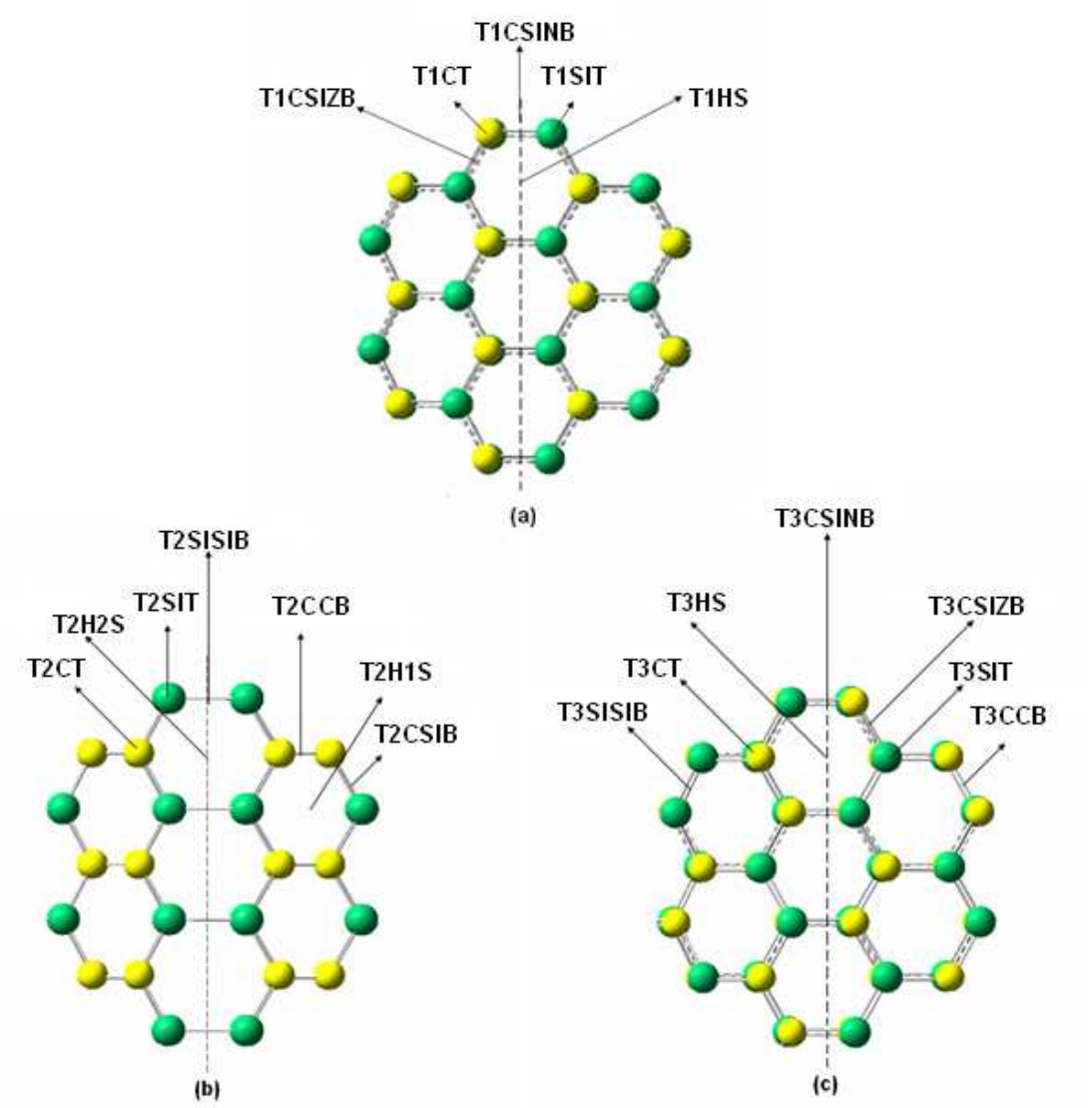

Figure 3.1 Atomic arrangements and different adsorption sites for (a) type 1, (b) type 2 and (c) type 3 nanotubes. The carbon atoms are yellow and silicon atoms are green. The dashed lines represent the orientation of tube axis.

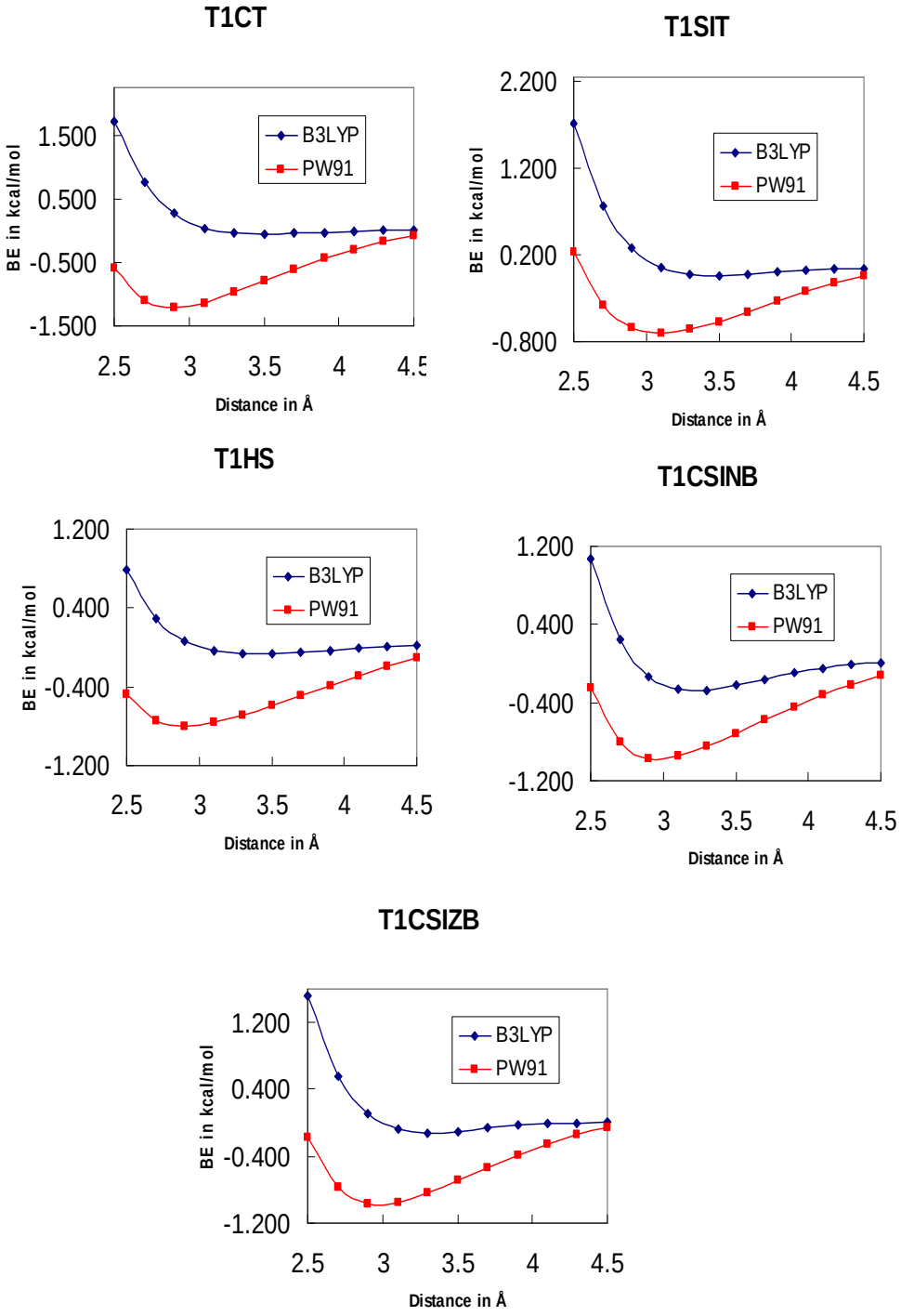

Figure 3.2 Binding energy vs. distance for type 1 approach sites for (9, 9) nanotubes, when hydrogen molecular adsorption takes place from outside.

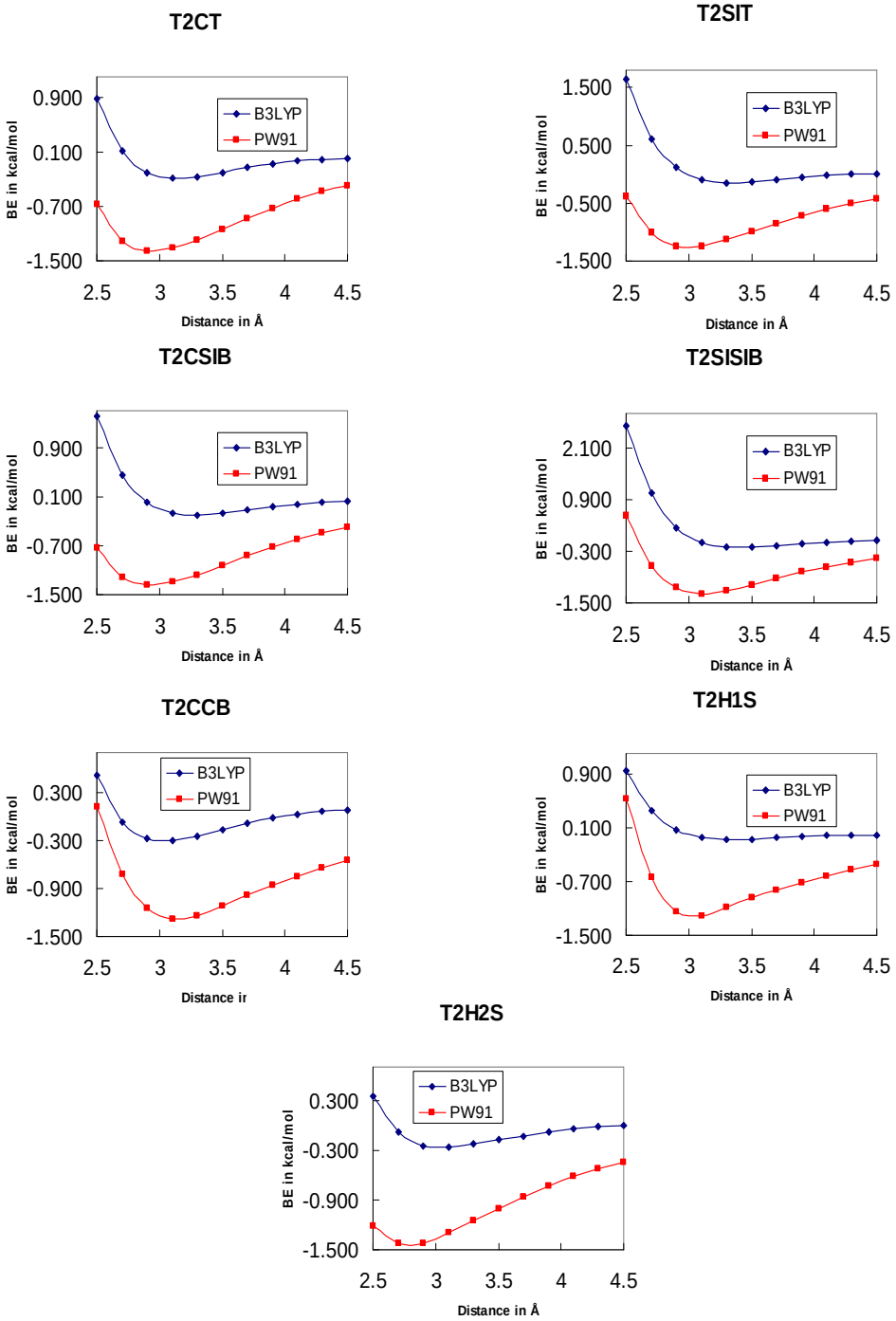

Figure 3.3 Binding energy vs. distance for type 2 approach sites for (9, 9) nanotubes, when hydrogen molecular adsorption takes place from outside.

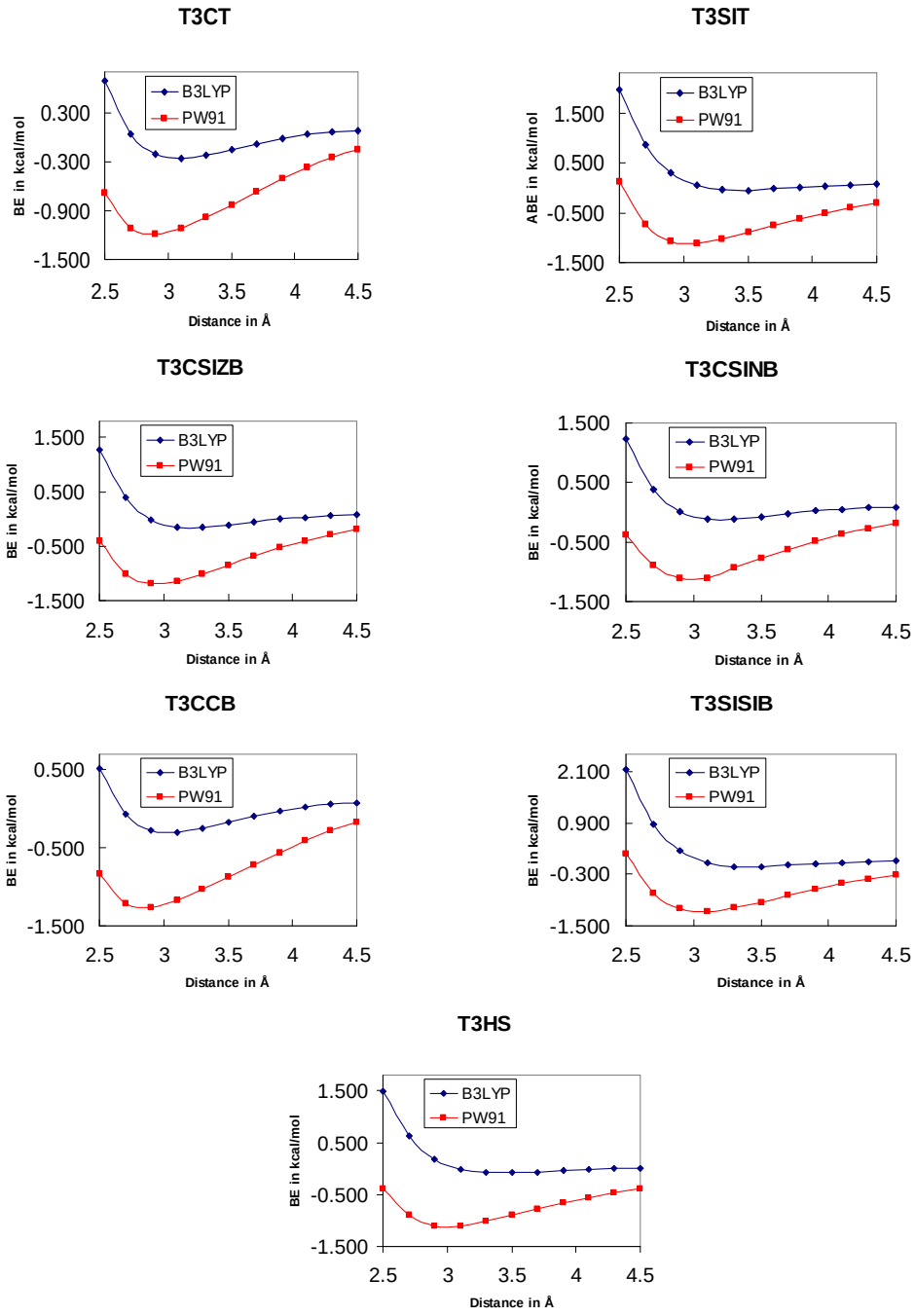

Figure 3.4 Binding energy vs. distance for type 3 approach sites for (9, 9) nanotubes, when hydrogen molecular adsorption takes place from outside.

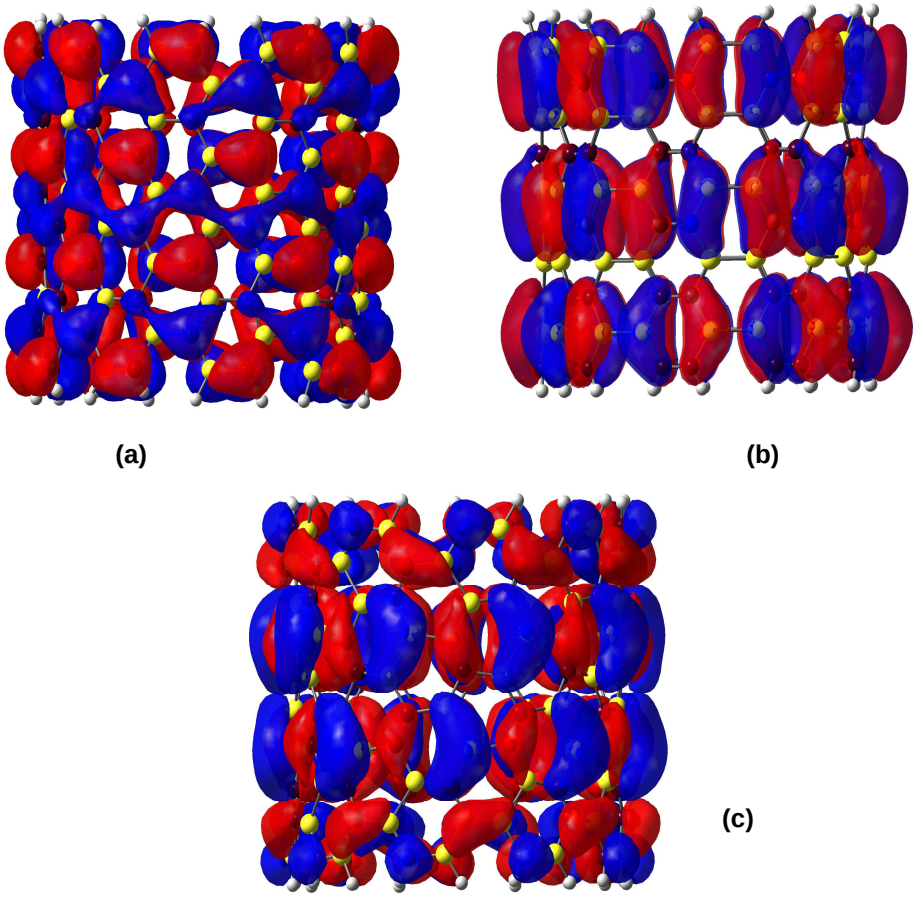

Figure 3.5 HOMO (highest occupied molecular orbital) plots for type 1, type 2 and type 3 (9, 9) bare SiCNT nanotube obtained using B3LYP method. The C atoms have been shown in brown and the Si atoms in yellow.

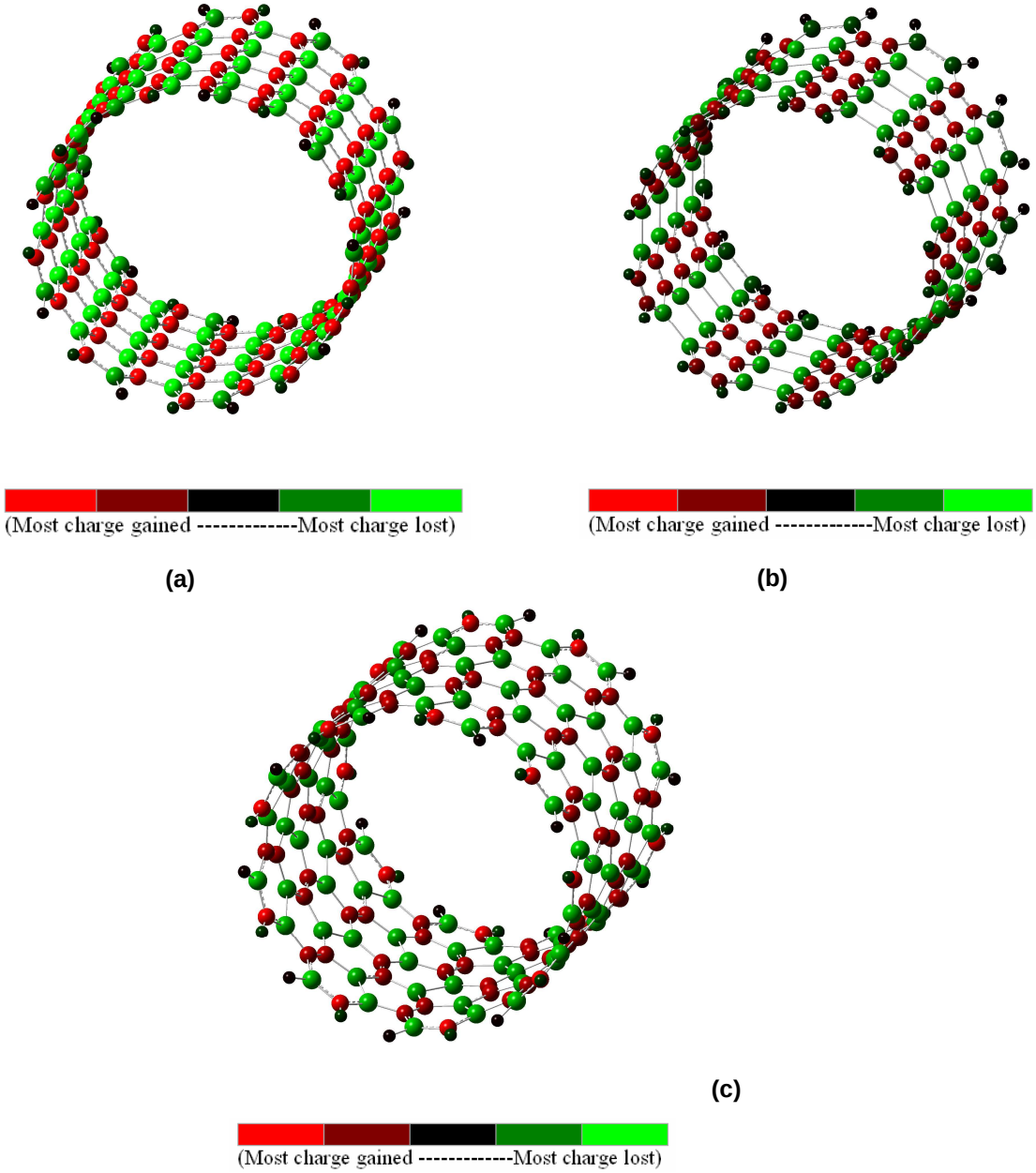

Figure 3.6 Mulliken charge distributions for (a) type 1, (b) type 2 and (c) type 3, (9, 9) nanotubes using B3LYP method. Carbon atoms gained and silicon atoms lost charge.

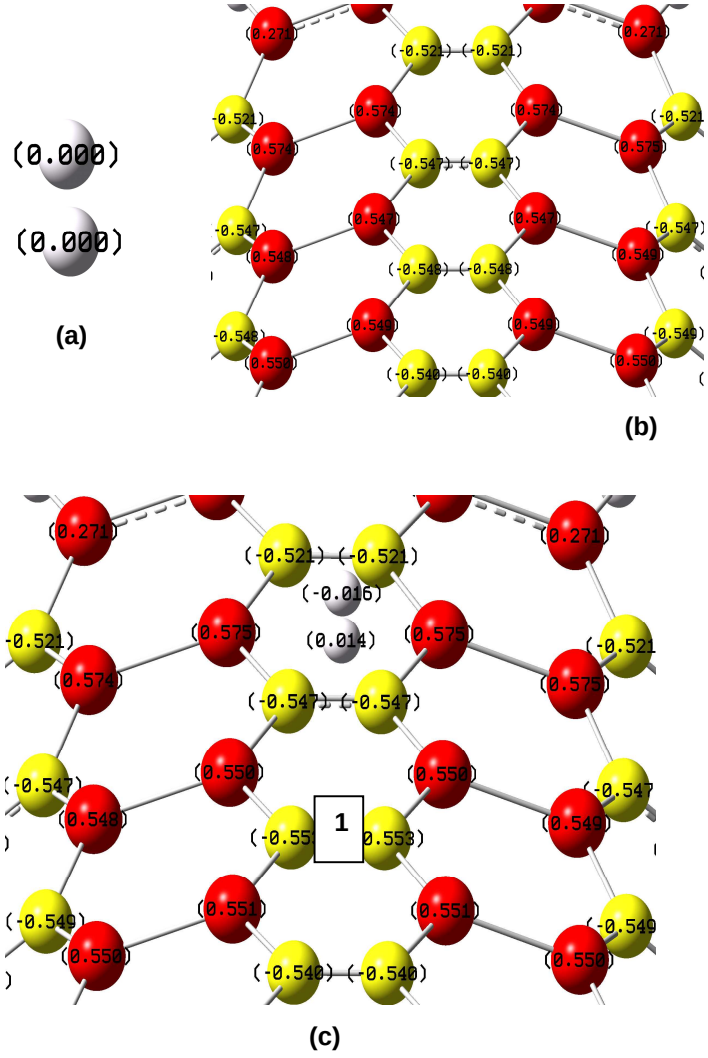

Figure 3.7 (a) Hydrogen molecule optimized using B3LYP method. (b) Type 2 bare SiCNT (9, 9) optimized using B3LYP method. (c) Type 2 SiCNT (9, 9) + Hydrogen molecule using B3LYP method. The hydrogen molecule is perpendicular to 1 as shown in the Figure above. This is the T2CCB position. The carbon atoms shown in yellow are gaining charge and the silicon atoms shown in red are losing charge. The numbers in bracket indicate the Mulliken charge for each atom.

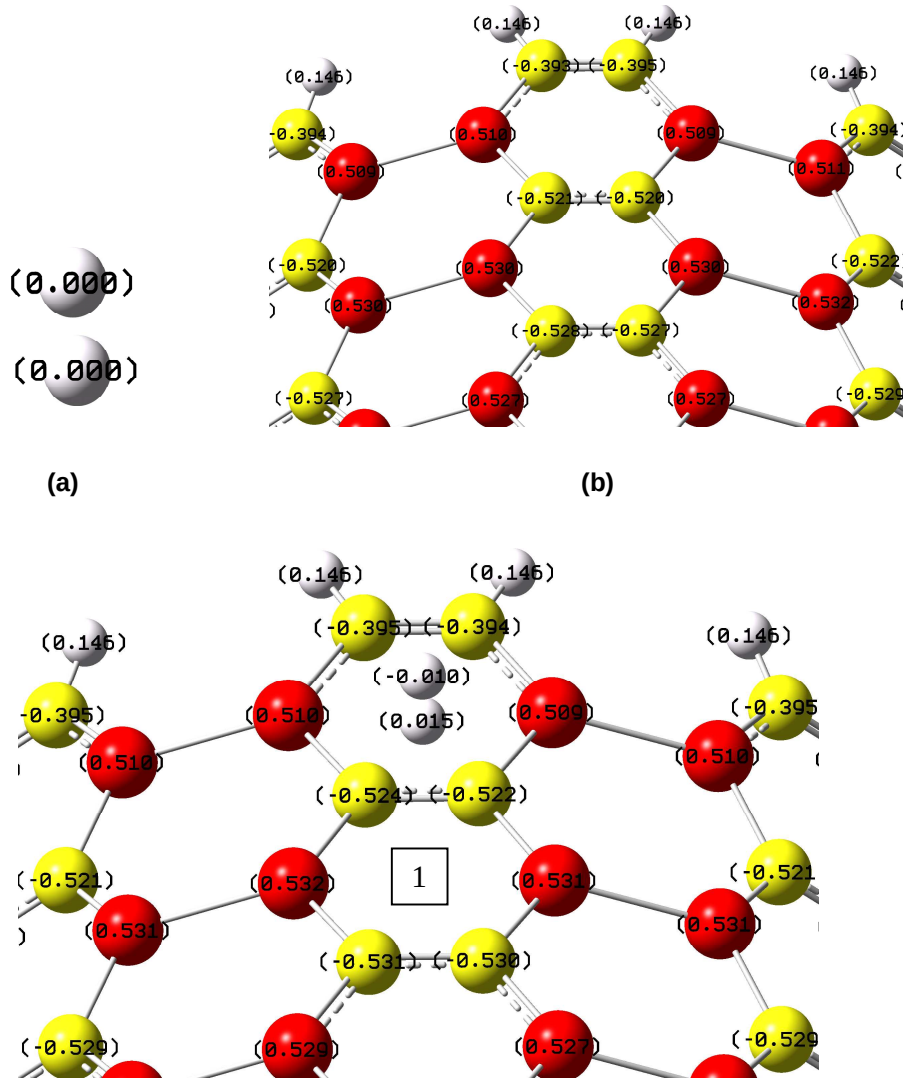

Figure 3.8 (a) Hydrogen molecule optimized using PW91 method. (b) Type 2 bare SiCNT (9, 9) optimized using PW91 method. (c) Type 2 SiCNT (9, 9) + Hydrogen molecule using PW91 method. The hydrogen molecule is perpendicular to 1 as shown in the Figure above. This is the T2H2S position. The carbon atoms shown in yellow are gaining charge and the silicon atoms shown in red are losing charge. The numbers in bracket indicate the Mulliken charge for each atom.

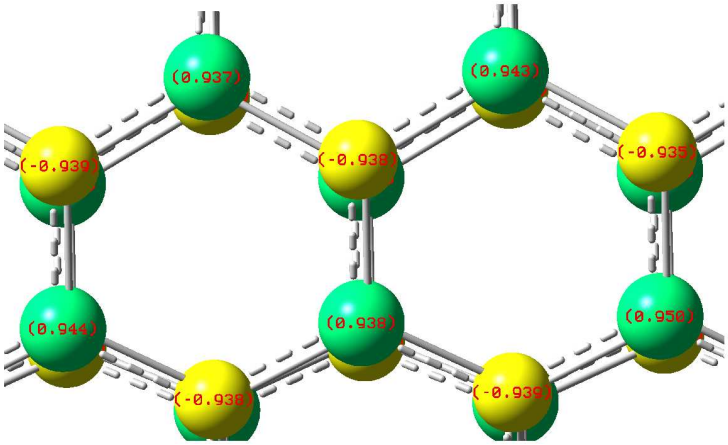

(a)

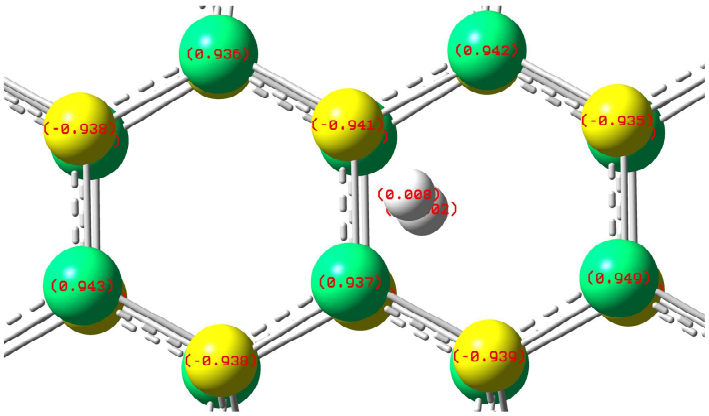

(b)

Figure 3.9 Mulliken charge plot of (a) type 1 (5, 5) bare SiCNT (b) type 1 (5, 5) SiCNT along with the hydrogen molecule adsorbed from inside at T1CT site. The carbon atoms are yellow, silicon atoms are green and the hydrogen atoms are white.

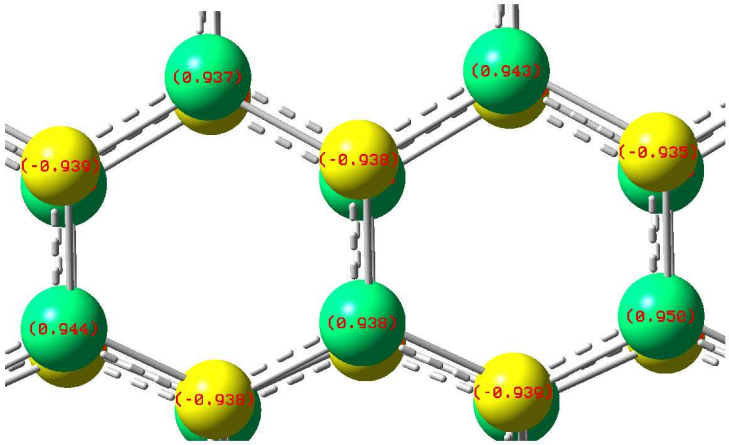

(a)

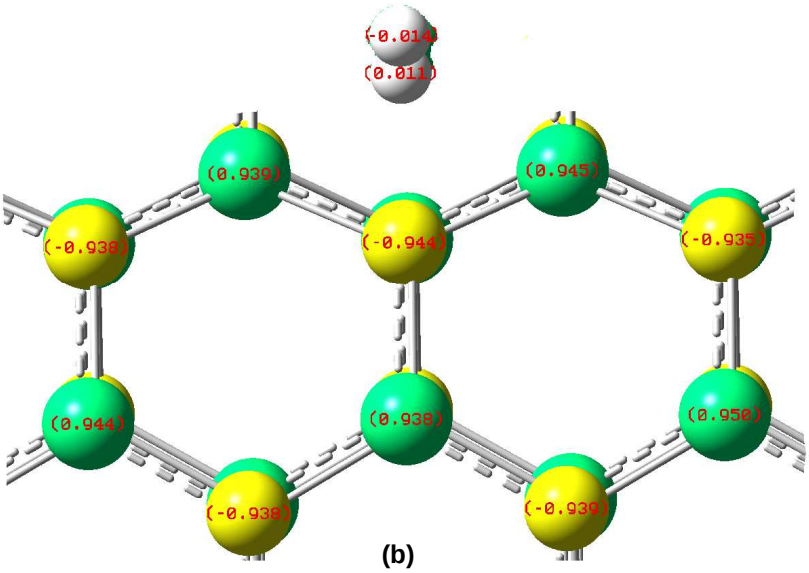

(b)

Figure 3.10 Mulliken charge plot of (a) type 1 (5, 5) bare SiCNT (b) type 1 (5, 5) SiCNT along with the hydrogen molecule adsorbed from the outer wall at T1CT site. The carbon atoms are yellow, silicon atoms are green and the hydrogen atoms are white.

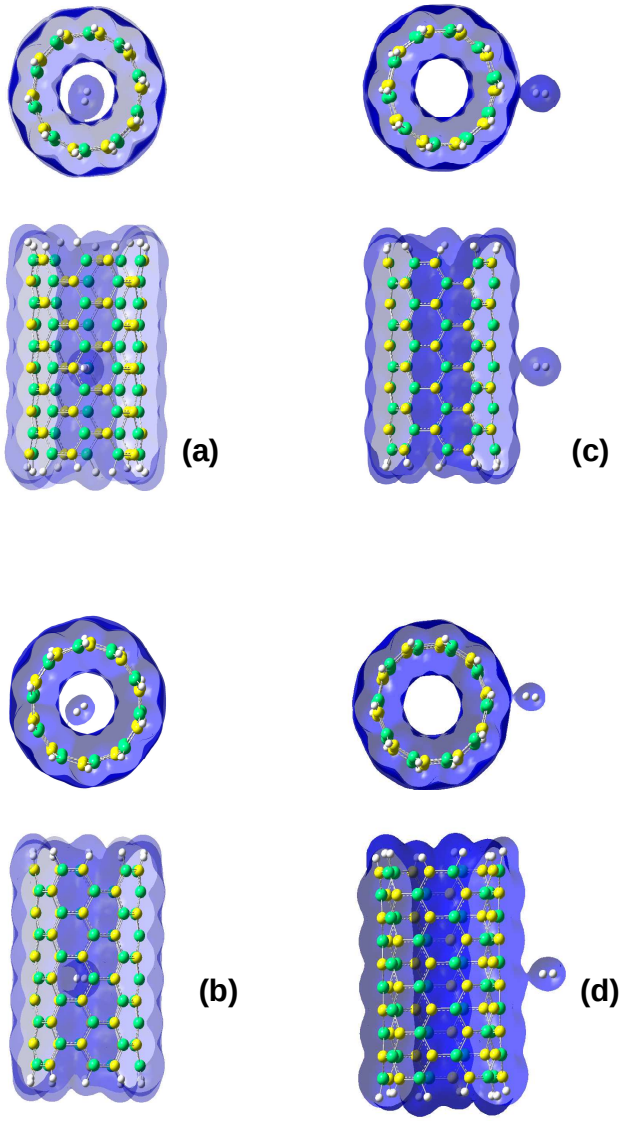

Figure 3.11 Electron charge density plot for (a) adsorption of the hydrogen molecule from inside the nanotube for type 1 (5, 5) TICT site (b) inside adsorption for type 1 (5, 5) T1CSINB site (c) outer wall adsorption for type 1 (5, 5) T1CT site (d) outer wall adsorption for type 1 (5, 5) T1CSIZB site. All plots have been plotted under similar conditions using an isovalue of 0.002.

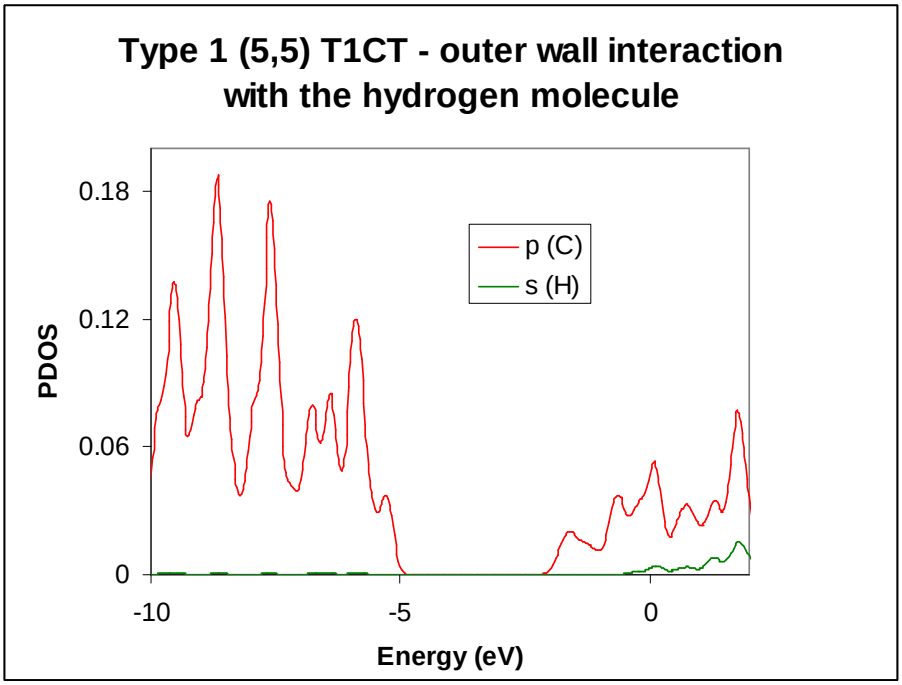

Figure 3.12 Partial density of state plot for the outer wall interaction of the hydrogen molecule with type 1 (5, 5) TICT site. The contribution of the hydrogen molecule and the nearest C atom has been shown in the PDOS.

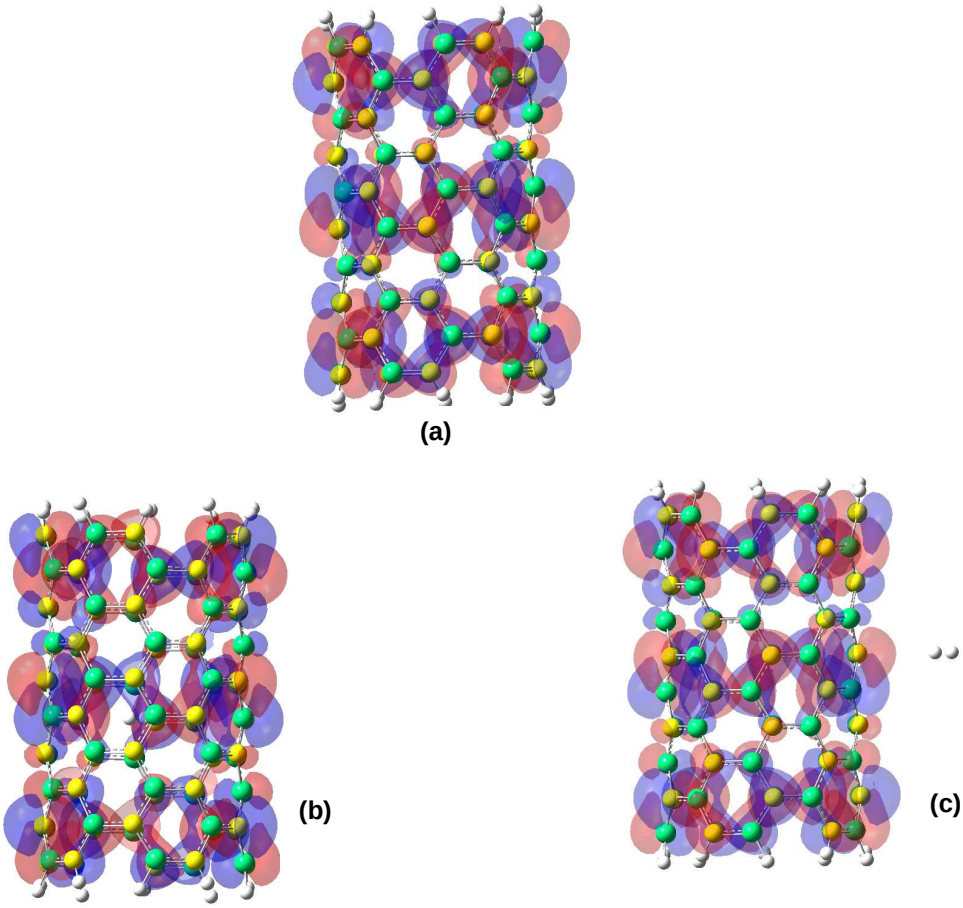

Figure 3.13 HOMO plots for (a) bare type 1 (5, 5) SiCNT (b) optimized type 1 (5, 5) SiCNT with hydrogen molecule placed inside the nanotube at T1CT site (c) optimized type 1 (5, 5) SiCNT with the hydrogen molecule approaching the nanotube from the outer wall at T1CT site.

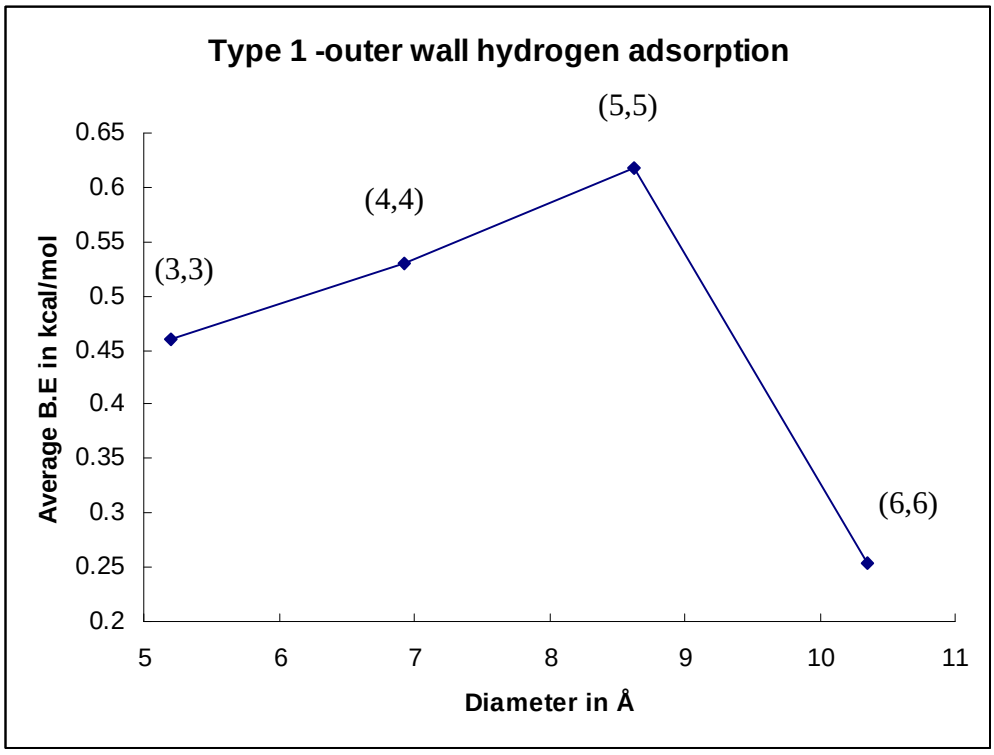

Figure 3.14 Diameter vs. average binding energy of the adsorbed hydrogen molecule for various type 1 structures, with the hydrogen molecule being adsorption from the outer wall.

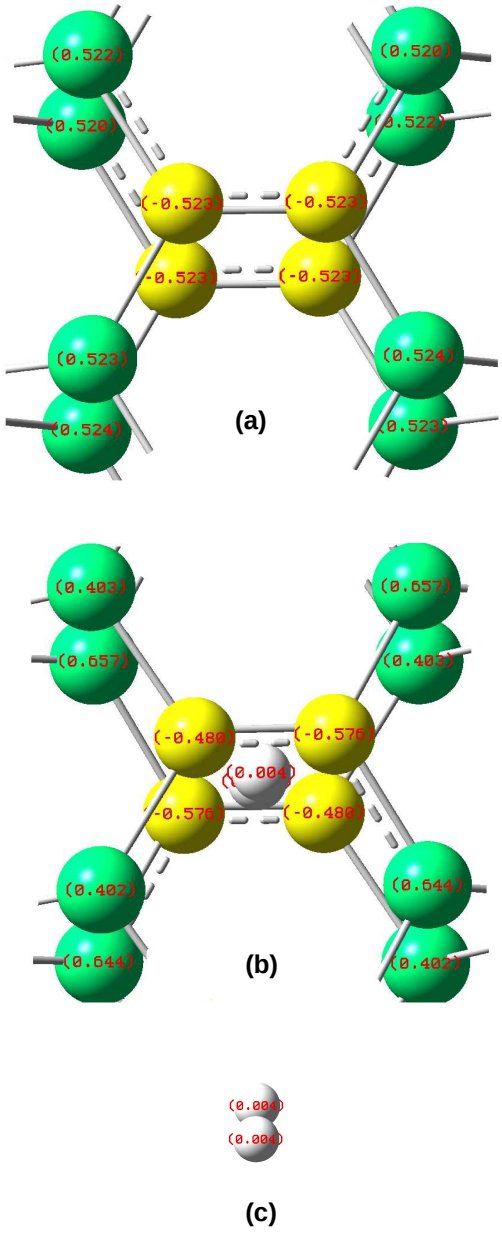

Figure 3.15 Mulliken charge plot of (a) type 2 (4, 4) bare SiCNT (b) type 2 (4, 4) SiCNT along with the hydrogen molecule adsorbed from inside at T2CCB site (c) partial charge on the encapsulated hydrogen molecule. The carbon atoms are yellow, silicon atoms are green and the hydrogen atoms are white.

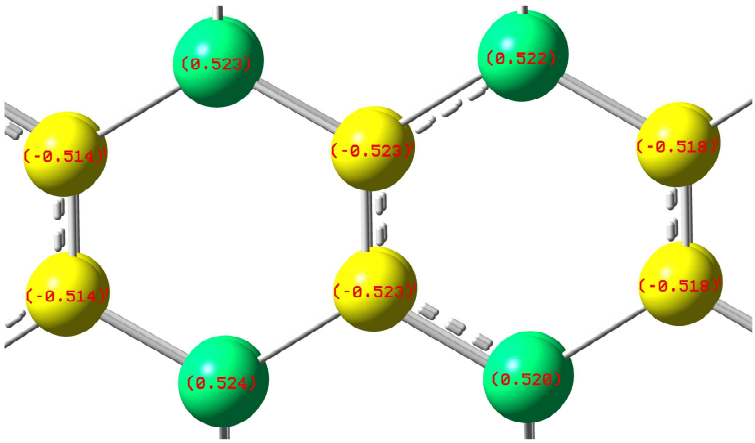

(a)

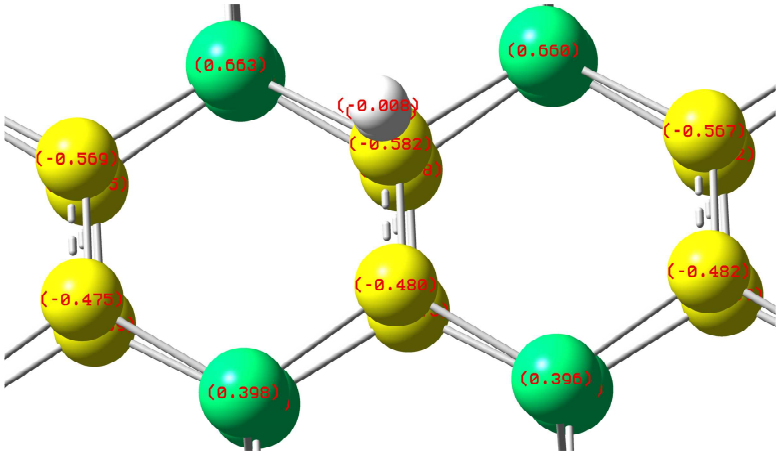

(b)

Figure 3.16 Mulliken charge plot of (a) type 2 (4, 4) bare SiCNT (b) type 2 (4, 4) SiCNT along with the hydrogen molecule adsorbed from outside at T2CT site (c) partial charge on the encapsulated hydrogen molecule. The carbon atoms are yellow, silicon atoms are green and the hydrogen atoms are white.

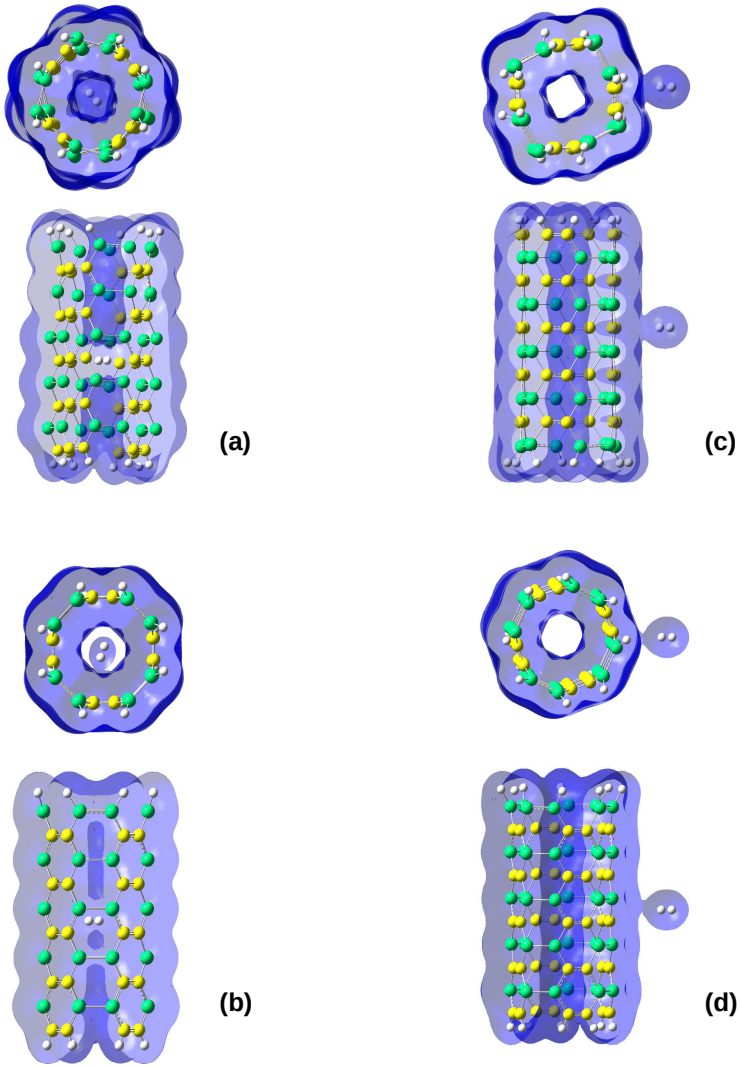

Figure 3.17 Electron charge density plot for (a) adsorption of the hydrogen molecule from inside the nanotube for type 2 (4, 4) T2CCB site (b) inside adsorption for type 2 (4, 4) T2CSIB site (c) outer wall adsorption for type 2 (4, 4) T2CT site (d) outer wall adsorption for type 2 (4, 4) T2CSIB site. All plots have been plotted under similar conditions using an isovalue of 0.002.

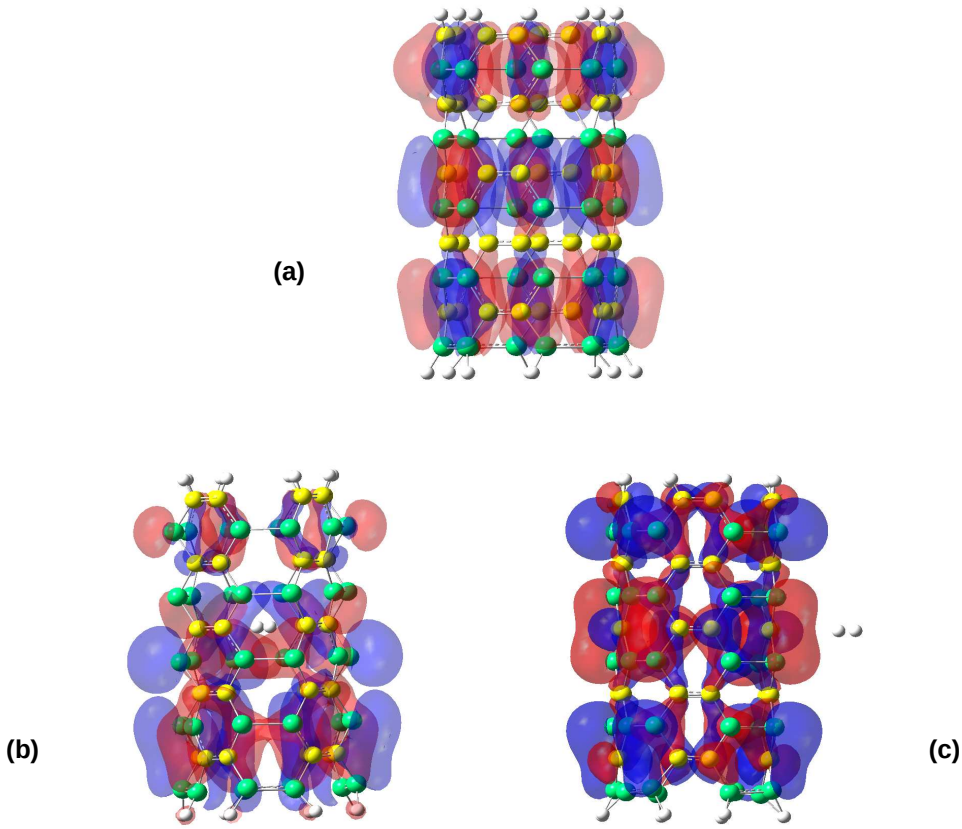

Figure 3.18 HOMO plots for (a) bare type 2 (4, 4) SiCNT (b) optimized type 2 (4, 4) SiCNT with hydrogen molecule placed inside the nanotube at T2CCB site (c) optimized type 2 (4, 4) SiCNT with the hydrogen molecule approaching the nanotube from the outer wall at T2CT site.

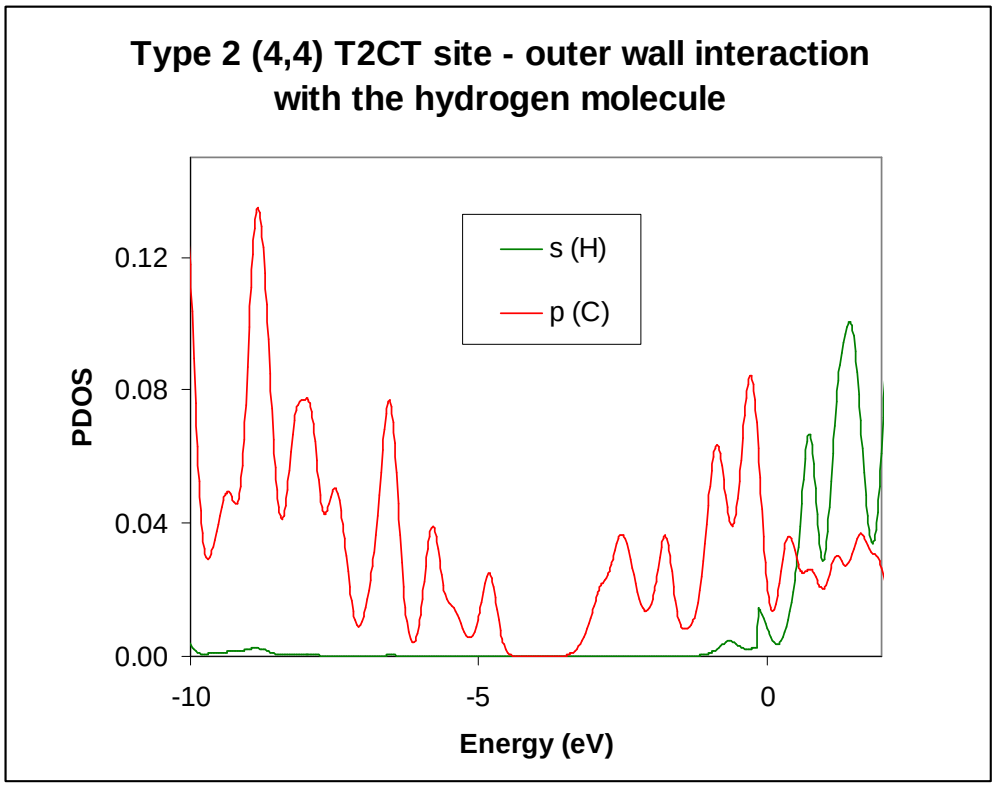

Figure 3.19 Partial density of state plot for the outer wall interaction of the hydrogen molecule with type 2 (4, 4) T2CT site. The contributions of the hydrogen molecule and the nearest C atom have been used for the PDOS plot.

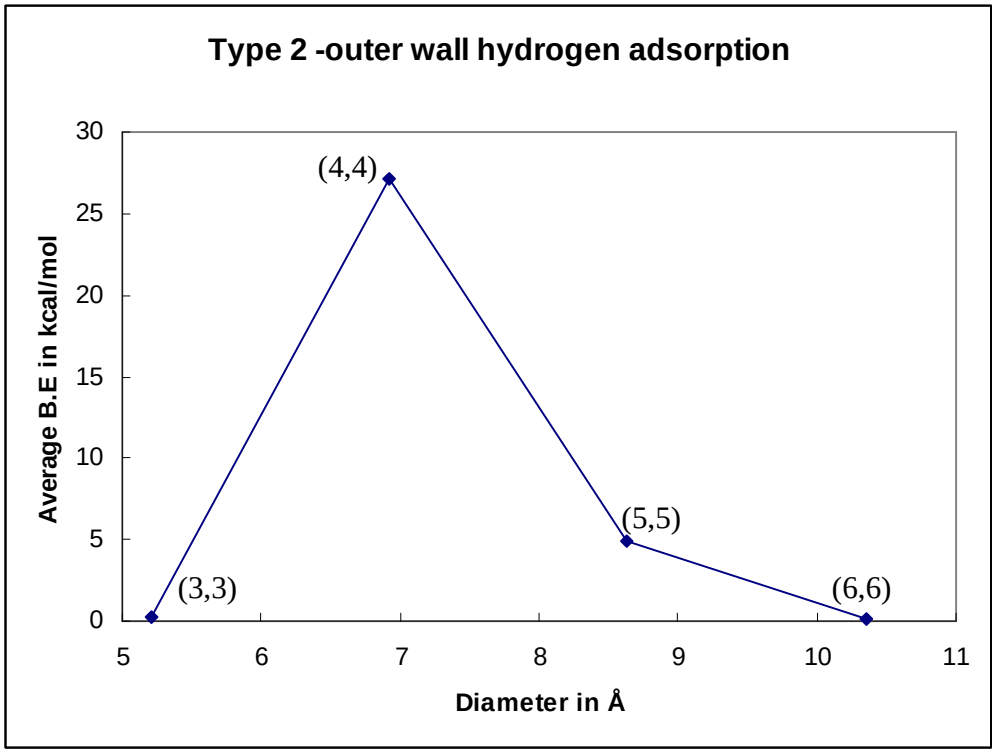

Figure 3.20 Diameter vs. average binding energy of the adsorbed hydrogen molecule for various type 2 structures, with the hydrogen molecule adsorbed from the outer wall.

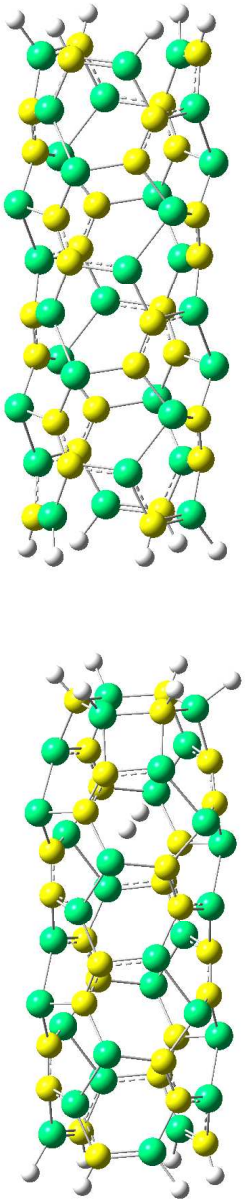

Figure 3.21 (a) type 3 (3, 3) bare SiCNT (b) type 3 (3, 3) SiCNT with hydrogen molecule adsorbed from inside at T3CSIZB site.

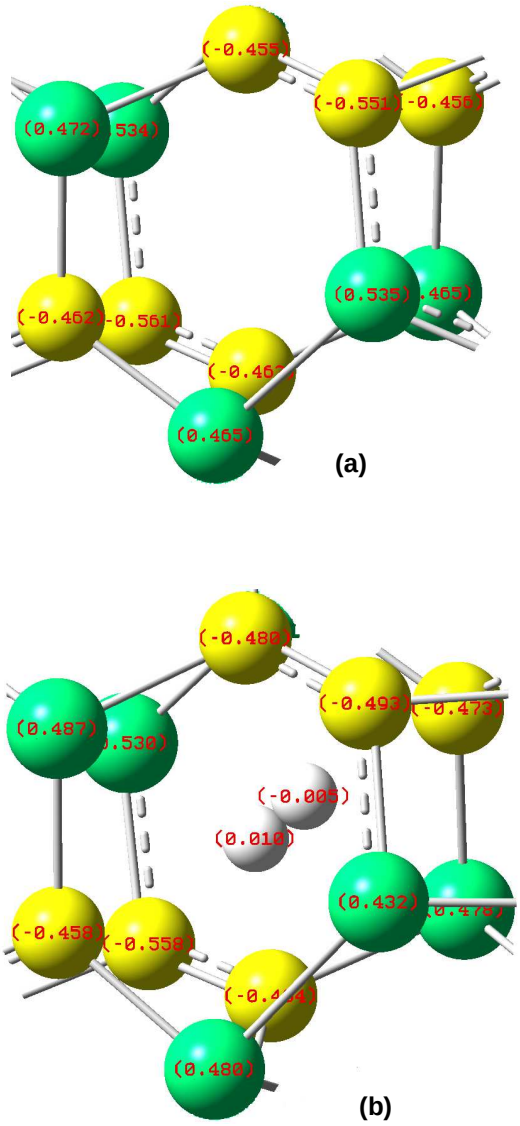

Figure 3.22 Mulliken charge plot of (a) type 3 (3, 3) bare SiCNT (b) type 3 (3, 3) SiCNT along with the hydrogen molecule adsorbed from inside at T3CSIZB site. The carbon atoms are yellow, silicon atoms are green and the hydrogen atoms are white.

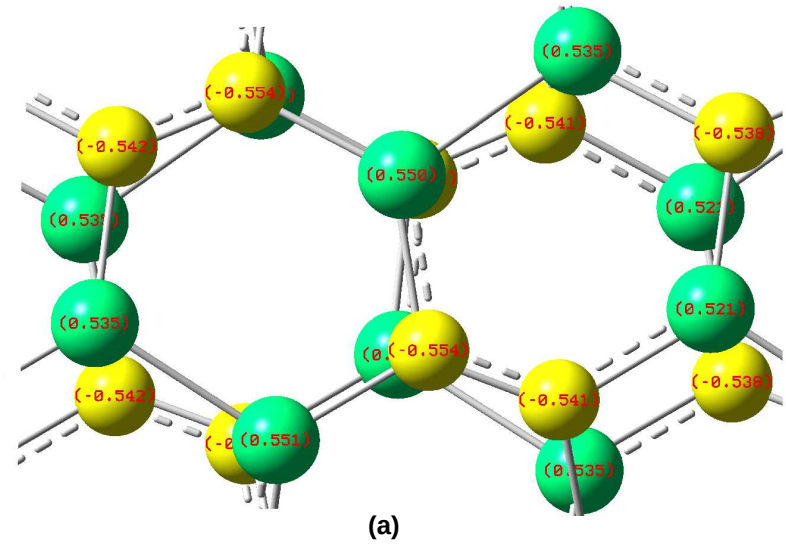

(a)

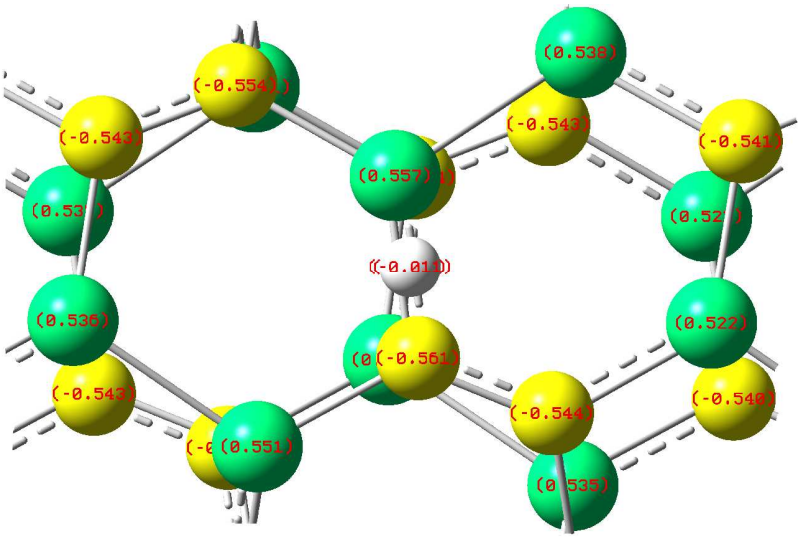

(b)

Figure 3.23 Mulliken charge plot of (a) type 3 (6, 6) bare SiCNT (b) type 3 (6, 6) SiCNT along with the hydrogen molecule adsorbed from outside at T3CSINB site. The carbon atoms are yellow, silicon atoms are green and the hydrogen atoms are white.

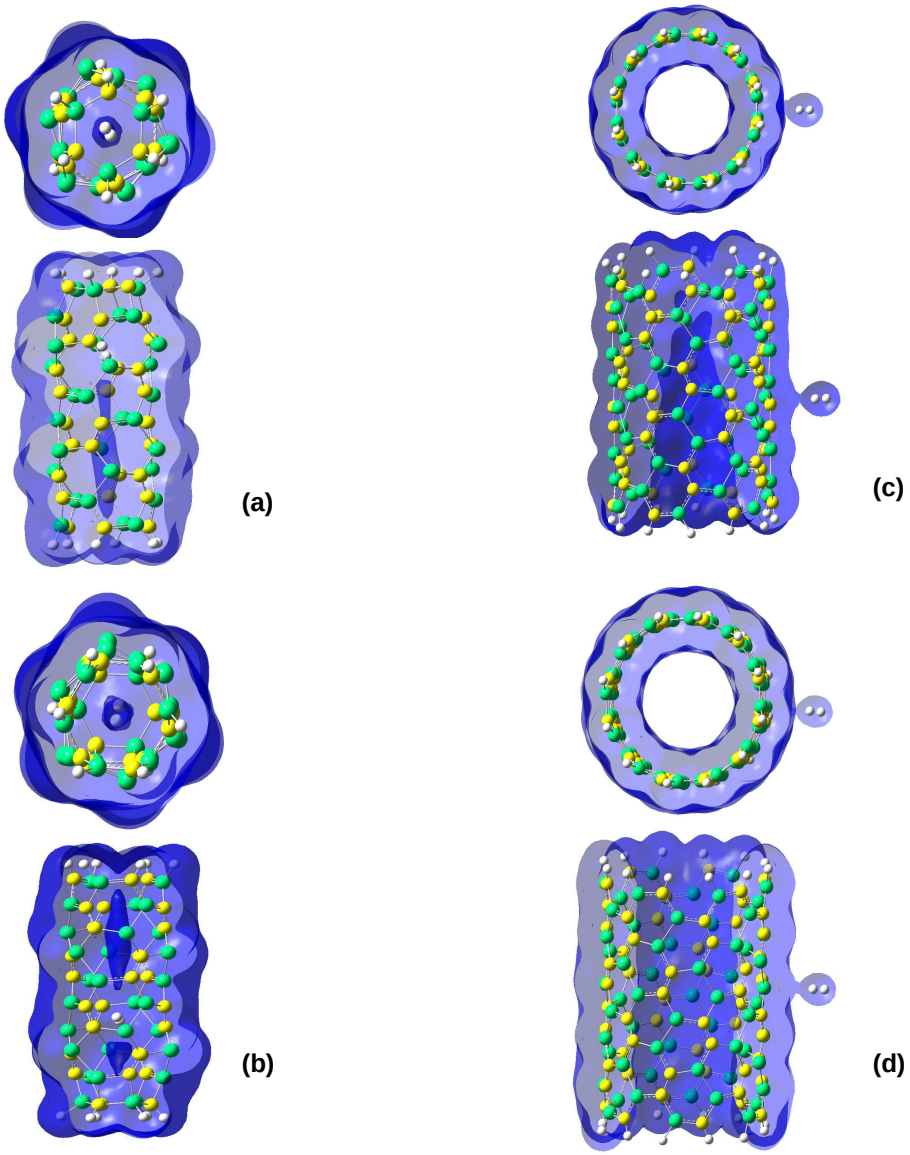

Figure 3.24 Electron charge density plot for (a) adsorption of the hydrogen molecule from inside the nanotube for type 3 (3, 3) T3CSIZB site (b) inside adsorption for type 3 (3, 3) T2CSINB site (c) outer wall adsorption for type 3 (6, 6) T3CSINB site (d) outer wall adsorption for type 3 (6, 6) T3SIT site. All plots have been plotted under similar conditions using an isovalue of 0.002.

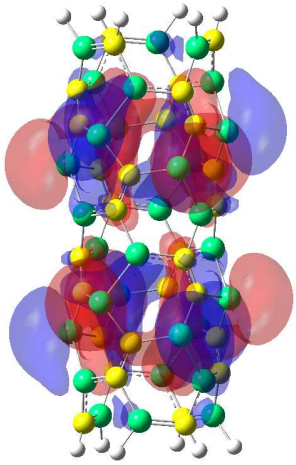

(a)

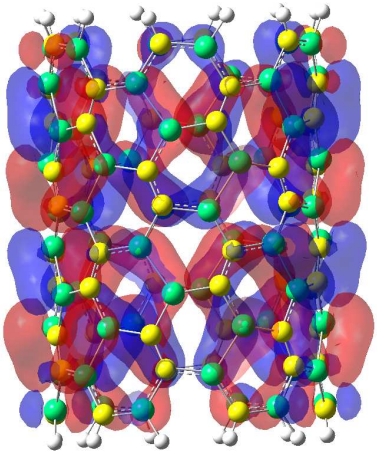

(c)

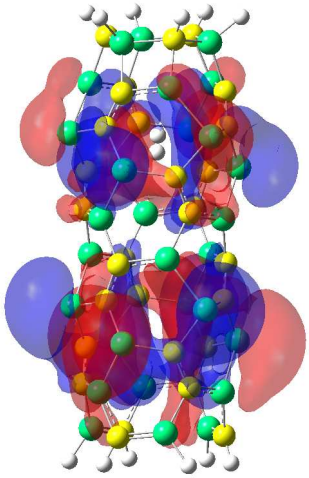

(b)

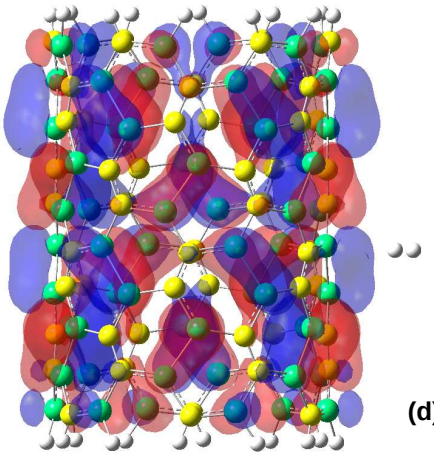

(d)

Figure 3.25 HOMO plots for (a) bare type 3 (3, 3) SiCNT (b) optimized type 3 (3, 3) SiCNT with hydrogen molecule placed inside the nanotube at T3CSIZB site (c) bare type 3 (6, 6) SiCNT (d) optimized type 3 (6, 6) SiCNT with the hydrogen molecule approaching the nanotube from the outer wall at T3CSINB site.

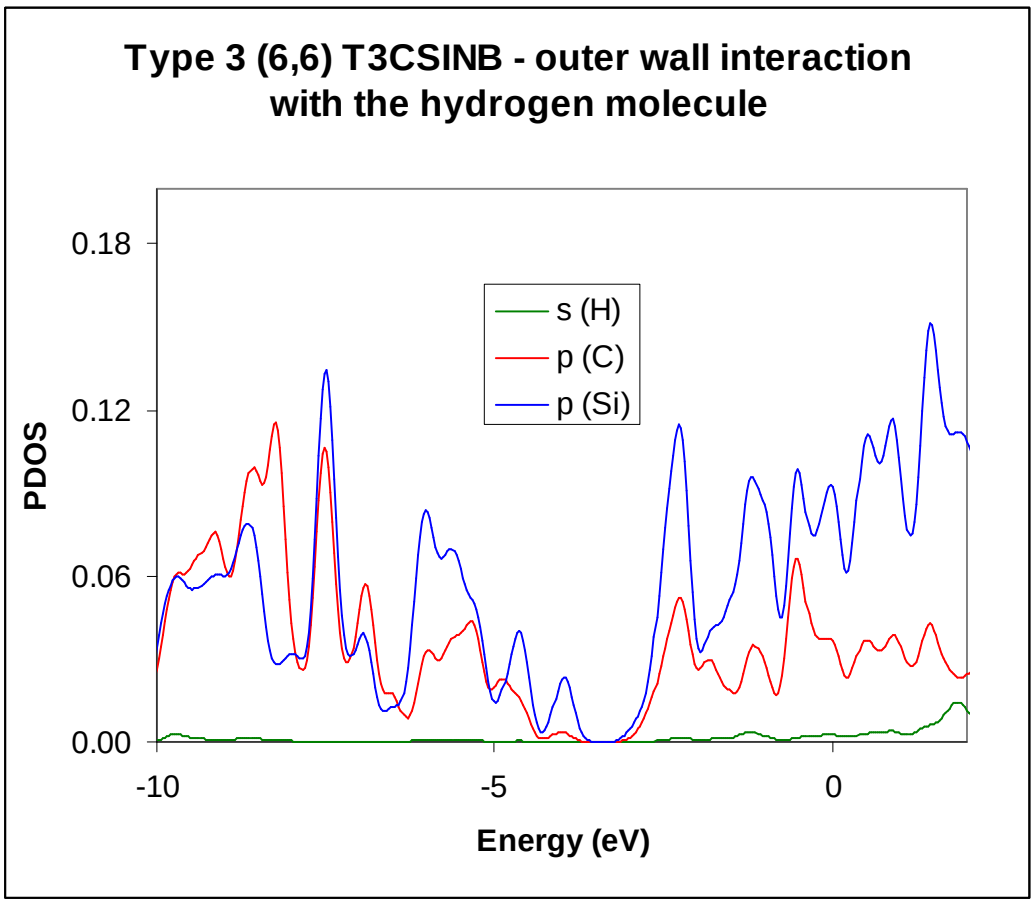

Figure 3.26 Partial density of state plot for the outer wall interaction of the hydrogen molecule with type 3 (6, 6) T3CSINB site. The contributions from two adjacent C and Si atoms for the site and the approaching hydrogen molecule have been used for the PDOS plot.

CHAPTER 4

CO-ADSORPTION OF HYDROGEN MOLECULES IN SIC NANOTUBES

4.1 Available site arrangements in different types of nanotubes

As a natural extension of the single molecular hydrogen adsorption, co-adsorption of two hydrogen molecules has been studied on the same structures used previously for single molecule adsorption and under the same set of conditions. The details have been provided here. A hydrogen molecule is first adsorbed at any of the uniquely available sites in each of the structures. Another hydrogen molecule can be placed in each of the remaining sites available for a particular type. While designating the configuration of the overall structure which includes the bare nanotube and the two adsorbed hydrogen molecules, the type of structure is designated first. The site name where the first hydrogen molecule is placed is stated next. This is followed by a zero which again is followed by the site name for adsorption of the second hydrogen molecule, except the type name, which is mentioned only once at the beginning while designating the “site arrangement” or “site configuration”. For example [Figure. 4.1] for co-adsorption at T1HS site in type 1 nanotube, after the adsorption of the first hydrogen molecule, there are 4 possible adsorption sites for the second molecule. These are T1CSINB, T1CT, T1CSIZB and T1SIT. So when both hydrogen molecules are adsorbed, one at T1HS site and say the other one at T1CSINB site, the overall configuration of the structure is designated as T1HS0CSINB. Similarly the other possible co-adsorption site arrangements for type 1 structures are T1HS0CT, T1HS0CSIZB and T1HS0SIT. This is with the first molecule placed at T1HS site. The hybrid density functional B3LYP is used as the functional for co-adsorption of hydrogen molecules. The basis set and other computational details are the same as in other single molecular hydrogen adsorption calculations, carried out previously.

4.2 Co-adsorption results and discussions

The binding energy (BE) is obtained by comparing the total energy of the spin-optimized composite system SiCNT+2*H_2 with the total energies of the optimized separated systems, namely SiCNT and the two H_2 molecules with the 3-21G* basis set:

BE = E (SiCNT) + 2*E (H2) – E (SiCNT+H2) (1)

Co-adsorption of hydrogen molecules in type 1 SICNT, with the hydrogen molecules approaching the nanotube from the inner walls, do not show any binding after optimization of the structure. This differs from single hydrogen molecular interaction with type 1 nanotubes where at least three sites, two in (5, 5) and one in (6, 6) show binding. For adsorption at the outer wall of the nanotube, the best binding is given by type 1 (4, 4), with the hydrogen molecules in the T1CSIZB0SIT site configuration. The binding energy in this case is 1.50 kcal/mol [Table 4.1]. The least binding site for type 1 armchair structures ranging from (3, 3) to (6, 6), for outer wall co-adsorption is (6, 6) T1HS0CT site configuration. The binding energy in this case is 0.68 kcal/mol. (3, 3) and (5, 5) structures in type 1 nanotubes do not display any binding when the hydrogen molecules interact with the nanotube from the outer wall. Only two site arrangements in type 1 (4, 4) and three site arrangements in type 1 (6, 6) nanotubes show binding. The bond length of the hydrogen molecules in the structures in type 1 nanotubes where the hydrogen molecules have been co-adsorbed varies between 0.747 Å and 0.748 Å. The distance of the co-adsorbed hydrogen molecules from the nanotube wall are in the range of 3 Å. However, no specific correlation has found between parameters like the distance of the co-adsorbed hydrogen molecules from the nanotube wall and the binding energy. From the data obtained it looks that the distance in this case is dependant on the overall structural configuration. Also the distance between the centers of the two hydrogen molecules which have been co-adsorbed is independent of the binding energy which is guided here more by the overall geometry of the optimized co-adsorbed structure. It is also worth mentioning that the binding energy 1.50 kcal/mol of type 1 (4, 4) T1CSIZB0SIT site arrangement obtained during

co-adsorption is better than the most favorable binding energy of type 1 (4, 4) structures obtained during single hydrogen molecular interaction. It is also better than the best binding energy sites in type 1, which is the energy attained in (5, 5) structures T1CT site. Even the least binding site arrangement during co-adsorption in type 1 (6, 6) nanotubes, which is T1HS0CT site arrangement having a binding energy of 0.68 kcal/mol compares favorably to 0.46 kcal/mol which is the binding energy of the most favorable binding site in type 1 (6, 6) structure. From [Figure. 4.3] we find that the HOMO delocalization initially present in the bare type 1 (6, 6) SICNT nanotube gets localized. The HOMO shifts to one end of the nanotube. However this does not necessarily relate to the binding energy of co-adsorption of the hydrogen molecules. Compared to type 1 (4, 4) T1CSIZB0SIT site arrangement, which gives the best binding energy for type 1 nanotube for outer wall co-adsorption of the hydrogen molecules, the charge overlap of type 1 (6, 6) T1HS0CT site arrangement is considerably less as seen in the electron charge density plot [Figure. 4.4]. Also from the Mulliken charge analysis of optimized type 1 (4, 4) SICNT with two hydrogen molecules placed outside the nanotube in T1CSIZB0SIT site configuration, it is found that hydrogen atoms farthest away from the nanotube walls has a charge loss of -0.022e and -0.024e [Figure. 4.5]. This can be compared to the charge loss of -0.020e and -0.019e of the hydrogen atoms farthest from the nanotube wall in case of type 1 (6, 6) SICNT with two hydrogen molecules placed outside the nanotube in T1HS0CT site configuration [Figure. 4.6].

For outer wall co-adsorption of the hydrogen molecules in type 2 (4, 4) nanotubes the number of binding sites arrangements are considerably more as compared to type 2 (3, 3). Also a very high comparative binding energy of 38.26 kcal/mol is obtained in case of type 2 (4, 4) T2CT0SISIB site configuration which is more than the best binding energy value of 37.52 kcal/mol obtained in case of single hydrogen molecule adsorption obtained in our previous study [Figure. 3.8]. In case of outer wall co-adsorption in type 2 (4, 4) structure twenty site arrangements where binding takes place have been found. The average binding in all these

sites arrangements with the exception of T2CSIB0SISIB is more than 1eV and the binding is chemisorption in nature. In particular, five out of six possible site arrangements where one of the two hydrogen molecules is placed in T2CT or T2CCB site shows extremely high binding energy. In case of co-adsorption in type 2 (5, 5) structures again twenty site arrangements have been found where binding occurs. In particular the site arrangement where one of the hydrogen molecules is placed at T2CCB position shows high binding energy ranging from 0.6eV to 0.7eV. For type 2 (5, 5) structures with outer wall molecular co-adsorption of the hydrogen molecules, the two adsorbed hydrogen molecules are at two diametrically opposite ends of the nanotube. The separation between the centers of the adsorbed hydrogen molecules are in the order of 13 Å to 15 Å. Only seven favorable site arrangements have been found in case of outer wall co-adsorption of the hydrogen molecules for type 2 (6, 6) structures. This trend is in line with our previous study involving hydrogen molecular adsorption on the same structures. The least favorable site arrangement for binding in case of type 2 SiCNT, outer wall adsorption is type 2 (6, 6) T2SISIB0H2S. The binding energy obtained in this case is 0.02 kcal/mol. In case of HOMO plots for optimized type 2 (4, 4) SICNT with hydrogen molecules placed outside the nanotube in T2CT0SISIB site configuration, the delocalization of the HOMO at layers perpendicular to the nanotube wall get partially localized in areas around the same layer [Figure. 4.7]. For the least possible binding site in case of type 2 structures for outside co-adsorption, which is type 2 (6, 6) T2SISIB0H2S site configuration, the HOMO delocalization largely remains unaffected before and after co-adsorption [Figure. 4.8]. The charge overlap in case of type 2 (4, 4) T2CT0SISIB site configuration is distinctly more as compared to type 2 (6, 6) T2SISIB0H2S site configuration [Figure. 4.9]. The Mulliken charge analysis of the two above structures shows the hydrogen atoms farthest away from the nanotube walls has a charge loss of -0.019e and -0.009e in case of type 2 (4, 4) nanotube in T2CT0SISIB site configuration [Figure. 4.10]. This can be compared to the charge loss of -0.015e and -0.004e of the hydrogen atoms farthest from the nanotube wall in case of type 2 (6, 6) SICNT with two hydrogen

molecules placed outside the nanotube in T2SISIB0H2S site configuration [Figure. 4.11]. For type 2 co-adsorption of the hydrogen molecules at the inner wall of the nanotube, several (4, 4) site configurations show a very high comparative binding energy. The best binding energy site is type 2 (4, 4) T2SISIB0CSIB site configuration which exhibits a binding energy of 37.27 kcal/mol [Table 4.3]. Type 2 (5, 5) show lower binding energy compared to (4, 4) sites. The least binding energy in case of type 2 site configuration where binding does occur is type 2 (5, 5) and is equal to 13.97 kcal/mol [Table 4.3]. The HOMO delocalization of type 2 (4, 4) bare SICNT gets partially localized after co-adsorption of the hydrogen molecules as in T2SISIB0CSIB site configuration [Figure. 4.12]. In case of type 2 (5, 5) SICNT with hydrogen molecules placed inside the nanotube in T2H2S0SISIB site configuration, the localization after adsorption results in slight shift in the HOMO to one end of the nanotube after co-adsorption [Figure. 4.13]. The electron charge density plot for co-adsorption of two hydrogen molecules from inside the nanotube in type 2 (4, 4) T2SISIB0CSIB site configuration has been compared to the co-adsorption of two hydrogen molecules from inside the nanotube in type 2 (5, 5) T2H2S0SISIB site configuration. The charge overlap is strong in both cases. The Mulliken charge analysis of optimized type 2 (4, 4) SICNT with two hydrogen molecules approaching the nanotube wall from inside the nanotube in T2SISIB0CSIB site configuration, show the hydrogen atoms belonging to the adsorbed hydrogen molecules gaining charge. This holds true for both type 2 (4, 4) and type 2 (5, 5) inner wall co-adsorptions [Figure. 4.15, 4.16]. For outer wall adsorption, some atoms in the adsorbed hydrogen molecules gain charge while the other looses.

In case of co-adsorption of hydrogen molecules in type 3 structures from the outer wall, the site configuration which shows the best binding energy is type 3 (6, 6) T3CTO0CSIZB site configuration. The binding energy obtained is 1.58 kcal/mol. The least favorable binding site has a binding energy of 0.17 kcal/mol in case of type 3 (4, 4), T3SISIB0SIT site configuration [Table 4.4]. Thus in case of type 3 the nanotubes having higher diameter have a better or comparable binding energy than nanotubes having smaller diameter. This is the reverse trend as compared

to type 1 and type 2, where the nanotubes having smaller diameter also have better binding energy for co-adsorption. The electron density plots and the Mulliken charge analysis confirm the better binding site potential of type 3 (6, 6) T3CT0CSIZB configuration as compared to type 3 (4, 4), T3SISIB0SIT site configuration [Figure. 4.19 - 4.21]. The trend is however same as what was observed during molecular adsorption. For type 3 inner wall co-adsorption, only type 3 (6, 6) structures have shown binding. The most favorable binding site configuration is T3HS0SISIB which gives a binding energy of 0.64 kcal/mol as compared to T3SISIB0CSIZB adsorption site which gives the least binding energy of 0.10 kcal/mol. The HOMO plots for type 2 (4, 4) SiCNT with hydrogen molecules placed inside the nanotube in T2SISIB0CSIB site configuration and the T3HS0SISIB site configuration show no change in the original HOMO delocalization of the bare nanotube structure [Figure. 4.12].However the binding energy in both cases are low and the electron charge density plots and the Mulliken charge plots do not lead to any major comparison amongst the two.

Table 4.1 Optimized parameters of co-adsorbed structure for adsorption at type 1 nanotube wall. The hydrogen molecules are approaching the nanotube wall from outside.

Nanostructure name / Site name	Binding energy in kcal	Bond length of the first hydrogen molecule in Å	Bond length of the second hydrogen molecule in Å	Distance of the first hydrogen molecule from the nanotube wall in Å	Distance of the second hydrogen molecule from the nanotube wall in Å	Distance between the centre of the two hydrogen molecules in Å	Binding energy in kcal/mol
T144/ T1CSIZB0SIT	1.50	0.748	0.747	3.14	3.10	1.32	0.75
T144/ T1CSIZB0HS	1.45	0.748	0.748	3.07	3.47	4.17	0.73
T166/ T1CSINB0HS	0.79	0.748	0.747	3.18	2.99	3.41	0.40
T166/ T1CSINB0CSIZB	0.78	0.748	0.748	3.16	3.64	4.13	0.39
T166/ T1HS0CT	0.68	0.748	0.748	3.13	3.53	3.95	0.34

Table 4.2 Optimized parameters of co-adsorbed structure for adsorption at type 2 nanotube wall. The hydrogen molecules are approaching the nanotube wall from outside.

Nanostructure name / Site name	Binding energy in kcal	Bond length of the first hydrogen molecule in Å	Bond length of the second hydrogen molecule in Å	Distance of the first hydrogen molecule from the nanotube wall in Å	Distance of the second hydrogen molecule from the nanotube wall in Å	Distance between the centre of the two hydrogen molecules in Å	Binding energy in kcal/mol
T233/ T2SIT0CSIB	0.56	0.748	0.747	3.31	6.62	3.45	0.28
T244/ T2CT0SISIB	38.26	0.749	0.748	3.25	3.46	5.80	19.13
T244/ T2CT0H2S	36.91	0.748	0.747	3.85	3.40	5.95	18.46
T244/ T2H1S0SISIB	29.53	0.717	0.716	3.66	3.01	1.96	14.77
T244/ T2SIT0H2S	34.74	0.747	0.748	3.88	3.90	3.04	17.37
T244/ T2H1S0SIT	29.03	0.748	0.747	4.62	3.10	2.82	14.52
T244/ T2CT0CCB	37.14	0.749	0.749	3.31	3.38	3.02	18.57
T244/ T2SISIB0CCB	29.64	0.747	0.747	6.55	3.12	7.08	14.82
T244/ T2CT0SIT	38.19	0.748	0.749	3.28	3.27	5.31	19.10
T244/ T2CCB0CSIB	29.04	0.747	0.747	4.49	3.79	2.90	14.52

Table 4.2 – *Continued*

Nanostructure name / Site name	Binding energy in kcal	Bond length of the first hydrogen molecule in Å	Bond length of the second hydrogen molecule in Å	Distance of the first hydrogen molecule from the nanotube wall in Å	Distance of the second hydrogen molecule from the nanotube wall in Å	Distance between the centre of the two hydrogen molecules in Å	Binding energy in kcal/mol
T244/ T2CCB0H1S	29.41	0.747	0.748	3.84	3.27	2.91	14.71
T244/ T2CCB0SIT	35.01	0.747	0.747	3.92	3.79	4.10	17.50
T244/ T2CCB0H2S	28.99	0.747	0.748	4.94	3.91	5.26	14.50
T244/ T2CSIB0H1S	38.06	0.748	0.748	4.15	3.30	3.10	19.03
T244/ T2H1S0CT	29.87	0.748	0.747	3.85	3.72	3.15	14.94
T244/ T2H1S0H2S	29.23	0.747	0.748	3.20	3.15	3.95	14.62
T244/ T2CSIB0H1S	38.06	0.748	0.748	3.00	3.25	4.00	19.03
T244/ T2CSIB0SISIB	0.35	0.747	0.748	3.45	3.67	3.82	17.50
T244/ T2SIT0SISIB	34.45	0.747	0.747	3.32	3.56	3.88	17.23
T244/ T2SIT0CSIB	37.42	0.747	0.748	3.45	3.66	4.01	18.71
T244/ T2CT0H1S	29.87	0.748	0.748	3.54	3.29	3.97	14.94

.

Table 4.2 – *Continued*

Nanostructure name / Site name	Binding energy in kcal	Bond length of the first hydrogen molecule in Å	Bond length of the second hydrogen molecule in Å	Distance of the first hydrogen molecule from the nanotube wall in Å	Distance of the second hydrogen molecule from the nanotube wall in Å	Distance between the centre of the two hydrogen molecules in Å	Binding energy in kcal/mol
T255/ T2CT0H2S	15.74	0.748	0.747	3.65	3.43	13.88	7.87
T255/ T2CSIB0SIT	0.56	0.747	0.747	3.53	3.63	13.41	0.28
T255/ T2SIT0CT	0.31	0.747	0.748	3.89	3.11	13.50	0.16
T255/ T2SIT0SISIB	0.33	0.747	0.747	3.45	3.46	13.66	0.17

Table 4.2 – *Continued*

Nanostructure name / Site name	Binding energy in kcal	Bond length of the first hydrogen molecule in Å	Bond length of the second hydrogen molecule in Å	Distance of the first hydrogen molecule from the nanotube wall in Å	Distance of the second hydrogen molecule from the nanotube wall in Å	Distance between the centre of the two hydrogen molecules in Å	Binding energy in kcal/mol
T255/ T2CSIB0SISIB	0.43	0.747	0.747	3.86	3.95	15.12	0.22
T255/ T2SISIB0CCB	0.28	0.748	0.747	3.66	3.78	13.98	0.14
T255/ T2CT0SISIB	0.27	0.747	0.748	3.56	3.61	14.26	0.14
T255/ T2SISIB0H1S	14.68	0.748	0.747	3.60	3.62	13.99	7.34
T255/ T2SISIB0H2S	17.72	0.748	0.748	3.33	3.28	14.05	8.86
T255/ T2SIT0SISIB	0.33	0.747	0.747	3.31	3.88	15.01	0.17
T255/ T2CCB0CSIB	14.96	0.748	0.747	3.67	3.98	13.87	7.48
T255/ T2CCB0H1S	15.52	0.747	0.748	3.88	3.79	14.89	7.76
T255/ T2CT0H1S	0.47	0.748	0.748	3.72	3.56	13.56	0.24
T255/ T2H1S0CSIB	0.33	0.747	0.748	3.61	3.43	14.56	0.17
T255/ T2SIT0H1S	0.47	0.747	0.747	3.67	3.28	13.77	0.24
T255/ T2SIT0H2S	0.23	0.747	0.748	3.15	3.85	14.63	0.12

Table 4.2 – *Continued*

Nanostructure name / Site name	Binding energy in kcal	Bond length of the first hydrogen molecule in Å	Bond length of the second hydrogen molecule in Å	Distance of the first hydrogen molecule from the nanotube wall in Å	Distance of the second hydrogen molecule from the nanotube wall in Å	Distance between the centre of the two hydrogen molecules in Å	Binding energy in kcal/mol
T255/ T2CSIBO0CT	0.12	0.748	0.747	3.23	3.67	15.01	0.06
T255/ T2CSIB0SISIB	0.43	0.747	0.748	3.45	3.15	14.03	0.22
T255/ T2CCB0CT	14.47	0.748	0.747	3.75	3.98	13.57	7.24
T255/ T2CCB0SISIB	15.24	0.747	0.748	3.26	3.58	13.66	7.62
T266/ T2SIT0CCB	0.38	0.748	0.748	3.44	3.72	13.88	0.19
T266/ T2SIT0CSIB	0.36	0.747	0.747	3.21	3.56	13.69	0.18
T266/ T2SIT0CT	0.34	0.748	0.747	3.62	3.85	4.25	0.17
T266/ T2SIT0H1S	0.53	0.747	0.748	3.20	3.34	4.32	0.27
T266/ T2SISIB0H2S	0.02	0.747	0.748	3.25	2.96	4.85	0.01
T266/ T2H2S0CT	0.26	0.747	0.747	3.60	3.01	4.44	0.13
T266/ T2SIT0H2S	0.53	0.747	0.748	3.51	3.63	4.63	0.27

Table 4.3 Optimized parameters of co-adsorbed structure for adsorption at type 2 nanotube wall. The hydrogen molecules are approaching the nanotube wall from inside.

Nanostructure name / Site name	Binding energy in kcal	Bond length of the first hydrogen molecule in Å	Bond length of the second hydrogen molecule in Å	Distance of the first hydrogen molecule from the nanotube wall in Å	Distance of the second hydrogen molecule from the nanotube wall in Å	Distance between the centre of the two hydrogen molecules in Å	Binding energy in kcal/mol
T244/ T2SIT0CT	26.90	0.750	0.749	2.91	3.05	3.38	13.45
T244/ T2CT0H1S	37.14	0.749	0.750	2.93	2.97	3.21	18.57
T244/ T2SIT0CSIB	30.34	0.750	0.750	2.97	2.69	3.15	15.17
T244/ T2SIT0H2S	29.89	0.750	0.749	2.87	2.89	3.01	14.95
T244/ T2SISIB0CSIB	37.27	0.750	0.749	2.95	3.45	3.20	18.64
T244/ T2CCB0SISIB	30.72	0.750	0.750	2.81	2.76	3.19	15.36
T244/ T2CCB0CSIB	29.82	0.749	0.749	2.63	2.85	3.39	14.91
T244/ T2CCB0H1S	29.88	0.749	0.750	2.59	2.48	3.11	14.94
T244/ T2CCB0H2S	30.84	0.749	0.749	2.28	2.32	3.41	15.42
T244/ T2CCB0CT	29.69	0.750	0.750	2.61	2.45	3.56	14.85
T255/ T2CSIB0SISIB	16.93	0.749	0.747	4.23	4.18	2.67	8.47

Table 4.3 – *Continued*

Nanostructure name / Site name	Binding energy in kcal	Bond length of the first hydrogen molecule in Å	Bond length of the second hydrogen molecule in Å	Distance of the first hydrogen molecule from the nanotube wall in Å	Distance of the second hydrogen molecule from the nanotube wall in Å	Distance between the centre of the two hydrogen molecules in Å	Binding energy in kcal/mol
T255/ T2CSIB0SIT	15.70	0.749	0.748	4.11	4.48	2.62	7.85
T255/ T2H2S0SISIB	13.97	0.750	0.747	4.25	4.06	2.72	6.99

Table 4.4 Optimized parameters of co-adsorbed structure for adsorption at type 3 nanotube wall. The hydrogen molecules are approaching the nanotube wall from outside.

Nanostructure name / Site name	Binding energy in kcal	Bond length of the first hydrogen molecule in Å	Bond length of the second hydrogen molecule in Å	Distance of the first hydrogen molecule from the nanotube wall in Å	Distance of the second hydrogen molecule from the nanotube wall in Å	Distance between the centre of the two hydrogen molecules in Å	Binding energy in kcal/mol
T344/ T3CT0CSINB	0.71	0.747	0.748	3.31	3,45	3.21	0.36
T344/ T3CT0SISIB	0.60	0.747	0.747	3.46	3.17	3.09	0.30
T344/ T3SIT0CSIZB	0.33	0.748	0.747	3.20	3.17	3.05	0.17
T344/ T3SIT0CSINB	0.24	0.748	0.748	3.51	3.74	3.33	0.12
T344/ T3CT0CSIZB	0.40	0.747	0.748	3.11	2.97	3.28	0.20
T344/ T3CT0SIT	0.50	0.747	0.748	3.47	3.00	3.16	0.25
T344/ T3CT0CCB	0.41	0.748	0.748	4.06	3.91	3.13	0.21
T344/ T3SIT0CCB	0.49	0.748	0.747	3.07	2.98	3.02	0.25
T344/ T3SISIB0CCB	0.61	0.747	0.748	3.05	3.43	3.30	0.31
T344/ T3SISIB0SIT	0.17	0.748	0.748	3.36	3.14	3.07	0.09
T344/ T3SISIB0CSINB	0.86	0.747	0.747	3.66	3.42	3.22	0.43

Table 4.4 – *Continued*

Nanostructure name / Site name	Binding energy in kcal	Bond length of the first hydrogen molecule in Å	Bond length of the second hydrogen molecule in Å	Distance of the first hydrogen molecule from the nanotube wall in Å	Distance of the second hydrogen molecule from the nanotube wall in Å	Distance between the centre of the two hydrogen molecules in Å	Binding energy in kcal/mol
T344/ T3CSINB0CCB	0.64	0.747	0.747	3.31	3.18	3.12	0.32
T355/ T3CCB0CSINB	0.83	0.748	0.747	3.20	3.14	3.11	0.42
T355/ T3CCB0CT	0.35	0.748	0.748	3.19	3.12	3.00	0.18
T355/ T3CSINB0CSIZB	0.72	0.748	0.748	3.15	3.24	3.24	0.36
T355/ T3CCB0CSIZB	0.33	0.748	0.748	3.21	3.22	3.23	0.17
T355/ T3CSINB0CT	0.72	0.748	0.747	3.45	3.56	3.10	0.36
T355/ T3CSIZB0CT	0.64	0.748	0.747	3.11	3.22	3.19	0.32
T366/ T3CT0CSIZB	1.58	0.749	0.748	3.30	3.47	3.53	0.79
T366/ T3SISIB0SIT	1.03	0.747	0.748	3.29	3.67	3.46	0.52
T366/ T3CSINB0SIT	1.25	0.747	0.748	3.47	3.62	3.56	0.63
T366/ T3CSINB0CSIZB	0.56	0.747	0.747	3.12	3.08	3.74	0.28

Table 4.4 – *Continued*

Nanostructure name / Site name	Binding energy in kcal	Bond length of the first hydrogen molecule in Å	Bond length of the second hydrogen molecule in Å	Distance of the first hydrogen molecule from the nanotube wall in Å	Distance of the second hydrogen molecule from the nanotube wall in Å	Distance between the centre of the two hydrogen molecules in Å	Binding energy in kcal/mol
T366/ T3CSINB0HS	1.07	0.747	0.747	3.31	3.48	3.54	0.54
T366/ T3HS0CSIZB	1.48	0.748	0.747	3.13	3.70	3.17	0.74
T366/ T3HS0SIT	0.78	0.748	0.748	3.54	3.42	3.63	0.39

Table 4.5 Optimized parameters of co-adsorbed structure for adsorption at type 3 nanotube wall. The hydrogen molecules are approaching the nanotube wall from inside.

Nanostructure name / Site name	Binding energy in kcal	Bond length of the first hydrogen molecule in Å	Bond length of the second hydrogen molecule in Å	Distance of the first hydrogen molecule from the nanotube wall in Å	Distance of the second hydrogen molecule from the nanotube wall in Å	Distance between the centre of the two hydrogen molecules in Å	Binding energy in kcal/mol
T366/ T3HS0CT	0.36	0.748	0.747	3.21	3.45	3.24	0.18
T366/ T3HS0SISIB	0.64	0.747	0.747	3.28	3.95	3.27	0.32
T366/ T3HS0SIT	0.29	0.748	0.747	3.21	3.31	3.54	0.15
T366/ T3SIT0CSINB	0.43	0.747	0.748	3.26	3.17	3.19	0.22
T366/ T3SIT0CSIZB	0.32	0.748	0.747	3.41	3.23	3.25	0.16
T366/ T3SIT0SISIB	0.27	0.747	0.747	3.17	3.19	3.18	0.14
T366/ T3CCB0CT	0.30	0.748	0.748	3.22	3.45	3.26	0.15
T366/ T3CCB0CSINB	0.27	0.748	0.748	3.18	3.40	3.17	0.14
T366/ T3CCB0CSIZB	0.32	0.747	0.747	3.25	3.47	3.34	0.16
T366/ T3CCB0HS	0.13	0.748	0.748	3.28	3.21	3.22	0.07
T366/ T3HS0CSIZB	0.61	0.747	0.748	3.22	3.41	3.19	0.31

Table 4.5 – *Continued*

Nanostructure name / Site name	Binding energy in kcal	Bond length of the first hydrogen molecule in Å	Bond length of the second hydrogen molecule in Å	Distance of the first hydrogen molecule from the nanotube wall in Å	Distance of the second hydrogen molecule from the nanotube wall in Å	Distance between the centre of the two hydrogen molecules in Å	Binding energy in kcal/mol
T366/ T3CT0HS	0.40	0.747	0.748	4.21	3.49	3.31	0.20
T366/ T3SIT0CCB	0.59	0.747	0.747	3.46	3.98	3.23	0.30
T366/ T3SIT0HS	0.35	0.747	0.747	3.14	3.89	3.34	0.18
T366/ T3SISIB0CCB	0.40	0.747	0.747	4.21	3.26	3.45	0.20
T366/ T3SISIB0CSINB	0.40	0.747	0.748	3.45	3.01	3.00	0.20
T366/ T3SISIB0CSIZB	0.10	0.747	0.747	4.76	3.25	3.34	0.05
T366/ T3SISIB0CT	0.50	0.747	0.748	3.97	3.00	3.17	0.25

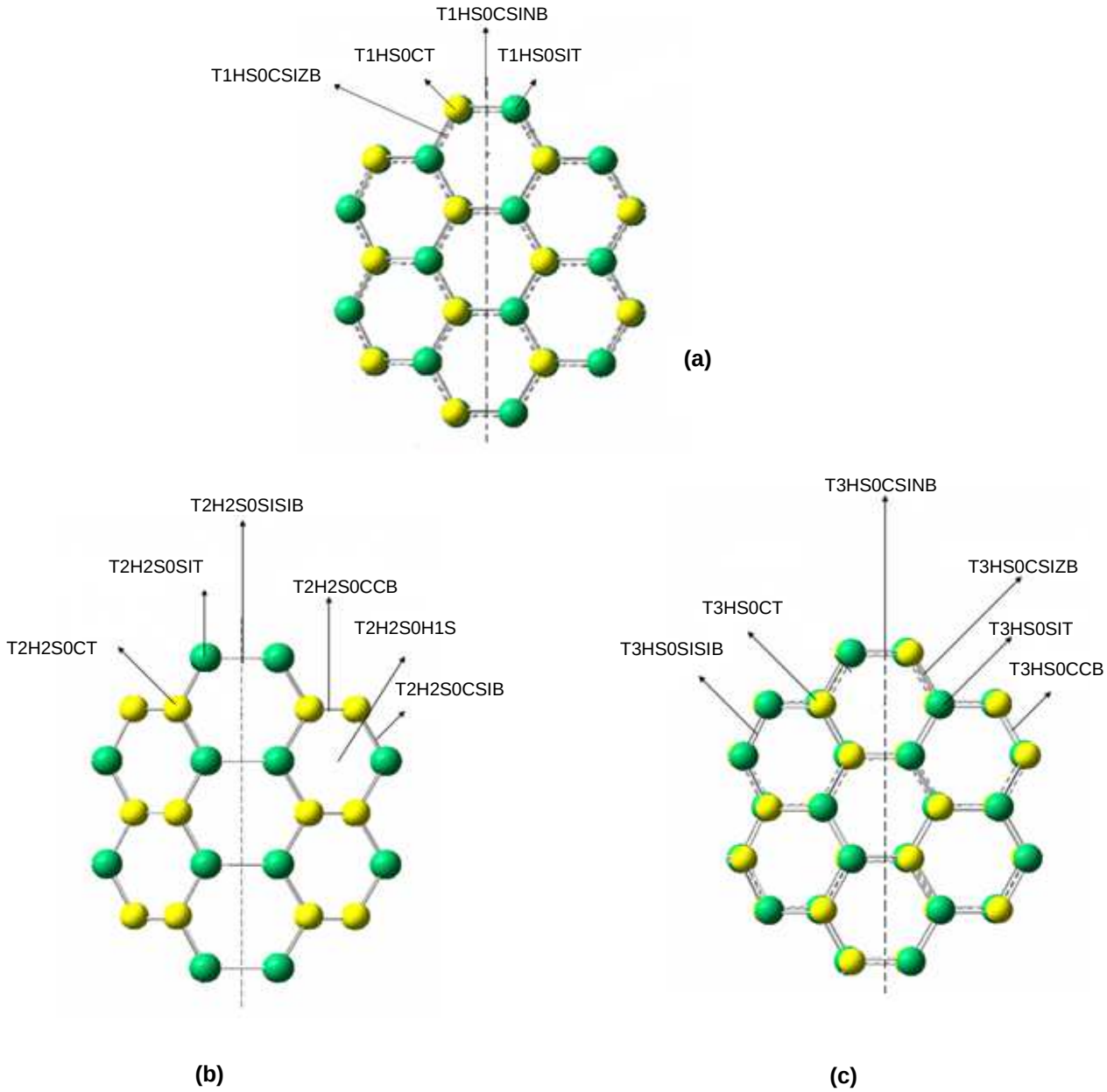

Figure 4.1 Atomic arrangements and different co-adsorption sites for (a) T1HS, (b) T2H2S and (c) T3HS nanotubes. The carbon atoms are yellow and silicon atoms are green. The dashed lines represent the orientation of tube axis.

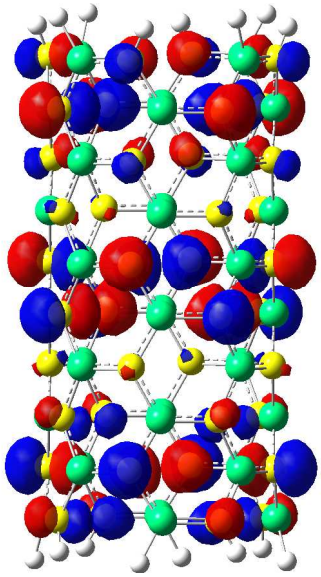

(a)

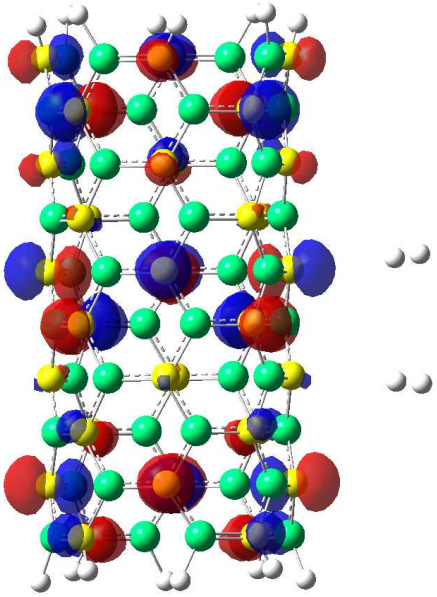

(b)

Figure 4.2 HOMO plots for (a) bare type 1 optimized (4, 4) SICNT (b) optimized type 1 (4, 4) SICNT with hydrogen molecules placed inside the nanotube in T1CSIZB0SIT site configuration. The two hydrogen molecules are approaching the nanotube from the outer wall.

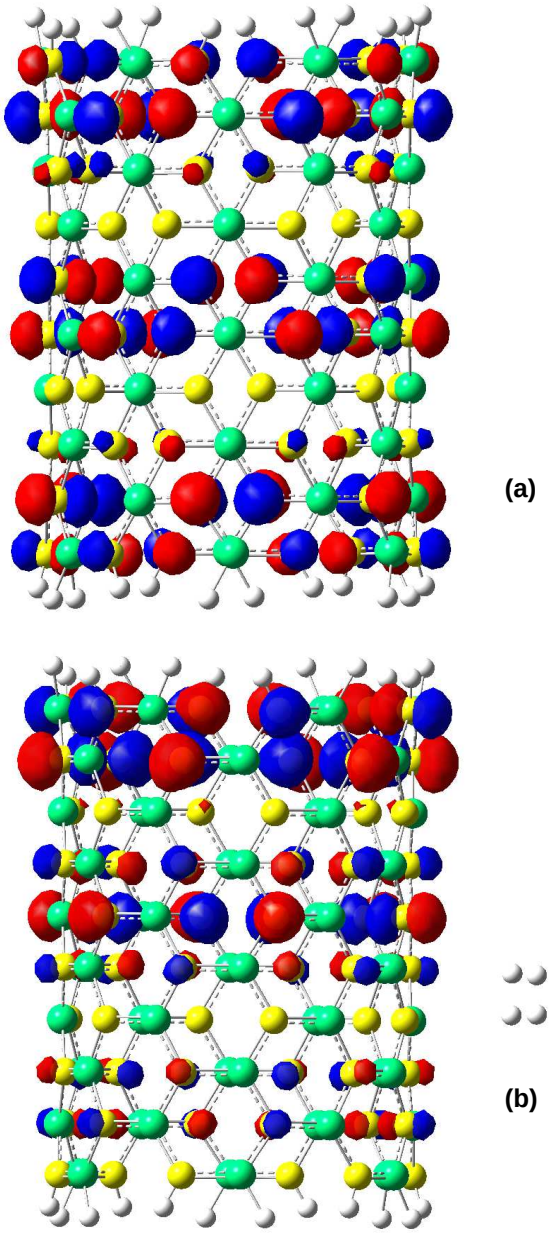

Figure 4.3 HOMO plots for (a) bare type 1 optimized (6, 6) SICNT (b) optimized type 1 (6, 6) SICNT with hydrogen molecules placed inside the nanotube in T1HS0CT site configuration. The two hydrogen molecules are approaching the nanotube from the outer wall.

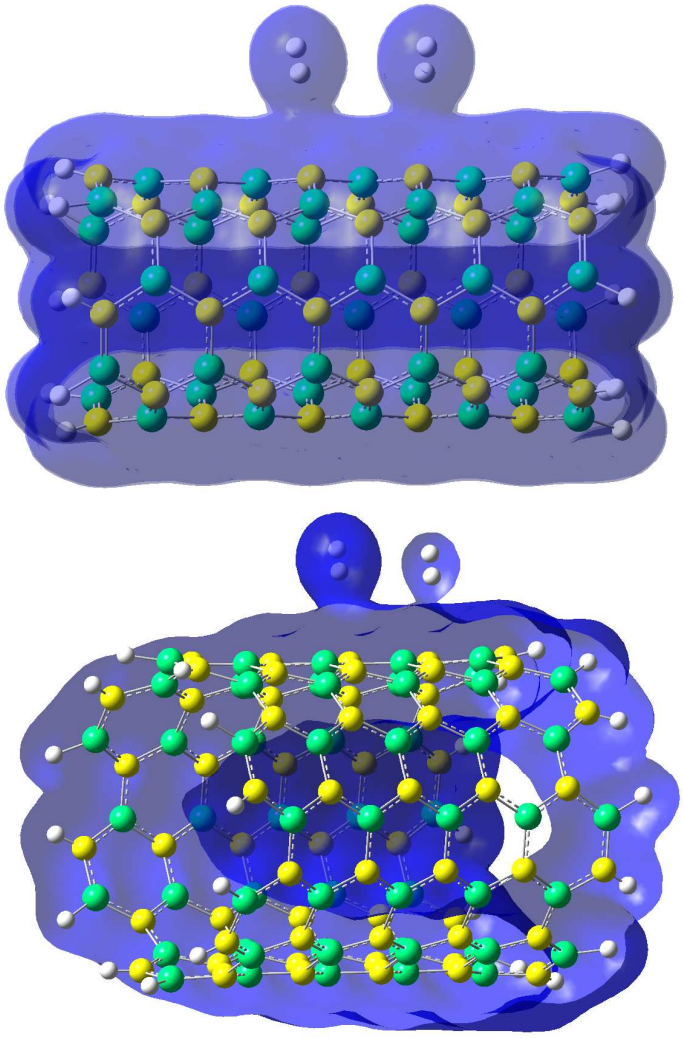

(a)

(b)

Figure 4.4 Electron charge density plot for (a) co-adsorption of two hydrogen molecules from outside the nanotube in type 1 (4, 4) T1CSIZB0SIT site configuration (b) co-adsorption of two hydrogen molecules from outside the nanotube in type 1 (6, 6) T1HS0CT site configuration. All plots have been plotted under similar conditions using an isovalue of 0.002.

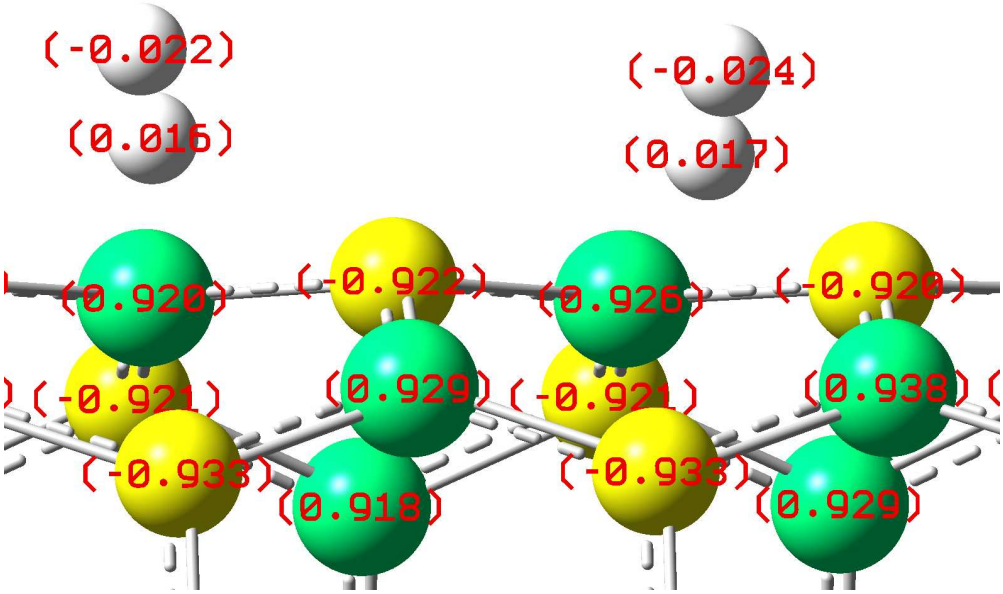

Figure 4.5 Mulliken charge plot of optimized type 1 (4, 4) SICNT with two hydrogen molecules placed outside the nanotube in T1CSIZB0SIT site configuration. The carbon atoms are yellow, silicon atoms are green and the hydrogen atoms are white.

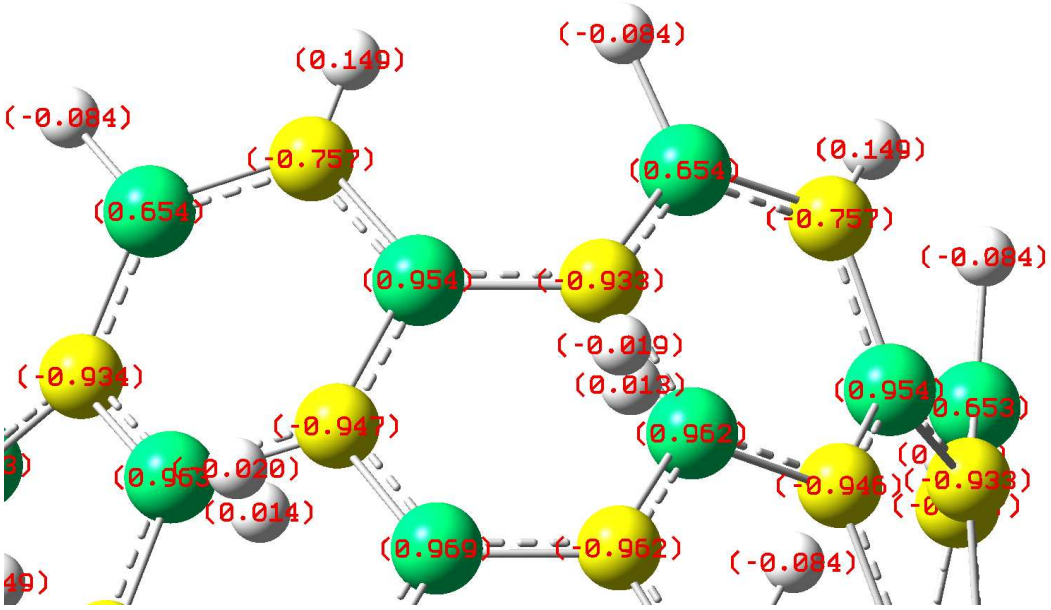

Figure 4.6 Mulliken charge plot of optimized type 1 (6, 6) SICNT with two hydrogen molecules placed outside the nanotube in T1HS0CT site configuration. The carbon atoms are yellow, silicon atoms are green and the hydrogen atoms are white.

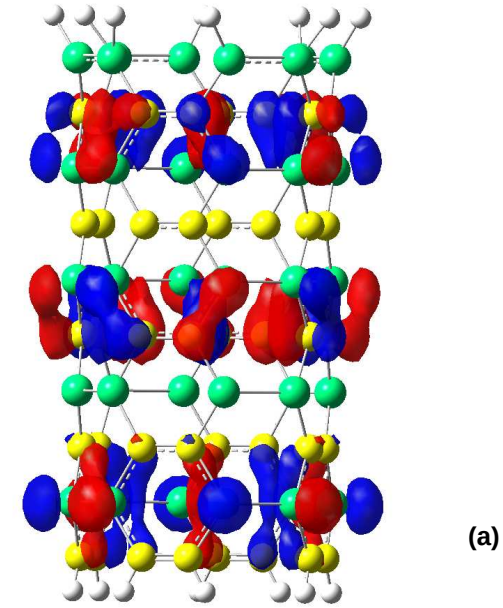

(a)

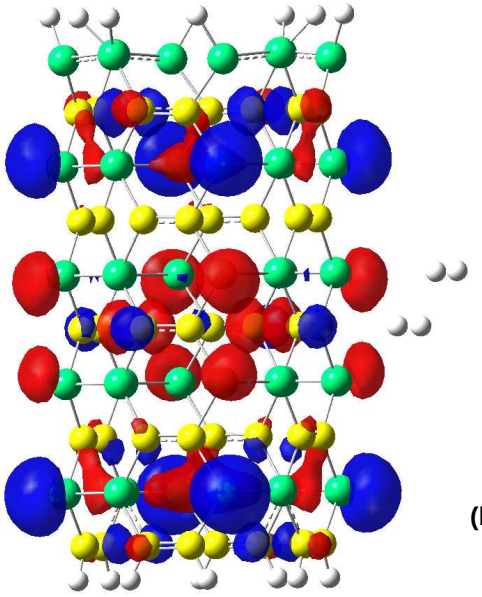

(b)

Figure 4.7 HOMO plots for (a) bare type 2 optimized (4, 4) SiCNT (b) optimized type 2 (4, 4) SiCNT with hydrogen molecules co-adsorbed outside the nanotube in T2CT0SISIB site configuration. The two hydrogen molecules are approaching the nanotube from the outer wall.

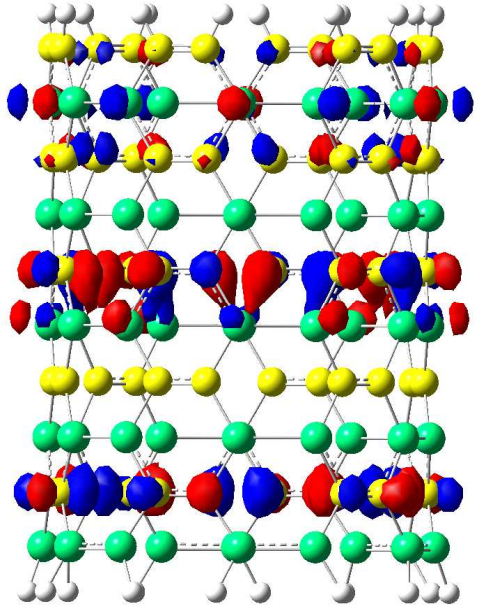

(a)

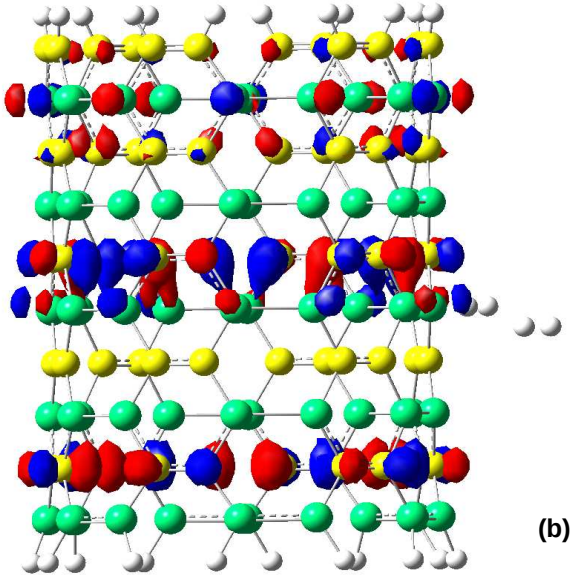

(b)

Figure 4.8 HOMO plots for (a) bare type 2 optimized (6, 6) SiCNT (b) optimized type 2 (6, 6) SiCNT with hydrogen molecules placed outside the nanotube in T2SISIB0H2S site configuration. The two hydrogen molecules are approaching the nanotube from the outer wall.

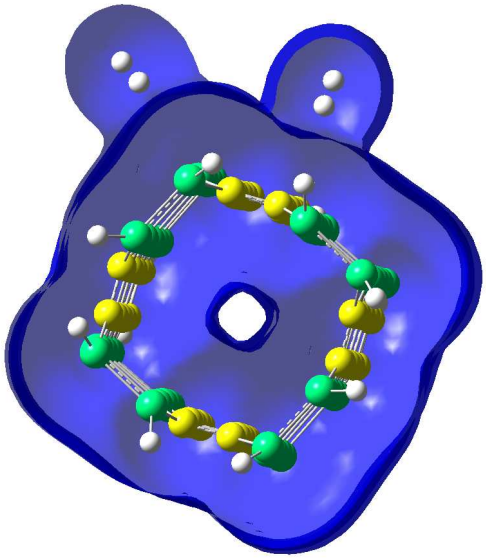

(a)

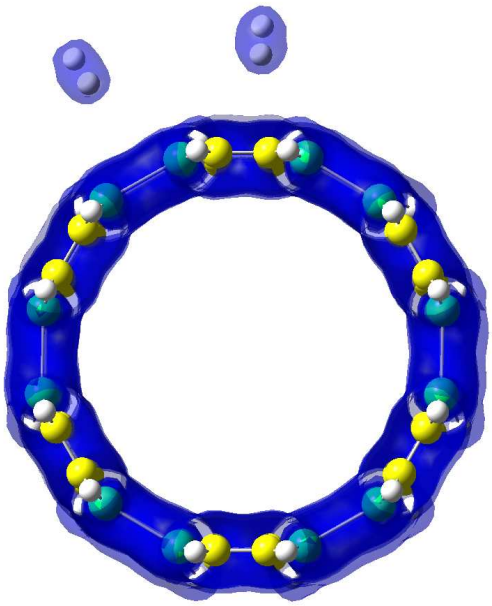

(b)

Figure 4.9 Electron charge density plot for (a) co-adsorption of two hydrogen molecules from outside the nanotube in type 2 (4, 4) T2CT0SISIB site arrangement (b) co-adsorption of two hydrogen molecules from outside the nanotube in type 2 (6, 6) T2SISIB0H2S site arrangement. All plots have been plotted under similar conditions using an isovalue of 0.002.

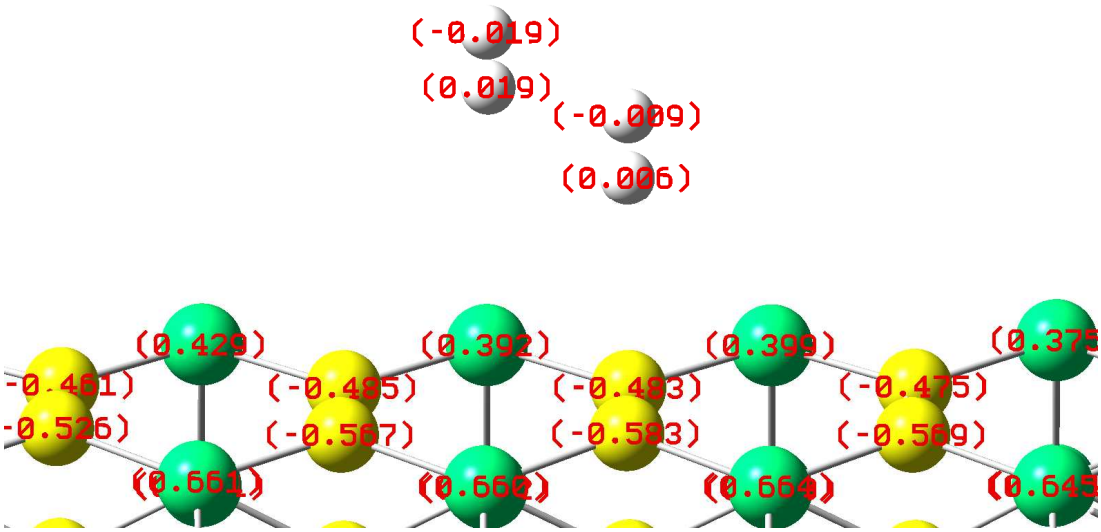

Figure 4.10 Mulliken charge plot of optimized type 2 (4, 4) SICNT with two hydrogen molecules placed outside the nanotube in T2CT0SISIB site configuration. The carbon atoms are yellow, silicon atoms are green and the hydrogen atoms are white.

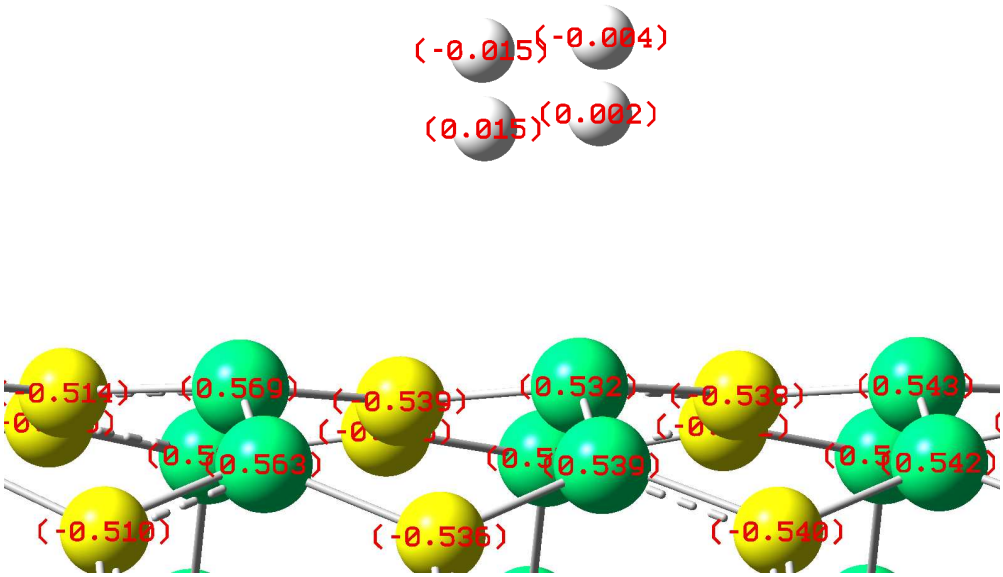

Figure 4.11 Mulliken charge plot of optimized type 2 (6, 6) SICNT with two hydrogen molecules placed outside the nanotube in T2SISIB0H2S site configuration. The carbon atoms are yellow, silicon atoms are green and the hydrogen atoms are white.

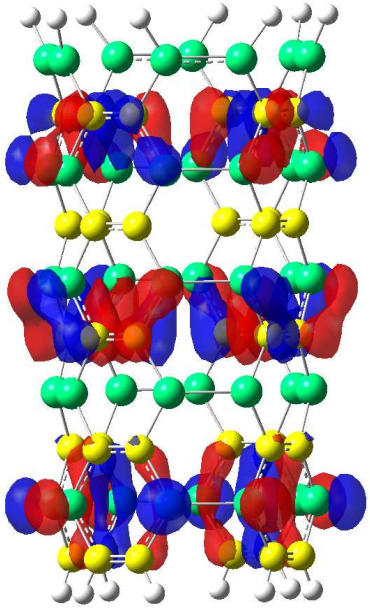

(a)

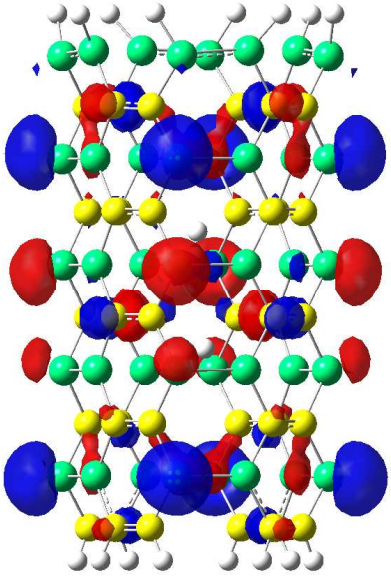

(b)

Figure 4.12 HOMO plots for (a) bare type 2 optimized (4, 4) SiCNT (b) optimized type 2 (4, 4) SiCNT with hydrogen molecules placed inside the nanotube in T2SISIB0CSIB site configuration. The two hydrogen molecules are approaching the nanotube from the inner wall.

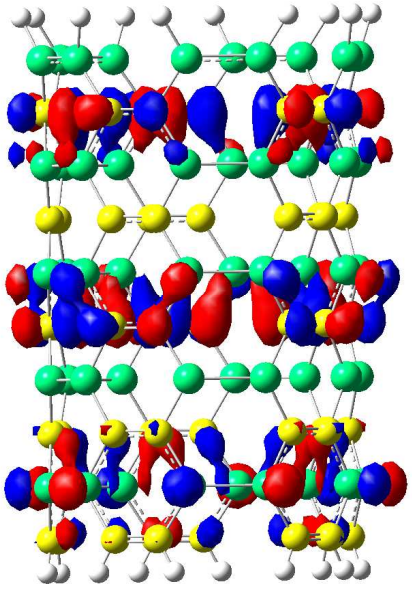

(a)

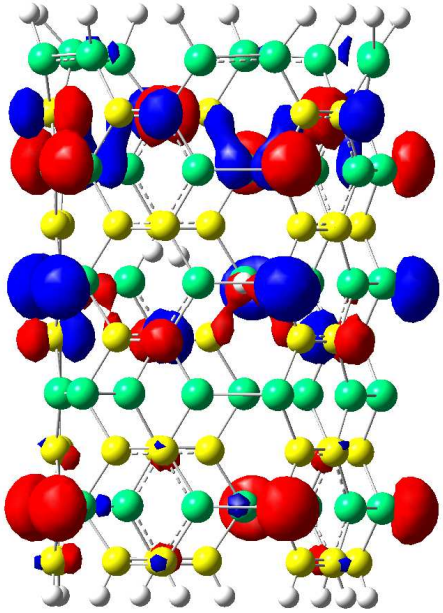

(b)

Figure 4.13 HOMO plots for (a) bare type 2 optimized (5, 5) SICNT (b) optimized type 2 (5, 5) SICNT with hydrogen molecules placed inside the nanotube in T2H2S0SISIB site configuration. The two hydrogen molecules are approaching the nanotube from the inner wall.

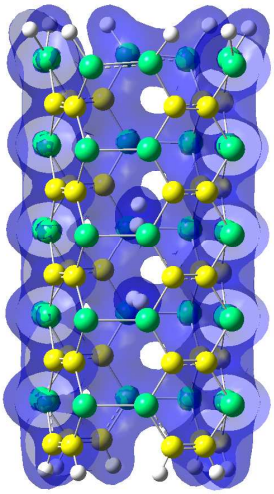

(a)

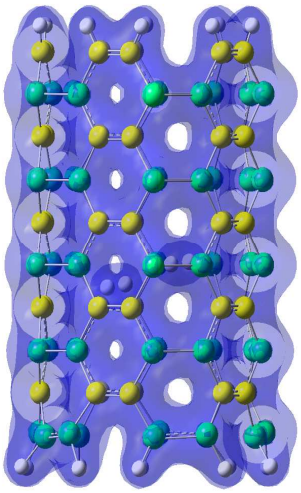

(b)

Figure 4.14 Electron charge density plot for (a) co-adsorption of two hydrogen molecules from inside the nanotube in type 2 (4, 4) T2SISIB0CSIB site configuration (b) co-adsorption of two hydrogen molecules from inside the nanotube in type 2 (5, 5) T2H2S0SISIB site configuration. All plots have been plotted under similar conditions using an isovalue of 0.002.

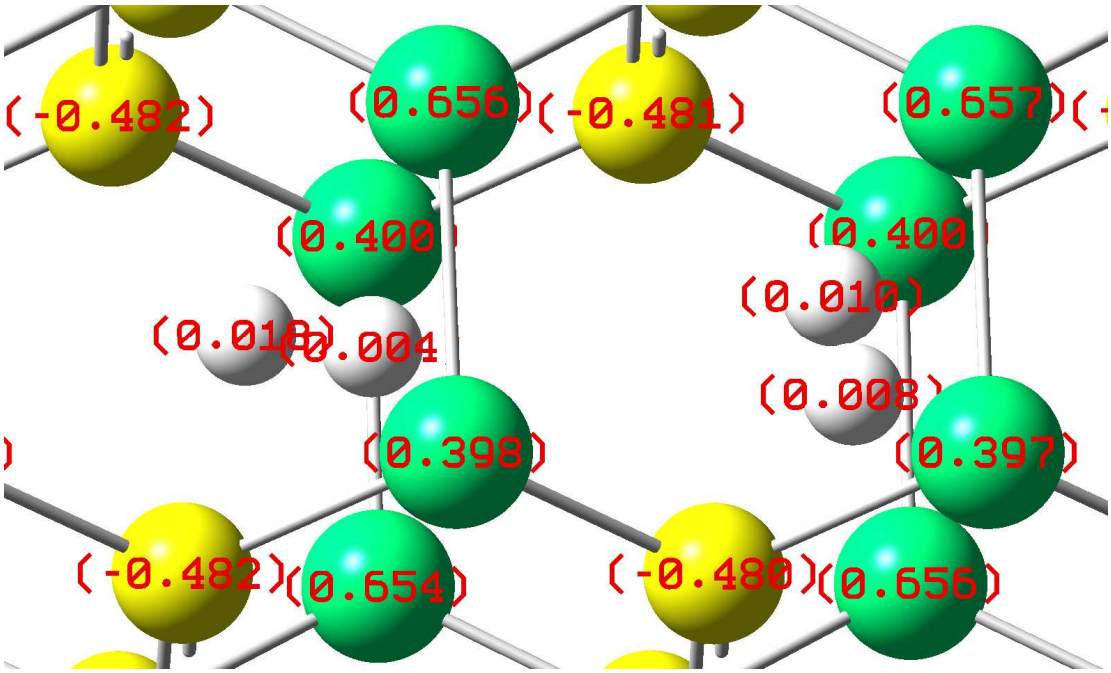

Figure 4.15 Mulliken charge plot of optimized type 2 (4, 4) SICNT with two hydrogen molecules placed inside the nanotube in T2SISIB0CSIB site configuration. The carbon atoms are yellow, silicon atoms are green and the hydrogen atoms are white.

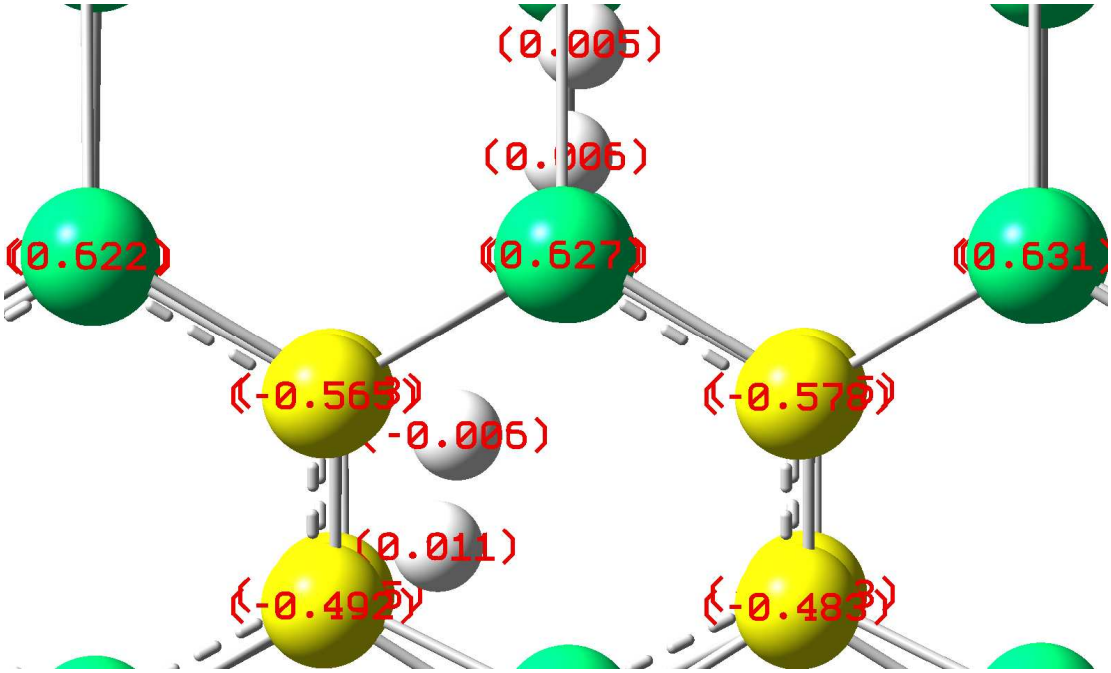

Figure 4.16 Mulliken charge plot of optimized type 2 (5, 5) SICNT with two hydrogen molecules placed inside the nanotube in T2H2S0SISIB site configuration. The carbon atoms are yellow, silicon atoms are green and the hydrogen atoms are white.

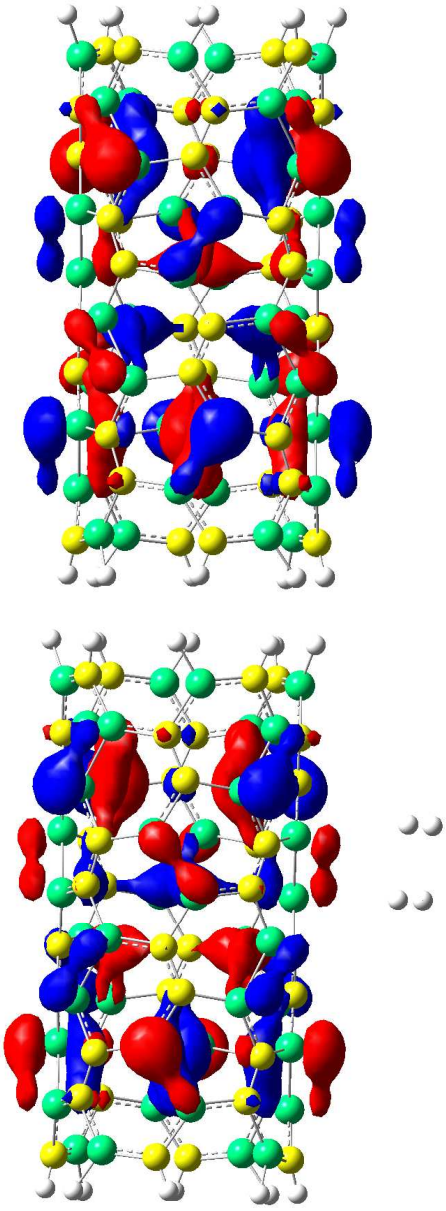

Figure 4.17 HOMO plots for (a) bare type 3 optimized (4, 4) SICNT (b) optimized type 3 (4, 4) SICNT with hydrogen molecules placed inside the nanotube in T3SISIB0SIT site configuration. The two hydrogen molecules are approaching the nanotube from the outer wall.

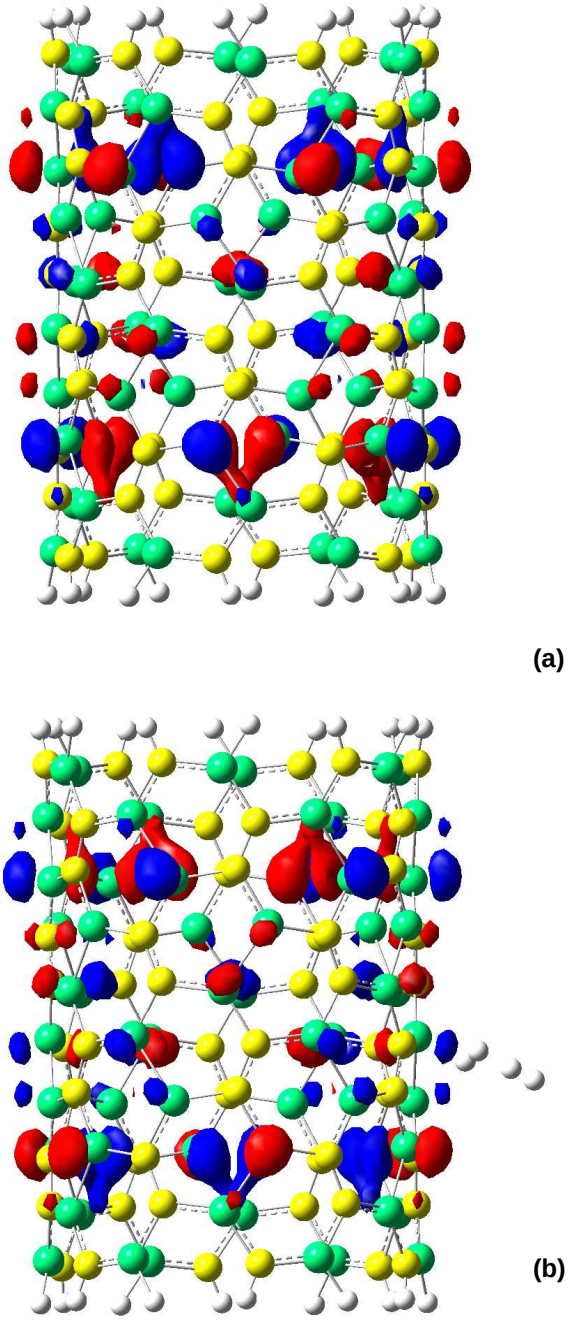

Figure 4.18 HOMO plots for (a) bare type 3 optimized (6, 6) SICNT (b) optimized type 3 (6, 6) SICNT with hydrogen molecules placed inside the nanotube in T3CT0CSIZB site configuration. The two hydrogen molecules are approaching the nanotube from the outer wall.

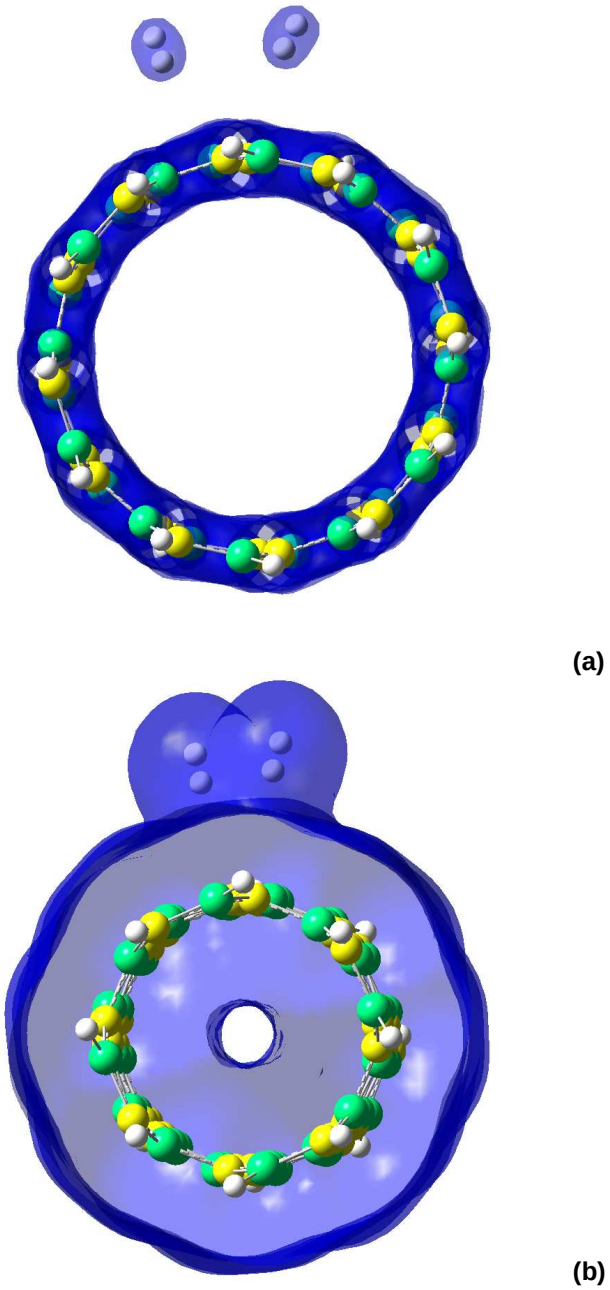

(a)

(b)

Figure 4.19 Electron charge density plot for (a) co-adsorption of two hydrogen molecules from outside the nanotube in type 3 (4, 4) T3SISIB0SIT site configuration (b) co-adsorption of two hydrogen molecules from outside the nanotube in type 3 (6, 6) T3CT0CSIZB site configuration. All plots have been plotted under similar conditions using an isovalue of 0.002.

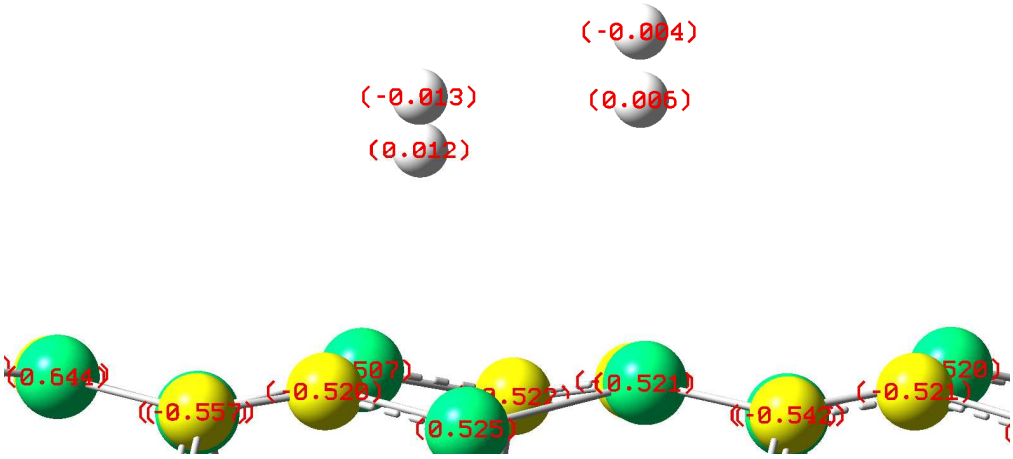

Figure 4.20 Mulliken charge plot of optimized type 3 (4, 4) SICNT with two hydrogen molecules placed outside the nanotube in T3SISIB0SIT site configuration. The carbon atoms are yellow, silicon atoms are green and the hydrogen atoms are white.

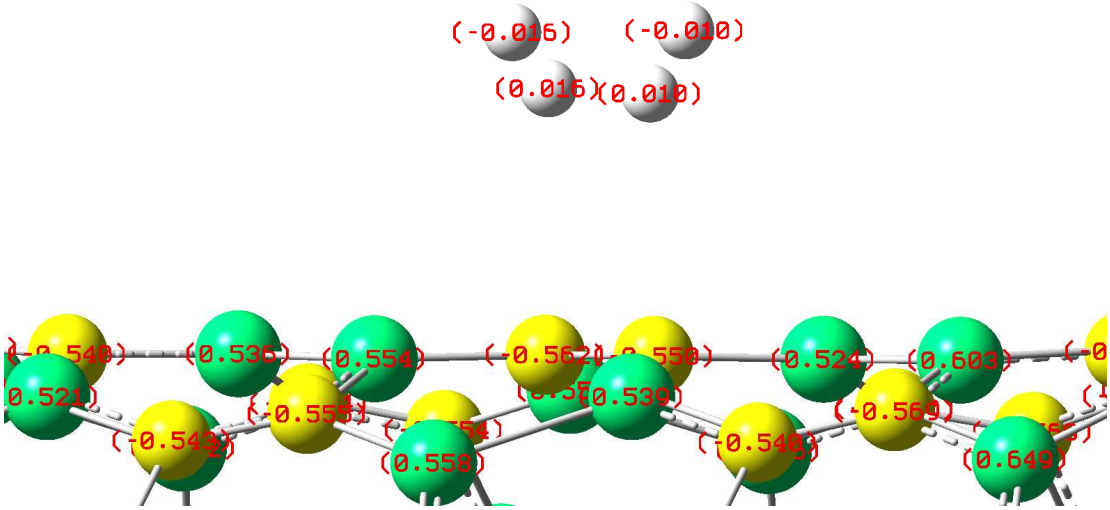

Figure 4.21 Mulliken charge plot of optimized type 3 (6, 6) SICNT with two hydrogen molecules placed outside the nanotube in T3CT0CSIZB site configuration. The carbon atoms are yellow, silicon atoms are green and the hydrogen atoms are white.

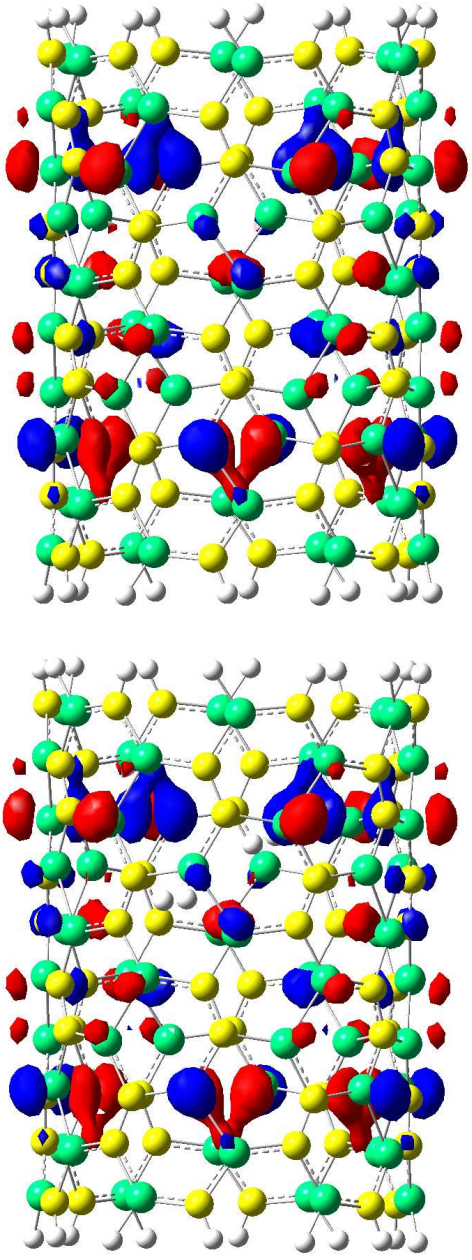

Figure 4.22 HOMO plots for (a) bare type 3 optimized (6, 6) SICNT (b) optimized type 3 (6, 6) SICNT with hydrogen molecules placed inside the nanotube in T3HS0SISIB site configuration. The two hydrogen molecules are approaching the nanotube from the inner wall.

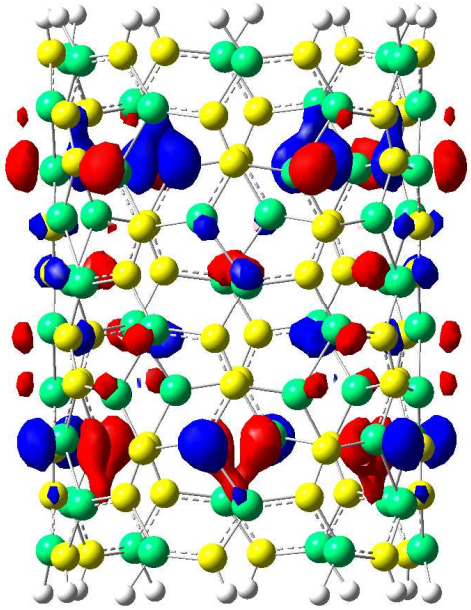

(a)

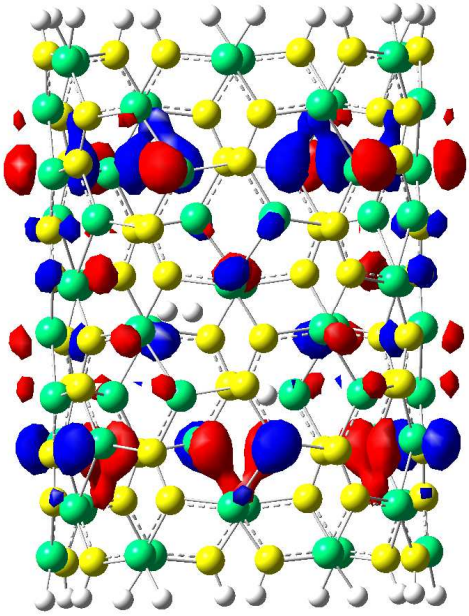

(b)

Figure 4.23 HOMO plots for (a) bare type 3 optimized (6, 6) SICNT (b) optimized type 3 (6, 6) SICNT with hydrogen molecules placed inside the nanotube in T3SISIB0CSIZB site configuration. The two hydrogen molecules are approaching the nanotube from the inner wall.

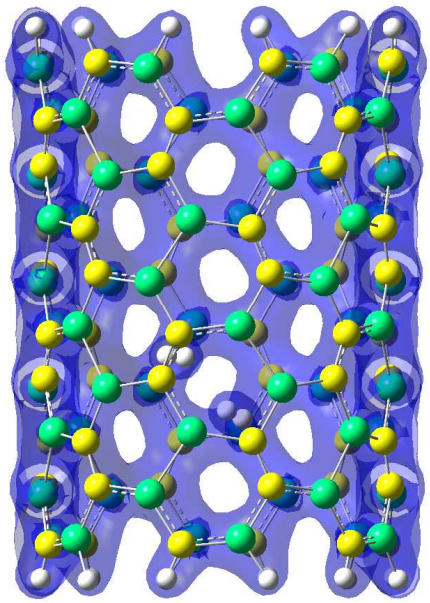

Figure 4.24 Electron charge density plot for co-adsorption of two hydrogen molecules from inside the nanotube in type 3 (6, 6) T3HS0SISIB site configuration. All plots have been plotted under similar conditions using an isovalue of 0.002.

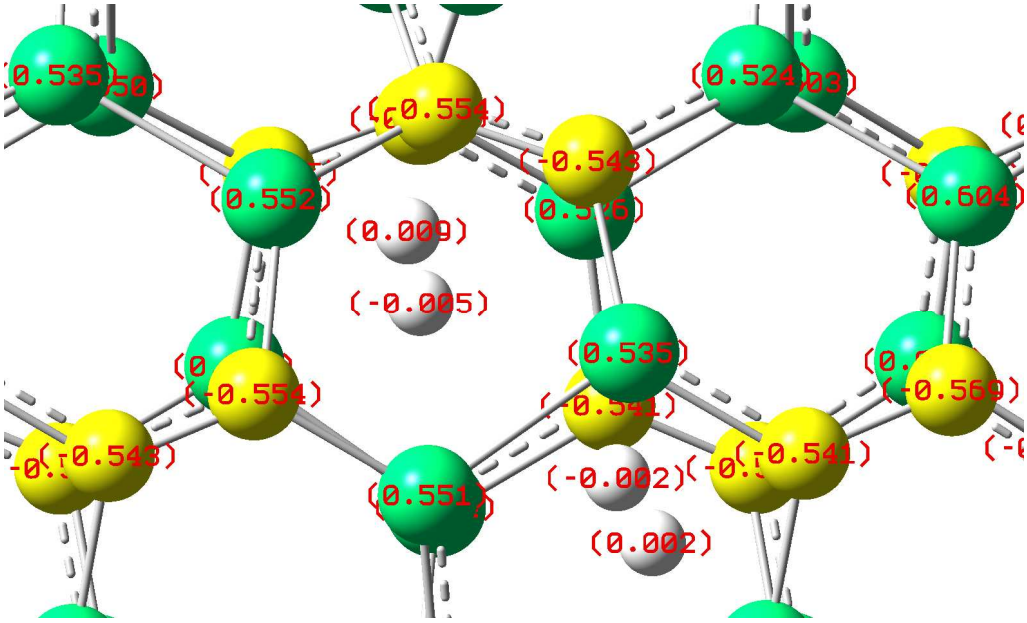

Figure 4.25 Mulliken charge plot of optimized type 3 (6, 6) SICNT with two hydrogen molecules placed inside the nanotube in T3HS0SISIB site configuration. The carbon atoms are yellow, silicon atoms are green and the hydrogen atoms are white.

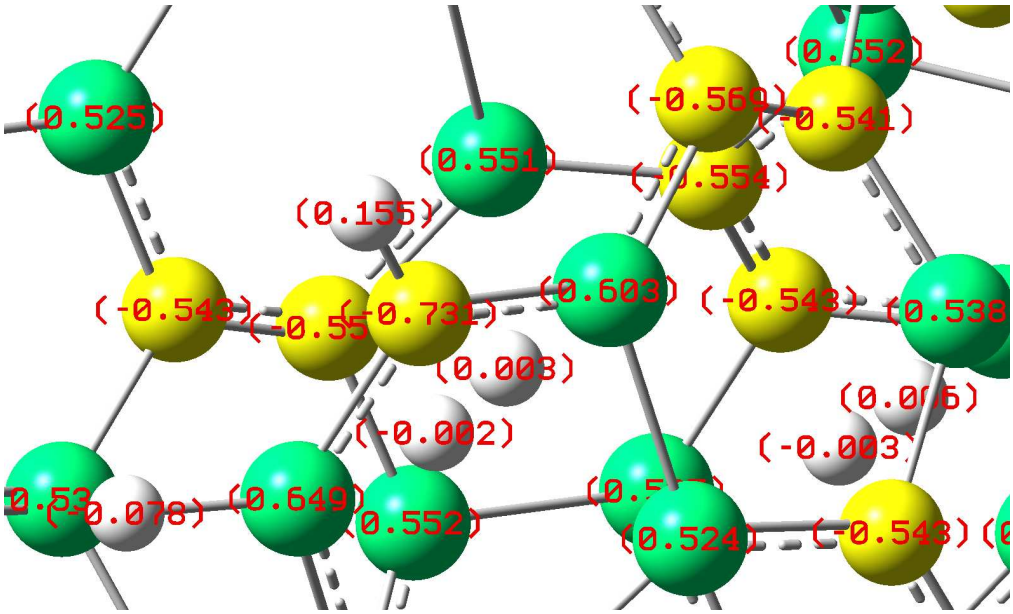

Figure 4.26 Mulliken charge plot of optimized type 3 (6, 6) SICNT with two hydrogen molecules placed inside the nanotube in T3SISIB0CSIZB site configuration. The carbon atoms are yellow, silicon atoms are green and the hydrogen atoms are white.

CHAPTER 5
CONCLUSIONS AND SUGGESTIONS FOR FUTURE WORK

In the first part of our study, we have studied molecular hydrogen adsorption on three different types of single walled (9, 9) SiC nanotubes in armchair configurations. Our studies indicate that SiCNT can be a good media for hydrogen storage, with types 2 and 3 nanotubes being possibly better storage medium as compared to type 1. Studies involving optimization of single molecule hydrogen adsorption have revealed that carbon top and the carbon-carbon bridge sites have a higher adsorption binding energy compared to silicon top sites. The above results suggest that higher adsorption binding energy can be achieved for sp^2 like bonding nanostructures. In all cases the adsorption binding energy obtained for PW91 method has been found to be higher than B3LYP method. This is on expected lines as B3LYP is a hybrid density functional compared to the pure density functional PW91. Most importantly, the first part of our study revealed that better binding sites are available in type 1 armchair structures as compared to sites studied by Mpourmpakis *et al.* [34].

In the next part of our study, optimization of various armchair nanotube structures ranging from (3, 3) to (6, 6), belonging to all three types and co-adsorption of two hydrogen molecules have been carried out. These structures include all three nanotube types. Results from our studies have confirmed that type 2 structures have better binding with the adsorbed hydrogen molecule as compared to type 1 and type 3. Furthermore, in this study we find that for the adsorption taking place inside the nanotube, optimized configuration is obtained when the hydrogen molecule is at the center of the nanotube as in T2CCB site in type 2 (4, 4) structure. This leads to both charge and geometric symmetry resulting in high binding energy of the order of 1eV. The adsorption in this case is chemisorption, unlike most sites in other structures where

the adsorption is predominantly physisorption. The average binding energy obtained is maximum in type 2 followed by type 3 and type 1 nanotubes, for inside adsorption. For hydrogen adsorption from outside the nanotube, the most preferred structure is once again type 2 (4, 4). Additionally, most sites in this structure show an adsorption binding energy of more than 1eV when the hydrogen molecule is adsorbed from outside. For outer wall adsorption, the maximum average binding energy of the hydrogen molecule is in type 2 structures followed by type 1 and then closely followed by type 3. Therefore, by changing the atomic configuration as well as diameter of the nanotube we can obtain the desired adsorption binding energy. Also, from the Mulliken charge analysis plots, it is quite evident that for the hydrogen molecular adsorption taking place inside the nanotube, excellent binding occurs when the final optimized structure is charge symmetric in nature. This can lead to other similar structures and sites in other polar nanotubes, displaying similar symmetric behavior, hence higher binding energy. However, for outer wall adsorption of the hydrogen molecule it is the local structure which as a whole determines the adsorption binding energy of the hydrogen molecule. The electronic charge density plots clearly illustrate that the charge overlap between the hydrogen molecule and the nanotube is most prominent in case of the more preferred binding sites. On the whole, except for one structure in type 2 and type 3, the adsorption in most sites which have been studied is predominantly physisorption in nature. The partial density of state plots also indicates that the nature of adsorption is predominantly physisorption. While addressing the storage capacity issue, we considered the number of sites where binding takes place and found that the storage capacity of up to 7.45% can be achieved for type 2 (5, 5) structures. Hence, it is an excellent candidate for hydrogen storage. The above trend in the binding energy values have been confirmed in the co-adsorption study of hydrogen molecules in nanotubes ranging from (3, 3) to (4, 4) and for all three types. The binding energies are on the whole extremely site dependant. For certain type 2 (4, 4) site configuration it has been found to exceed binding energy obtained during single molecular hydrogen adsorption. Most site arrangement which

show binding in type 2 (4, 4), both inside as well as outer wall co-adsorption, display binding energy of more than 1eV. Hence, these adsorptions can be classified as chemisorption in nature. Through the co-adsorption study, we also find that in case of type 3 nanotubes only (6, 6) nanotubes show binding for inner wall co-adsorption and for outer wall co-adsorption. The binding in type 3 (6, 6) nanotubes is sometimes better or equivalent to smaller diameter nanotube structures belonging to the same type. The co-adsorption study shows better binding as compared to single molecular adsorption in particular cases. It thus raises the possibility of getting excellent binding results when real time experiments are conducted. The binding energy can be further tailor made to suit our needs by modifying the nanotube diameter and using different atomic configuration. Even though types 2 and type 3 have slightly lower stability compared to type 1 as reported by our group [33], the binding energy properties we get in type 2 and type 3 are encouraging. In a similar way, zigzag nanotubes have lower stability as compared to armchair nanotubes and work on them has already been carried out previously in our group [33]. Hence studies on zigzag nanotubes can be worthwhile. Studies involving interaction of hydrogen molecules on transition metal coated SiCNTs can also be explored.

REFERENCES

[1] http://www.daimlerchrysler.com.

[2] H.Cheng, Q. Yang, and C. Liu, Carbon, 39, 1447-1454 (2001)

[3] U.S. Patent 4,580, 404

[4] K.A.G Amankwah, J. A. Schwarz, Int. J. Hydrogen Energy, 14, 437 (1989)

[5] J. Jagiello, T.J. Bandosz, K. Putyera, J A Schwarz, J. Chem.Soc., Faraday Trans., 91, 2929 (1995)

[6] A.C Dillon, K.M Jones, T.A Bekkedahl, C.H Kiang, D.S. Bethune, M.J Heben, Nature, 386, 377 (1997)

[7] H. Freimuth, H. Wiechert, H.J. Lauter, Surf. Sci., 189, 548 (1987)

[8] J. Cui, S.C. Jr. Fain, H. Freimuth, H. Wiechert, H.P. Schildberg, H.J. Lauter, J. Phys. ReV. Lett., 60, 1848 (1988)

[9] K. Watanabe, M. Soma, T. Ohishi, K. Tamaru, Nature, 233, 160 (1971)

[10] P.Lagarnge, A. Metror, A. Herold, Comp. Rend., 275, 160 (1971)

[11] R. Ströbel, L. Jörissen, T. Schliermann, V. Trapp, W. Schütz, K. Bohmhammel, G.Wolf and J.Garche, J. Power Sources, 84, 221 (1999)

[12] F. E. Pinkerton, B. G. Wicke, C. H. Olk, G. G. Tibbetts, G. P. Meisner, M. S. Meyer and J. F. Herbst, J. Phys. Chem. B., 104, 9460 (2000)

[13] R. T. Yang, Carbon, 38, 623 (2000)

[14] H. G. Schimmel, G. J. Kearley, M. G. Nijkamp, C. T. Visser, K. P. de Jong and F. M. Mulder, Chem. Eur. J., 9, 4764 (2003)

[15] http://www1.eere.energy.gov/hydrogenandfuelcells/pdfs/milliken_ee_storage.pdf

[16] S. Iijima, Nature, 354, 56 (1991)

[17] A. C. Dillon and M. J. Heben, Appl. Phys. A, 72, 133 (2001)

[18] S. H. Jhi and Y-K. Kwon, Phys. Rev. B., 69, 245407 (2004)

[19] M. T. Yin and M. L. Cohen, Phys. Rev. B., 29, 6996 (1984)

[20] X. H. Sun, C. P. Li, W. K. Wong, N. B. Wong, C. S. Lee, S. T. Lee and B.K. Teo, J. Am. Chem. Soc., 124, 14464 (2002)

[21] N. Keller, C. Pham-Huu, G. Ehret, V. Keller and M. J. Ledoux, Carbon, 41, 2131 (2003)

[22] E. Borowiak-Palen, M. H. Ruemmeli, T. Gemming, M. Knupfer, K. Biedermann, A. Leonhardt, T. Pihler, R. J. Kalenczuk, J. Appl. Phys., 97, 056102 (2005)

[23] T. Taguchi, N. Igawa, H. Yamamoto, S. Shamoto, S. Jitsukawa, Physica E, 28, 431 (2005)

[24] J-M. Nhut, R. Vieira, L. Pesant, J.-P. Tessonnier, N. Keller, G. Ehret, C. Pham-Huu, M.J. Ledoux, Catal. Today, 76, 11 (2002)

[25] C. Pham-Huu, N. Keller, G. Ehret, M. J. Ledoux, J. Catal., 200, 400 (2001)

[26] A. Huczko, M. Bystrzejewski, H. Lange, A. Fabianowska, S. Cudzilo, A. Panas, and M. Szala, J. Phys. Chem. B, 109, 16244 (2005)

[27] T. Meng, C-Y. Wang, S.-Y. Wang, Chem. Phys. Lett., 437, 224 (2007)

[28] M. W. Zhao, Y. Y. Xia, F. Li, R. Q. Zhang and S.-T Lee, Phys. Rev. B, 71, 085312 (2005)

[29] A. Gali, Phys. Rev. B., 75, 085416 (2007)

[30] R. He, Z. Chu, X. Li, Y. Si, Key Eng. Mater., 368,647 (2008)

[31] G. Mavrandonakis, E. Froudakis, M. Schnell and M. Muhlhä, Nano Lett., 3, 1481 (2003)

[32] M. Menon, E. Richter and A. N. Andriotis, Phys. Rev. B., 69, 115322 (2004)

[33] K. M. Alam and A. K. Ray, Phys. Rev. B., 77, 035436 (2008)

[34] G. Mpourmpakis, G. E. Froudakis, G. P. Lithoxoos and J. Samios, Nano Lett., 6, 1581 (2006)

[35] S. Mukherjee and Asok K. Ray, J. Comput. Theor. Nanosci., 5, 1210 (2008)

[36] R. G. Parr and W. Yang, *Density Functional Theory of Atoms and Molecules* (Oxford University Press, New York, 1989).

[37] P. Hohenberg and W. Kohn, Phys. Rev., 136, B864 (1964)

[38] W. Kohn and L. J. Sham, Phys Rev., 140, A1133 (1965)

[39] D. M. Ceperley and B. J. Adler, Phys. Rev. Lett., 45, 566 (1980)

[40] W. Kohn, A.D. Becke and R. G. Parr, J. Phys. Chem., 100, 12974 (1996)

[41] R. O. Jones and O. Gunnarsson, Rev. Mod. Phys., 61, 689 (1989)

[42] G. Sentore and N. H. March, Rev. Mod. Phys., 66, 445 (1996)

[43] J. F. Dobson, G. Vignale and M. P. Das (Eds.), *Electronic Density Functional Theory: Recent Progress and New Directions, (Plenum Press, New York and London, 1998)*

[44] D. R. Hartree, Proc. Cambridge PHilos. Soc., 24, 89 (1928)

[45] V. Fock, Z. Phys., 61, 126 (1930)

[46] J. C. Slater, Phys. Rev., 35, 210 (1930)

[47] C. Coulson, Rev. Mod. Phys., 32, 170 (1960)

[48] L. H. Thomas, Proc. Cambridge Plilos. Soc., 23, 542 (1927)

[49] E. Fermi, Z. Phys., 48, 73 (1928)

[50] P. A. M. Dirac, Proc. Cambridge Plilos. Soc., 26, 376 (1930)

[51] U. von Barth and L. Hedin, J. Phys. C:Solid State Phys., 5, 1629 (1972)

[52] O. Gunnarsson and B. I. Lundqvist, Phys. Rev., 13, 4274 (1976)

[53] S. H. Vosko, L. Wilk and M. Nusair, Can. J. Phys., 58, 1200 (1980)

[54] M. Rasolt and D. J.W. Geldart, Phys. Rev. B, 34, 1325 (1986)

[55] J. P. Perdew, Phys. Rev. B, 33, 8822 (1986); 34, 7406 (1984)

[56] A. D. Becke, J. Chem. Phys., 98, 1372 (1993); 98, 5648 (1993)

[57] C. Lee, W. Yang and R. G. Parr, Phys. Rev. B , 37, 785 (1988)

[58] J. P. Perdew, J. A. Chevary, S. H. Vosko, K. A. Jackson, M. R. Pederson, D. J. Singh, and C. Fiolhais, Phys. Rev. B, 48, 4978 (1993); K. Burke, J. P. Perdew, and Y. Wang, in Electronic

Density Functional Theory: Recent Progress and New Directions, Ed. J. F. Dobson, G. Vignale, and M. P. Das (Plenum, New York, 1998).

[59] J. P. Perdew, K. Burke and M. Ernzerhof, Phys. Rev. Lett., 77, 3865 (1996); 78, 1396 (1997).

[60] J. P. Perdew, Electronic Structure of Solids'91, edited by P. Ziesche and H. Eschig (Akademie Verlag, Berlin, 1991); J. P. Perdew and Y. wang, Phys. Rev. B, 46, 12947 (1992); Phys. Rev. B, 46, 6671 (1992)

[61] W. J. Hehre, L. Radom, P. V. R. Schleyer and J. A. Pople, Ab Initio Molecular Orbital Theory (Wiley, New York, 1986).

[62] J. P. Perdew, R. G. Parr, M. Levy, J. L. Balduz, Phys. Rev. Lett., 49, 1691 (1982)

[63] J. P. Perdew, M. Levy, Phys. Rev. Lett., 51, 1884 (1983)

[64] J. Muscat, A. Wander and N. Harrison, Chem. Phys. Lett., 34, 397 (2001)

[65] J. Heyd and G. Scuseria, J. Chem. Phys., 121, 1187 (2004)

[66] V. Barone, J. E. Peralta, M. Wert, J. Heyd, and G. E. Scuseria, Nano Lett., 5, 1621 (2005)

[67] V. Barone, J. E. Peralta, and G. E. Scuseria, Nano Lett., 5, 1830 (2005)

[68] V. Barone, O. Hod, and G. E. Scuseria, Nano Lett., 6, 2748 (2006)

[69] M. Y. Han, B. Ozyilmaz, Y. Zhang, and P. Kim, Phys. Rev., Lett. 98, 206805 (2007)

[70] J. P. Perdew, K. Burke and Y. Wang, Phys. Rev. B, 54, 16533 (1996)

[71] Gaussian 03, Revision A.1, M. J. Frisch, M. J. Frisch, G. W. Trucks, H. B. Schlegel, G. E. Scuseria, M. A. Robb, J. R. Cheeseman, J. A. Montgomery, Jr., T. Vreven, K. N. Kudin, J. C. Burant, J. M. Millam, S. S. Iyengar, J. Tomasi, V. Barone, B. Mennucci, M. Cossi, G. Scalmani, N. Rega, G. A. Petersson, H. Nakatsuji, M. Hada, M. Ehara, K. Toyota, R. Fukuda, J. Hasegawa, M. Ishida, T. Nakajima, Y. Honda, O. Kitao, H. Nakai, M. Klene, X. Li, J. E. Knox, H. P. Hratchian, J. B. Cross, C. Adamo, J. Jaramillo, R. Gomperts, R. E. Stratmann, O. Yazyev, A. J. Austin, R. Cammi, C. Pomelli, J. W. Ochterski, P. Y. Ayala, K. Morokuma, G. A. Voth, P. Salvador, J. J. Dannenberg, V. G. Zakrzewski, S. Dapprich, A. D. Daniels, M. C. Strain, O.

Farkas, D. K. Malick, A. D. Rabuck, K. Raghavachari, J. B. Foresman, J. V. Ortiz, Q. Cui, A. G. Baboul, S. Clifford, J. Cioslowski, B. B. Stefanov, G. Liu, A. Liashenko, P. Piskorz, I. Komaromi, R. L. Martin, D. J. Fox, T. Keith, M. A. Al-Laham, C. Y. Peng, A. Nanayakkara, M. Challacombe, P. M. W. Gill, B. Johnson, W. Chen, M. W. Wong, C. Gonzalez, and J. A. Pople, Gaussian Inc. Pittsburgh, Pa, (2003)

[72] M. Zhao, Y. Xia, F. Li, R. Q. Zhang and S. T. Lee, Phys. Rev. B., 71, 085312 (2005)

[73] S. Mukherjee and Asok K. Ray, J. Comput. Theor. Nanosci., 5, 1210 (2008)

[74] N.M. O'Boyle, J.G. Vos, GaussSum 0.9, Dublin City University, 2005. Available at: <http://gausssum.sourceforge.net>.

[75] T. Meng, C-Y. Wang, S.-Y. Wang, Chem. Phys. Lett., 437, 224 (2007)

BIOGRAPHICAL INFORMATION

The author completed his undergraduate degree in Metallurgical Engineering from National Institute of Technology, Karnataka, India. During these programs he has completed courses on Engineering Physics and semiconductor materials. Thereafter he worked in Essar Steel, India for four months. Later on he worked as Manager Business Development in Unisoft (India) Pvt. Ltd., Bangalore, India. In order to get back to academics he joined as a MS student at the University of Texas at Arlington, Materials Science Dept. To have a deeper understanding towards basic sciences and getting attracted to physics he joined Dr. A. K. Ray's group as a physics graduate student. Right now he is pursuing a Master of Science degree in physics in the area of condensed matter physics.

His current research interests are theoretical nanotechnology, interaction of hydrogen molecules with nanotubes and exploring the possibility of hydrogen storage in nanotubes. Specifically he has been working with silicon carbide nanotubes as part of his master's thesis. Under the mentorship of Dr. A. K. Ray, the author published his work in the Journal of Computational and Theoretical Nanocsience. In future he intends to work both in the industry and academia and contribute meaningfully to the scientific community at large.